ISSN 2686-7575 (Online)

ТОНКИЕ ХИМИЧЕСКИЕ ТЕХНОЛОГИИ

Fine Chemical Technologies

- Theoretical Bases of Chemical Technology
- Chemistry and Technology of Organic Substances
- Chemistry and Technology of Medicinal Compounds and Biologically Active Substances
- Synthesis and Processing of Polymers and Polymeric Composites
- Chemistry and Technology of Inorganic Materials
- Analytical Methods in Chemistry and Chemical Technology
- Mathematical Methods and Information Systems in Chemical Technology

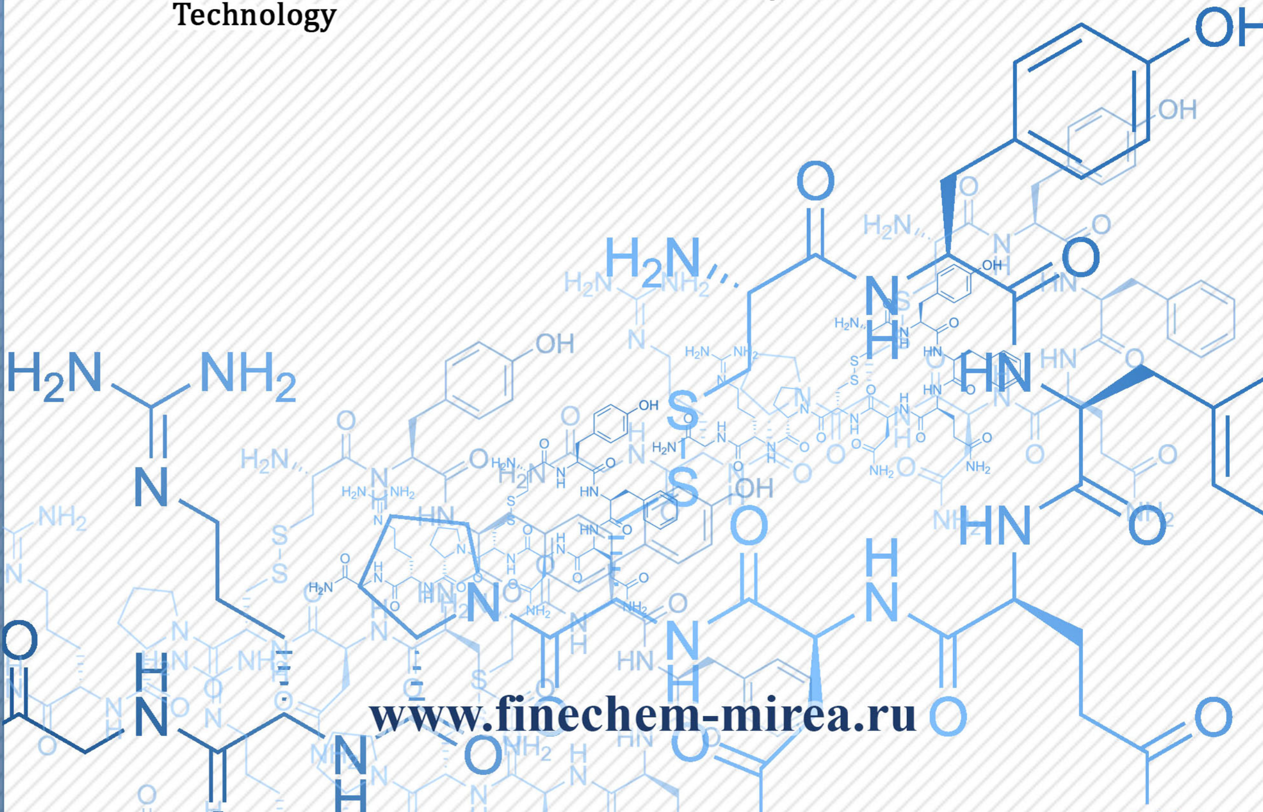

15(2)

2020

www.finechem-mirea.ru

ISSN 2686-7575 (Online)

ТОНКИЕ ХИМИЧЕСКИЕ ТЕХНОЛОГИИ

Fine Chemical Technologies

- Theoretical Bases of Chemical Technology
- Chemistry and Technology of Organic Substances
- Chemistry and Technology of Medicinal Compounds and Biologically Active Substances
- Synthesis and Processing of Polymers and Polymeric Composites
- Chemistry and Technology of Inorganic Materials
- Analytical Methods in Chemistry and Chemical Technology
- Mathematical Methods and Information Systems in Chemical Technology

Tonkie Khimicheskie Tekhnologii =
Fine Chemical Technologies
Vol. 15, No. 2, 2020

Тонкие химические технологии =
Fine Chemical Technologies
Том 15, № 2, 2020

https://doi.org/10.32362/2410-6593-2020-15-2
www.finechem-mirea.ru

https://doi.org/10.32362/2410-6593

Tonkie Khimicheskie Tekhnologii
= Fine Chemical Technologies
2020, vol. 15, no. 2

The peer-reviewed scientific and technical journal Fine Chemical Technologies highlights the modern achievements of fundamental and applied research in the field of fine chemical technologies, including theoretical bases of chemical technology, chemistry and technology of medicinal compounds and biologically active substances, organic substances and inorganic materials, synthesis and processing of polymers and polymeric composites, analytical and mathematical methods and information systems in chemistry and chemical technology.

Founder and Publisher

Federal State Budget
Educational Institution
of Higher Education
"MIREA – Russian Technological University"
78, Vernadskogo pr., Moscow 119454, Russian Federation.

Six issues a year are published.
The journal was founded in 2006. The name was Vestnik MITHT until 2015 (ISSN 1819-1487).

The journal is included into the List of peer-reviewed science press of the State Commission for Academic Degrees and Titles of the Russian Federation.
The journal is indexed:
DOAJ, Chemical Abstracts, Science Index, RSCI, Ulrich's International Periodicals Directory

Editor-in-Chief:

Deputy Editor-in-Chief:

Editorial staff:

86, Vernadskogo pr., Moscow 119571, Russian Federation.
Phone: +7(495) 246-05-55 (#2-88)
E-mail: *vestnik@mitht.ru*

Registration Certificate ПИ № ФС 77–74580, issued on December 14, 2018 by the Federal Service for Supervision of Communications, Information Technology, and Mass Media of Russia

The subscription index of *Pressa Rossii*: **36924**

www.finechem-mirea.ru

Тонкие химические технологии
= Fine Chemical Technologies
2020, том 15, № 2

Научно-технический рецензируемый журнал «Тонкие химические технологии» освещает современные достижения фундаментальных и прикладных исследований в области тонких химических технологий, включая теоретические основы химической технологии, химию и технологию лекарственных препаратов и биологически активных соединений, органических веществ и неорганических материалов, синтез и переработку полимеров и композитов на их основе, аналитические и математические методы и информационные системы в химии и химической технологии.

Учредитель и издатель

федеральное государственное бюджетное
образовательное учреждение
высшего образования
«МИРЭА – Российский технологический университет»
119454, РФ, Москва, пр-кт Вернадского, д. 78.

Периодичность: 6 раз в год.
Журнал основан в 2006 году. До 2015 года издавался под названием «Вестник МИТХТ» (ISSN 1819-1487).

Журнал входит в Перечень ведущих рецензируемых научных журналов ВАК РФ.
Индексируется:
DOAJ, Chemical Abstracts, РИНЦ (Science Index), RSCI, Ulrich's International Periodicals Directory

Главный редактор:

Заместитель главного редактора:

Редакция:

119571, Москва, пр. Вернадского, 86, оф. Л-119.
Тел.: +7(495) 246-05-55 (#2-88)
E-mail: *vestnik@mitht.ru*

Свидетельство о регистрации СМИ: ПИ № ФС 77-74580 от 14.12.2018 г. выдано Федеральной службой по надзору в сфере связи, информационных технологий и массовых коммуникаций (Роскомнадзор)

Индекс по Объединенному каталогу «Пресса России»: **36924**

Editorial Board

Zinesh S. Abisheva – Corresponding Member of the National Academy of Sciences of Kazakhstan, Dr. Sci. (Eng.), Professor, Institute of Metallurgy and Ore Beneficiation, K.I. Satpaev Kazakh National Research Technical University, Almaty, Kazakhstan. Scopus Author ID 6601954283, ResearcherID O-8453-2017, http://orcid.org/0000-0002-4506-0694, *abisheva_z@mail.ru.*

Sergey P. Verevkin – Dr. Sci. (Eng.), Professor, University of Rostock, Rostock, Germany. Scopus Author ID 7006607848, ResearcherID G-3243-2011, *Sergey.verevkin@uni-rostock.de.*

Dmitry V. Drobot – Dr. Sci. (Chem.), Professor, MIREA – Russian Technological University, Moscow, Russian Federation. Scopus Author ID 35580931100, *dvdrobot@mail.ru.*

Konstantin Yu. Zhizhin – Corresponding Member of the Russian Academy of Sciences, Dr. Sci. (Chem.), Professor, N.S. Kurnakov Institute of General and Inorganic Chemistry of the RAS, Moscow, Russian Federation. Scopus Author ID 6701495620, ResearcherID C-5681-2013, http://orcid.org/0000-0002-4475-124X, *kyuzhizhin@igic.ras.ru.*

Igor V. Ivanov – Dr. Sci. (Chem.), Professor, MIREA – Russian Technological University, Moscow, Russian Federation. Scopus Author ID 34770109800, ResearcherID I-5606-2016, http://orcid.org/0000-0003-0543-2067, *ivanov_i@mirea.ru.*

Anatolii A. Ischenko – Dr. Sci. (Chem.), Professor, MIREA – Russian Technological University, Moscow, Russian Federation. Scopus Author ID 6701507307, *aischenko@yasenevo.ru.*

Carlos A. Cardona – PhD (Eng.), Professor, National University of Columbia, Manizales, Colombia. Scopus Author ID 7004278560, ResearcherID G-8554-2016, http://orcid.org/0000-0002-0237-2313, *ccardonaal@unal.edu.co.*

Oskar I. Koifman – Corresponding Member of the Russian Academy of Sciences, Dr. Sci. (Chem.), Professor, Ivanovo University of Chemical Technology, Ivanovo, Russian Federation. Scopus Author ID 6602070468, ResearcherID R-1020-2016, http://orcid.org/0000-0002-1764-0819, *president@isuct.ru.*

Valery F. Kornyushko – Dr. Sci. (Eng.), Professor, MIREA – Russian Technological University, Moscow, Russian Federation, *vfk256@mail.ru.*

Elvira T. Krut'ko – Dr. Sci. (Eng.), Professor, Belarusian State Technological University, Minsk, Belarus. Scopus Author ID 6602297257, *ela_krutko@mail.ru.*

Anatolii I. Miroshnikov – Academician of the Russian Academy of Sciences, Dr. Sci. (Chem.), Professor, M.M. Shemyakin and Yu.A. Ovchinnikov Institute of Bioorganic Chemistry of the RAS, Member of the Presidium of the RAS, Chairman of the Presidium of the RAS Pushchino Research Center, Moscow, Russian Federation. Scopus Author ID 7006592304, ResearcherID G-5017-2017, *aiv@ibch.ru.*

Yuri P. Miroshnikov – Dr. Sci. (Chem.), Professor, MIREA – Russian Technological University, Moscow, Russian Federation. Scopus Author ID, 6603349573, *miroshnikov@mirea.ru.*

Редакционная коллегия

Абишева Зинеш Садыровна – член-корр. Национальной Академии Наук Республики Казахстан, д.т.н., профессор, Институт металлургии и обогащения, Казахский национальный технический университет имени К. И. Сатпаева, Алматы, Казахстан. Scopus Author ID 6601954283, ResearcherID O-8453-2017, http://orcid.org/0000-0002-4506-0694, *abisheva_z@mail.ru.*

Верёвкин Сергей Петрович – д.т.н., профессор Университета г. Росток, Росток, Германия. Scopus Author ID 7006607848, ResearcherID G-3243-2011, *Sergey.verevkin@uni-rostock.de.*

Дробот Дмитрий Васильевич – д.х.н., профессор, МИРЭА – Российский технологический университет, Москва, Российская Федерация. Scopus Author ID 35580931100, *dvdrobot@mail.ru.*

Жижин Константин Юрьевич – член-корр. Российской академии наук, д.х.н., профессор, Институт общей и неорганической химии им. Н.С. Курнакова РАН, Москва, Российская Федерация. Scopus Author ID 6701495620, ResearcherID C-5681-2013, http://orcid.org/0000-0002-4475-124X, *kyuzhizhin@igic.ras.ru.*

Иванов Игорь Владимирович – д.х.н., профессор, МИРЭА – Российский технологический университет, Москва, Российская Федерация. Scopus Author ID 34770109800, ResearcherID I-5606-2016, http://orcid.org/0000-0003-0543-2067, *ivanov_i@mirea.ru.*

Ищенко Анатолий Александрович – д.х.н., профессор, МИРЭА – Российский технологический университет, Москва, Российская Федерация. Scopus Author ID 6701507307, *aischenko@yasenevo.ru.*

Кардона Карлос Ариэль – профессор Национального университета Колумбии, Манизалес, Колумбия. Scopus Author ID 7004278560, ResearcherID G-8554-2016, http://orcid.org/0000-0002-0237-2313, *ccardonaal@unal.edu.co.*

Койфман Оскар Иосифович – член-корр. Российской академии наук, д.х.н., профессор, Ивановский химико-технологический университет, Иваново, Российская Федерация. Scopus Author ID 6602070468, ResearcherID R-1020-2016, http://orcid.org/0000-0002-1764-0819, *president@isuct.ru.*

Корнюшко Валерий Федорович – д.т.н., профессор, МИРЭА – Российский технологический университет, Москва, Российская Федерация, *vfk256@mail.ru.*

Крутько Эльвира Тихоновна – д.т.н., профессор Белорусского государственного технологического университета, Минск, Беларусь. Scopus Author ID 6602297257, *ela_krutko@mail.ru.*

Мирошников Анатолий Иванович – академик Российской академии наук, д.х.н., профессор, Институт биоорганической химии им. академиков М.М. Шемякина и Ю.А. Овчинникова РАН, член Президиума РАН, председатель Президиума Пущинского научного центра РАН, Москва, Российская Федерация. Scopus Author ID 7006592304, ResearcherID G-5017-2017, *aiv@ibch.ru.*

Мирошников Юрий Петрович – д.х.н., профессор, МИРЭА – Российский технологический университет, Москва, Российская Федерация. Scopus Author ID 6603349573, *miroshnikov@mirea.ru.*

Aziz M. Muzafarov – Academician of the Russian Academy of Sciences, Dr. Sci. (Chem.), Professor, A.N. Nesmeyanov Institute of Organoelement Compounds of the RAS, Moscow, Russian Federation. ResearcherID G-1644-2011, https://orcid.org/0000-0002-3050-3253, *aziz@ineos.ac.ru.*

Ivan A. Novakov – Academician of the Russian Academy of Sciences, Dr. Sci. (Chem.), Professor, Volgograd State Technical University, Volgograd, Russian Federation. Scopus Author ID 7003436556, ResearcherID I-4668-2015, http://orcid.org/0000-0002-0980-6591, *president@vstu.ru.*

Alexander N. Ozerin – Corresponding Member of the Russian Academy of Sciences, Dr. Sci. (Chem.), Professor, Enikolopov Institute of Synthetic Polymeric Materials of the RAS, Moscow, Russian Federation. Scopus Author ID 7006188944, ResearcherID J-1866-2018, https://orcid.org/0000-0001-7505-6090, *ozerin@ispm.ru.*

Tapani A. Pakkanen – PhD, Professor, Head of Department of Chemistry, University of Eastern Finland, Joensuu, Finland. Scopus Author ID 7102310323, *tapani.pakkanen@uef.fi.*

Armando J.L. Pombeiro – Academician of the Academy of Sciences of Lisbon, PhD, Professor, Higher Technical Institute of the University of Lisbon, Lisbon, Portugal. Scopus Author ID 7006067269; ResearcherID I-5945-2012, https://orcid.org/0000-0001-8323-888X, *pombeiro@ist.utl.pt.*

Dmitrii V. Pyshnyi – Corresponding Member of the Russian Academy of Sciences, Dr. Sci. (Chem.), Professor, Institute of Chemical Biology and Fundamental Medicine, Siberian Branch of the Russian Academy of Sciences, Novosibirsk, Russian Federation. Scopus Author ID 7006677629, ResearcherID F-4729-2013, https://orcid.org/0000-0002-2587-3719, *pyshnyi@niboch.nsc.ru.*

Alexander S. Sigov – Academician of the Russian Academy of Sciences, Dr. Sci. (Phys. and Math.), Professor, President of MIREA – Russian Technological University, Moscow, Russian Federation. Scopus Author ID 35557510600, ResearcherID L-4103-2017, *sigov@mirea.ru.*

Vladimir A. Tverskoy – Dr. Sci. (Chem.), Professor, MIREA – Russian Technological University, Moscow, Russian Federation. Scopus Author ID 6604012434, 29567701900, ResearcherID H-8042-2017, https://orcid.org/0000-0003-4348-8854, *tverskoy@mitht.ru.*

Alexander M. Toikka – Dr. Sci. (Chem.), Professor, Institute of Chemistry, Saint Petersburg State University, St. Petersburg, Russian Federation. Scopus Author ID 6603464176, ResearcherID A-5698-2010, http://orcid.org/0000-0002-1863-5528, *a.toikka@spbu.ru.*

Andrzej W. Trochimczuk – Dr. Sci. (Chem.), Professor, Faculty of Chemistry, Wrocław University of Science and Technology, Wroclaw, Poland. Scopus Author ID 7003604847, *andrzej.trochimczuk@pwr.edu.pl.*

Aslan Yu. Tsivadze – Academician of the Russian Academy of Sciences, Dr. Sci. (Chem.), Professor, A.N. Frumkin Institute of Physical Chemistry and Electrochemistry of the RAS, Moscow, Russian Federation. Scopus Author ID 7004245066, ResearcherID G-7422-2014, *tsiv@phyche.ac.ru.*

Музафаров Азиз Мансурович – академик Российской академии наук, д.х.н., профессор, Институт элементоорганических соединений им. А.Н. Несмеянова РАН, Москва, Российская Федерация. ResearcherID G-1644-2011, https://orcid.org/0000-0002-3050-3253, *aziz@ineos.ac.ru.*

Новаков Иван Александрович – академик Российской академии наук, д.х.н., профессор, президент Волгоградского государственного технического университета, Волгоград, Российская Федерация. Scopus Author ID 7003436556, ResearcherID I-4668-2015, http://orcid.org/0000-0002-0980-6591, *president@vstu.ru.*

Озерин Александр Никифорович – член-корр. Российской академии наук, д.х.н., профессор, Институт синтетических полимерных материалов им. Н.С. Ениколопова РАН, Москва, Российская Федерация. Scopus Author ID 7006188944, ResearcherID J-1866-2018, https://orcid.org/0000-0001-7505-6090, *ozerin@ispm.ru.*

Пакканен Тапани – PhD, профессор, руководитель Департамента химии Университета Восточной Финляндии, Йоенсуу, Финляндия. Scopus Author ID 7102310323, *tapani.pakkanen@uef.fi.*

Помбейро Армандо – академик АН Лиссабона, PhD, профессор, президент Центра структурной химии Высшего технического института Университета Лиссабона, Португалия. Scopus Author ID 7006067269; ResearcherID I-5945-2012, https://orcid.org/0000-0001-8323-888X, *pombeiro@ist.utl.pt.*

Пышный Дмитрий Владимирович – член-корр. Российской академии наук, д.х.н., профессор, Институт химической биологии и фундаментальной медицины Сибирского отделения РАН, Новосибирск, Российская Федерация. Scopus Author ID 7006677629, ResearcherID F-4729-2013, https://orcid.org/0000-0002-2587-3719, *pyshnyi@niboch.nsc.ru.*

Сигов Александр Сергеевич – академик Российской академии наук, д.ф.-м.н., профессор, президент МИРЭА – Российского технологического университета, Москва, Российская Федерация. Scopus Author ID 35557510600, ResearcherID L-4103-2017, *sigov@mirea.ru.*

Тверской Владимир Аркадьевич – д.х.н., профессор, МИРЭА – Российский технологический университет, Москва, Российская Федерация. Scopus Author ID 6604012434, 29567701900, ResearcherID H-8042-2017, https://orcid.org/0000-0003-4348-8854, *tverskoy@mitht.ru.*

Тойкка Александр Матвеевич – д.х.н., профессор, Институт химии, Санкт-Петербургский государственный университет, Санкт-Петербург, Российская Федерация. Scopus Author ID 6603464176, ResearcherID A-5698-2010, http://orcid.org/0000-0002-1863-5528, *a.toikka@spbu.ru.*

Трохимчук Анджей – д.х.н., профессор, Химический факультет Вроцлавского политехнического университета, Вроцлав, Польша. Scopus Author ID 7003604847, *andrzej.trochimczuk@pwr.edu.pl.*

Цивадзе Аслан Юсупович – академик Российской академии наук, д.х.н., профессор, Институт физической химии и электрохимии им. А.Н. Фрумкина РАН, Москва, Российская Федерация. Scopus Author ID 7004245066, ResearcherID G-7422-2014, *tsiv@phyche.ac.ru.*

ТОНКИЕ
ХИМИЧЕСКИЕ
ТЕХНОЛОГИИ
Fine
Chemical
Technologies

15(2)
2020

CONTENTS

СОДЕРЖАНИЕ

Review Articles

Обзорные статьи

Theoretical Bases of Chemical Technology

Теоретические основы химической технологии

Chemistry and Technology of Organic Substances

Химия и технология органических веществ

Synthesis and Processing of Polymers and Polymeric Composites

Синтез и переработка полимеров и композитов на их основе

Chemistry and Technology of Inorganic Materials

Химия и технология неорганических материалов

Analytical Methods in Chemistry and Chemical Technology

Аналитические методы в химии и химической технологии

ISSN 2686-7575 (Online)
https://doi.org/10.32362/2410-6593-2020-15-2-7-20
UDC 535.012.2

Photoalignment and photopatterning: New liquid crystal technology for displays and photonics

Vladimir G. Chigrinov

School of Physics and Optoelectronic Engineering, Foshan University, Foshan, 528000 Peoples Republic of China
@Corresponding author, e-mail: eechigr@ust.hk

Objectives. *Since the end of the 20th century, liquid crystals have taken a leading position as a working material for the display industry. In particular, this is due to the advances in the control of surface orientation in thin layers of liquid crystals, which is necessary for setting the initial orientation of the layer structure in the absence of an electric field. The operation of most liquid crystal displays is based on electro-optical effects, arising from the changes in the initial orientation of the layers when the electric field is turned on, and the relaxation of the orientation structure under the action of surfaces after the electric field is turned off. In this regard, the high quality of surface orientation directly affects the technical characteristics of liquid crystal displays. The traditional technology of rubbing substrates, currently used in the display industry, has several disadvantages associated with the formation of a static charge on the substrates and surface contamination with microparticles. This review discusses an alternative photoalignment technology for liquid crystals on the surface, using materials sensitive to polarization of electromagnetic irradiation. Also, this review describes various applications of photosensitive azo dyes as photo-oriented materials.*

Results. *The alternative photoalignment technology, which employs materials sensitive to electromagnetic polarization, allows to create the orientation of liquid crystals on the surface without mechanical impact and to control the surface anchoring force of a liquid crystal. This provides the benefits of using the photoalignment technology in the display industry and photonics—where the use of the rubbing technology is extremely difficult. The optical image rewriting mechanism is discussed, using electronic paper with photo-inert and photoaligned surfaces as an example. Further, different ways of using the photoalignment technology in liquid crystal photonics devices that control light beams are described. In particular, we consider switches, controllers and polarization rotators, optical attenuators, switchable diffraction gratings, polarization image analyzers, liquid crystal lenses, and ferroelectric liquid crystal displays with increased operation speed.*

Conclusions. *The liquid crystal photoalignment and photopatterning technology is a promising tool for new display and photonics applications. It can be used for light polarization rotation; voltage controllable diffraction; fast switching of the liquid crystal refractive index; alignment of liquid crystals in super-thin photonic holes, curved and 3D surfaces; and many more applications.*

Keywords: *electro-optical effects in liquid crystals, liquid crystals in fiber optics, liquid crystal surface alignment, optical elements and materials for liquid crystal devices.*

For citation: Chigrinov V.G. Photoalignment and photopatterning: New liquid crystal technology for displays and photonics. *Tonk. Khim. Tekhnol. = Fine Chem. Technol.* 2020;15(2):7-20. https://doi.org/10.32362/2410-6593-2020-15-2-7-20

Фотоориентация и фотопаттернинг: Новая жидкокристаллическая технология для дисплеев и фотоники

В.Г. Чигринов

Школа физики и оптоэлектронного инжиниринга, Фошаньский Университет, Фошань, 528000 Китайская Народная Республика
@Автор для переписки, e-mail: eechigr@ust.hk

Цели. *С конца XX века жидкие кристаллы занимают лидирующее положение среди рабочих материалов для дисплейной индустрии. В частности, это стало возможным благодаря достижениям в области управления поверхностной ориентацией в тонких слоях жидких кристаллов, необходимой для задания исходной ориентационной структуры слоя в отсутствие электрического поля. Работа большинства жидкокристаллических дисплеев основана на электрооптических эффектах, возникающих за счет изменения исходной ориентации слоев при включении электрического поля и обратной релаксации ориентационной структуры под действием поверхностей после выключения электрического поля. По этой причине высокое качество поверхностной ориентации напрямую влияет на технические характеристики жидкокристаллических дисплеев. Используемая в настоящее время в дисплейной индустрии традиционная технологии натирания подложек имеет ряд недостатков, связанных с образованием на подложках статического заряда и загрязнением поверхности микрочастицами. В данном обзоре рассмотрена альтернативная технология фотоориентации жидких кристаллов на поверхности с использованием материалов, чувствительных к поляризации электромагнитного излучения. Также описаны различные приложения с использованием фоточувствительных азокрасителей в качестве фотоориентируемых материалов.*

Результаты. *Альтернативная технология фотоориентации позволяет создавать ориентацию жидких кристаллов на поверхности без механического воздействия, а также контролировать силу сцепления жидкого кристалла с поверхностью подложек. Это обеспечивает преимущество использования технологии фотоориентации в дисплейной индустрии и в фотонике, где применение технологии натирания крайне затруднительно. На примере электронной бумаги с фотоинертной и фоточувствительной поверхностями рассмотрен механизм оптической перезаписи изображения. Описаны различные варианты использования технологии фотоориентации в жидкокристаллических устройствах фотоники, обеспечивающих управление световыми пучками. В частности, рассмотрены переключатели, контроллеры и вращатели поляризации, оптические аттенюаторы, переключаемые дифракционные решетки, поляризационные анализаторы изображения, жидкокристаллические линзы, а также ферроэлектрические жидкокристаллические дисплеи с повышенным быстродействием.*

Выводы. *Технология фотоориентации и фотопаттернинга жидких кристаллов является многообещающей для новых приложений в области дисплеев и фотоники. Технология может быть использована для вращения поляризации света; дифракции, управляемой напряжением; быстрого переключения показателя преломления жидкого кристалла; ориентации жидких кристаллов в супертонких фотонных дырах, на искривленных и 3D поверхностях; и многого другого.*

Ключевые слова: *электрооптические эффекты в жидких кристаллах, жидкие кристаллы в волоконной оптике, поверхностная ориентация жидких кристаллов, оптические элементы и материалы для жидкокристаллических устройств.*

Для цитирования: Chigrinov V.G. Photoalignment and photopatterning: New liquid crystal technology for displays and photonics. *Tonk. Khim. Tekhnol. = Fine Chem. Technol.* 2020;15(2):7-20. https://doi.org/10.32362/2410-6593-2020-15-2-7-20

PHOTOALIGNMENT AND PHOTOPATTERNING TECHNOLOGY

The paper presents a comprehensive review of liquid crystal (LC) photoalignment technologies, based on the use of polarization-sensitive (photo-anisotropic) materials with anisotropic substances. Such materials demonstrate photo-induced optical anisotropy (birefringence and dichroism) upon absorbance of polarized (or non-polarized but direct) optical (ultraviolet (UV) or visible) irradiation. The mechanism of this effect can be explained as a result of photochemical mono- or bimolecular reactions, or orientation ordering, of photochemically stable molecules in solid state films. In fact, light–molecule anisotropic interactions have been in the focus of researchers for a long time, and it is still an intriguing topic. These materials have been shown to provide a high-quality alignment of molecules in an LC cell under specific light irradiation.

Over the past two decades, tremendous improvements have been made in the field of photoalignment [1–4]. Photoalignment materials are now commercially available. A number of new applications, apart from the alignment of LC displays (LCDs) and other LC devices, have been proposed and demonstrated. In particular, the use of photoalignment to activate optical elements in optical signal processing and communications is currently a major direction in display and photonics research.

Photopatterning via the advanced photoalignment technology can make a great contribution to the development of new classes of such devices. Photoalignment has obvious advantages over the usual “rubbing” treatment of glass substrates of LC display cells [5, 6]. The potential benefits of such techniques include [7, 8]:

– elimination of electrostatic charge, impurities, and mechanical damage of the surface;

– controllable pretilt angle and anchoring energy of the LC cell, high thermal and UV stability, and ionic purity;

– some advanced applications of LC in optical data processing, fiber communications, holography and many more—where the traditional “rubbing” treatment is impossible because of the high spatial resolution of the processing system, and/or the complicated geometry of the LC cell;

– capability of efficient LC alignment on flexible and curved substrates;

– manufacturing of new optical elements, e.g., patterned phase retarders and polarizers, tunable optical filters, polarization-insensitive optical lenses with electrically controlled focal length, *etc.*

In this review, we will analyze different applications of photoalignment and photopatterning based on azo dye layers. We will also discuss certain new applications of the photoalignment technology, including optically rewritable E-paper (ORW), and certain LC photonics devices, such as LC switches, polarization controllers and polarization rotators, variable optical attenuators, photonic crystal fibers filled with LC, switchable diffraction gratings, LC sensors, electrically tunable LC q-plates, LC optical elements with integrated Pancharatnam–Berry phases, fast ferroelectric LCs, and new, highly efficient photovoltaic, optoelectronic, and photonic devices.

OPTICALLY REWRITABLE LIQUID CRYSTAL ALIGNMENT

Traditionally, most approaches in LC E-paper were based on photo-degradation [9, 10] and photo-crosslinking mechanisms [11], thus the erasing and writing capabilities of photoalignment films were very limited [7, 12]. The only reversible writing and erasing process can be achieved by the photoalignment in solid films observed in sulfonic azo dye SD1 layers, explained in our pioneering work on its diffusion model [7, 12]. Optical LC alignment can be considered as rewritable, even though it encounters the complete image decay due to the exposure under direct sunlight, the image can be facilely restored or changed through a rewriting cycle via a specific exposure device. Photo-stability requirements of such optically rewriteable LC cells are practically diminished, since a display unit does not undergo reversible changes. The optically rewritable technology is a modified method of azo dye based photoalignment, which possesses a considerably high azimuthal anchoring energy, and has a unique feature of reversible in-plane reorientation via photoalignment—photosensitive molecules tend to reorient perpendicular to the polarization of incident light. Typically, an ORW LC cell is comprised of two substrates with different alignment materials (Fig. 1).

One aligning material is optically passive and keeps the alignment direction on one substrate. The other aligning material is optically active and can change its alignment direction after exposure to polarized light through the substrate. In comparison with electrically controlled plastic displays, ORW is significantly thinner, and does not require transparent conductive electrodes, thus indium tin oxide photolithography and etching on a plastic substrate are not needed. By controlling the alignment direction of the photoalignment azo dye layer, which is insoluble in the LC, the switching and continuous gray scale can be achieved. Hence, one can reach the transmission level that corresponds to the specified twist angle of LC in the ORW cell under the initial configuration of

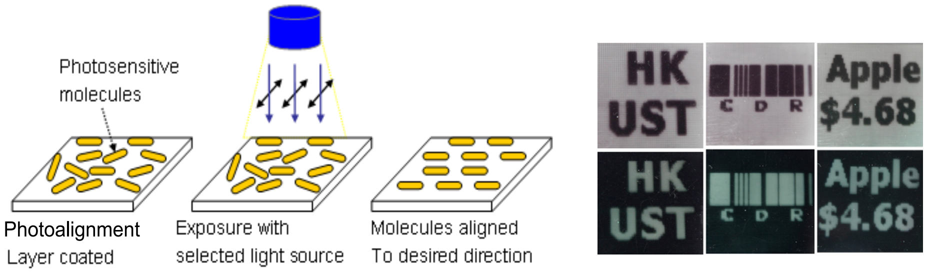

Fig. 1. Left to right: operation mechanism of ORW LC cell—an azo dye photoalignment film rotates its alignment direction in-plane, and eventually reorients perpendicular to the polarization of the writing beam; LC molecules are switched between homogeneous and twisted states controlled by the top photoalignment direction; images of ORW samples.

the polarizers. The tolerance of the cell gap variation of the ORW is very high, as no obvious change in LC transmission is observed when the cell gap changes by 50%, and the achromatic switching of all grey levels in ORW can be achieved [7, 12]. Each transmission level is stable, and the visualization of information on the ORW requires zero power consumption for a long time.

Due to the recent developments in ORW LCD and progress in LC photoalignment, it is possible to separate the E-paper display unit and the driving optoelectronic part, and a significant reduction in the complexity of the ORW E-paper structure makes both devices as cheap as paper [7, 12]. Thus, ORW E-paper is durable, economical and flexible. More research on ORW has revealed that a cheap and low power consuming, highly efficient blue light-emitting diode (LED) can be used as an alternative exposure light source, instead of expensive and highly consuming mercury lamps or lasers. The prototype of the ORW E-paper with the device structure based on a polarizer and plastic substrates was experimentally implemented [12] (Fig. 2).

Fig. 2. ORW E-paper in plastic substrates is highly resistant to mechanical pressure [12].

This prototype uses the optically rewritable alignment technology, and possesses a grey scale capability; it is truly stable, has no electrodes and does not require electric power to display the image with high contrast and wide viewing angles. Nowadays, a new function of the ORW E-paper based on the LC technology, has been developed: it can be used for displaying 3D images to enrich the performance of the single-side light printable ORW E-paper, which was originally designed for 2D images [7, 12].

The light-sensitive photoalignment materials and LC layers were developed to fulfill the following requirements [12]: optical writing/erasing time <2 s; energy of the writing beam <1 J/cm^2; more than 1000 reversible cycles; blue LED used as exposure light source. Because of the insufficient durability of contact bonding and the flexible conductor, E-paper displays have the issue of high complexity of the driving electronics. Therefore, an optically rewritable technique is highly desirable. The merits of the ORW E-paper include: no current–conducting layer; no drivers; high tolerance to layer thickness; low manufacturing cost (the price of the ORW E-paper is approximately equal to the price of two polarizers, i.e., around 20 USD/m^2). Due to the plastic substrates, the ORW E-paper, as a pioneering innovation in LCD E-paper, exhibits the outstanding flexibility characteristics, and will easily find its place on the market. Some possible applications of the ORW E-paper include light re-printable paper, labels, plastic card displays, 3D paper for security applications, and many more (Fig. 3).

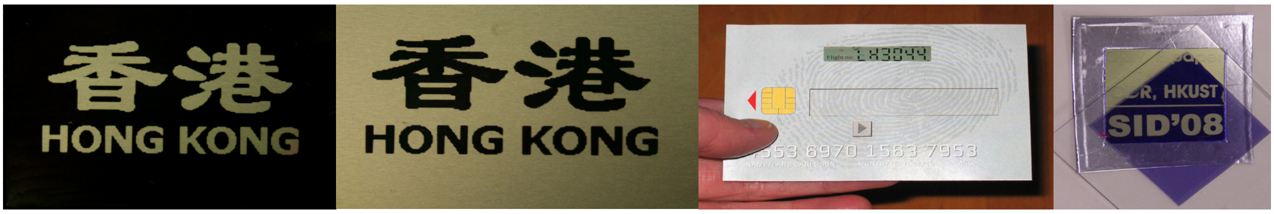

Fig. 3. Left to right: ORW E-paper for advertisements, plastic cards and security applications.

APPLICATION OF PHOTOALIGNMENT IN PHOTONIC LC DEVICES

LC photonic devices based on the photoalignment materials, including passive elements for fiber optical communication used in the fiber-to-the-home (FTTH) program, are becoming increasingly important. FTTH is a form of fiber optical delivery where the fiber extends from the central office to the subscriber's working or living space. Since the Gigabit and Terabit Ethernet can be efficiently used, configurations that bring the fiber right into a building can offer the highest speeds of voice, video, and data delivery. Fast-switching photoaligned LC cells, with microsecond and sub-microsecond switching time, have the potential to replace the currently used micro-electro-mechanical (MEM) switching devices in FTTH systems, with millisecond switching time [13].

The reliable passive optical components are still in high demand, and this trend will continue to grow for a long time. Some LC components, such as LC-based polarization controllers, phase retarders, and coaxial variable optical attenuators have already appeared on the market[1,2]. For example, a USA-based company Vescent Photonics announced that LC waveguides could be a great electro-optic technology platform for various applications, such as beam steerers, interferometers, lasers, tunable filters, *etc.*[3].

Further investigations on passive LC elements for fiber optical communication systems are needed. Silicon photonic devices (high-quality LC switches, voltage controllable filters, and variable optical attenuators) and photoalignment LC devices (e.g., polarization rotators and controllers) are to be developed. New prototypes for packaging are highly desired. New LC materials for fiber optical communications that work in the infrared (IR) range need to be tested. LC tunable sensors, including those based on complementary metal–oxide–semiconductor (CMOS) and LC lenses, are becoming very important for LC photonic applications.

LC switches

Switches for optical fiber networks are becoming more and more important. LC switches have certain advantages compared to MEM switches that are time commonly used for this purpose, for instance: (i) fast-switching time; (ii) low power consumption and controlling voltages; (iii) high reliability and durability [13]. Nevertheless, the characteristics of thermal drift and wavelength-dependent response time of LC switches should be avoided. We have investigated several LC electro-optical modes, which can be utilized for manufacturing LC switches for optical fiber networks [14].

1. LC switches can make use of the effect of total internal reflection in nematic LC [14]. The total internal reflection switch operates only in the transverse electric mode, and the most promising approach is based on the vertical aligned nematic configuration, realized by photoalignment. The switching time of 1 ms can be facilely achieved at the switching pulse amplitude of 5 V [14].

2. A bypass optical switch based on two nematic LC (NLC) cells with the switching time <200 μs was created from two temperature-stabilized photoaligned (NLC) cells [15]. Two subsequent NLC cells with mutually orthogonal optical axes compensate the relaxation of NLC birefringence when they are turned off simultaneously. Thus, the switching time of the two-cell switch can be as short as the turn-on time of the NLC cell. NLC cells can be designed for a certain fiber wavelength by adjusting the cell gap thickness.

3. An LC switch can be designed to control the light propagation in the plane of LC layers [16]. It was experimentally demonstrated that the propagation of the light beam can be noticeably changed by refraction and reflection of light at the sharp boundaries between the regions with different LC orientations induced by photoalignment. LC switches can be electrically controlled. Certain methods were proposed for optimizing the insertion loss and crosstalk of the 1 × 2 switch for practical photonic applications. It is possible to create an N × M switch and various optical processing data elements (e.g., attenuators) by using different photoalignment templates. There are many ways to optimize such types of LC devices, and employment of fast-operating ferroelectric liquid crystal layers is one of these approaches, which can provide the microsecond-level operation time.

Polarization controllers and polarization rotators, variable optical attenuators

Polarization controllers are optical elements that can convert an arbitrary input state of polarization (SOP) to a desired one, thus governing the unpredictable polarization change that stems from the polarization-dependent components of the optical fiber system. These optical elements can be made of three successively placed LC cells, which utilize the electrically controlled birefringence to modify the evolution of the SOP [17]. The switching

---

[1] Manufacturers of Innovative of Fiberoptics Components. Lightwaves2020 [Internet]. Milpitas, CA, USA: Lightwaves2020 Inc.; 2020 [Accessed January 15, 2020]. Available from: http://www.lightwaves2020.com

[2] Precision Electro-Optic and Laser Technologies. Vescent Photonics [Internet]. Golden, CO, USA: Vescent Photonics; 2020 [Accessed January 15, 2020]. Available from: https://www.vescent.com

[3] Precision Electro-Optic and Laser Technologies. Vescent Photonics [Internet]. Golden, CO, USA: Vescent Photonics; 2020 [Accessed January 15, 2020]. Available from: https://www.vescent.com

typically depends on the LC material, and is around 10 ms for the wavelength of 1.3 µm [17].

A polarization rotator is an optical element that can rotate the linear polarization of the input light to any desired polarization plane. The configuration of our proposed LC polarization rotator comprises a polarizer and two LC homogeneous cells, placed in such a way that their optical axes are at an angle of 45° to each other. One LC cell provides a voltage controllable phase change, and the other is fixed as a quarter wave plate [12]. Such optical element can rotate the light polarization state at any angle between 0° and 90°, depending on the voltage.

LC variable optical attenuators (VOA) typically have the attenuation range of 30 dB for the applied voltage of 12 V in the wavelength range between 1525 and 1575 nm [13], with the response time of approximately 10–30 ms. Some of these attenuators are dependent on the light scattering of a polymer network (PN) filled LC (PN-LC) cell. Due to the refractive index mismatching of the polymer and the LC in the absence of driving voltage, the light from the input fiber is scattered, and it can pass mostly through the PN-LC layer, because of the refractive index match of the polymer and the LC in the presence of applied voltage.

LC-filled photonic crystal fiber

Photonic crystal fiber (PCF) is a polymer or glass fiber with an array of tiny air holes running along the length of the fiber. The waveguide properties of such fibers can be controlled by filling the air holes with additional material [13, 18–21]. The refractive index of LC can be easily tuned by electric field or temperature, therefore LC is suitable for this purpose. The technique of light reconfigurable alignment of LC in glass micro-tubes and in PCF was developed (Fig. 4) [13, 18–21].

A fairly homogeneous alignment was verified by polarizing optical microscopy and Fourier-transform infrared spectroscopy (FTIR). Since the presented technique is based on properly developed photoalignment azo dye materials [22], it is a promising non-contact method of LC orientation in complicated photonic crystal structures. The order parameter *S* of LC was acquired from FTIR data, and the good quality of alignment was confirmed. Moreover, LC-filled thin porous films are to be investigated for the purpose of practical applications in electrically controlled optical attenuators and polarization-insensitive optical switches [23, 24].

Switchable diffraction gratings

Remnant high-efficiency polarization gratings are produced in nematic LC cells by exposing the azo dye molecule layers deposited on the substrate, to “interfering” beams with opposite circular polarizations [25]. The diffraction pattern is controlled by an electric signal applied across the LC cell. Polarization gratings are suitable for electrically controlled detection and discrimination of polarized components of light. All molecules of LC tend to be reoriented to a uniform homeotropic state at high voltage, and the modulation of LC alignment in the cell is terminated. Applications in LC optical switches are being discussed.

A diffraction grating was proposed by periodically defining the liquid crystal director distribution to form alternating planar aligned (PA) and twist nematic (TN) regions in an LC cell sandwiched between two crossed polarizers. Both 1D and 2D diffraction gratings demonstrate the diffraction efficiency of the total 1st order up to 12.0% and 18.2%, respectively (Fig. 5), due to their different voltage-dependent transmittance and phase modulation. When voltage was applied, four characteristic states were achieved, and the intensity of the 1st order could be suppressed by approximately 2 orders within 0.3 Vp-p at the driving voltage <2.5 Vp-p.

A Dammann grating based on hybrid photoaligned dual-frequency nematic LCs was demonstrated in 2016 [26–28]. The configuration of the Dammann grating is comprised of two substrates, one of which is coated with the homeotropic alignment, and the other substrate provides a planar, patterned alignment with mutually orthogonal easy axes in every two adjacent alignment domains. The produced polarization-independent Dammann grating could generate an optical array with equal light intensity distribution, which was characterized by the low uniformity deviation of ~0.081, diffraction efficiency of more than 58%, response time <1 ms, and low driving voltage of ~3 V/µm (Fig. 6).

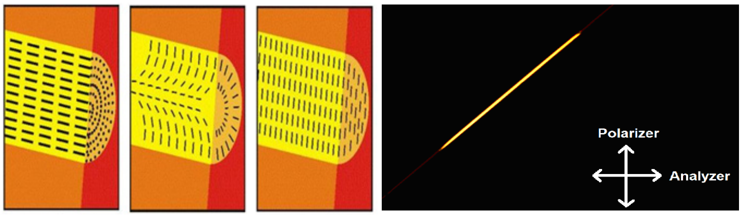

Fig. 4. Left to right: typical alignment of LC molecules in micro-capillary: planar, splay (axial, escaped radial), transverse; single-frame excerpt from a video recording of micro-capillaries filled with LC, in which two stable alignments (planar and tilted at 45º) have been obtained simultaneously [13, 21].

Optically rewritable technology for photonic devices

The ORW technology, pioneered in our research [12], can be successfully used for photonic applications. LC materials with optimized electro-optical properties provide a promising opportunity for application devices. As we know, there are no publications published by other groups on the application of optically rewritable technology for LC photonics devices. Several key devices have been developed, for example, light controllable LC plane waveguides, LC polarization-dependent elements, lenses and wave plates, LC polarization rotators and polarization controllers, light and voltage controllable diffraction gratings for optical filters, *etc*. One of such applications is shown in Fig. 7.

Using ORW photoalignment techniques, the smooth collimating refractive interface can be written by light in front of the waveguide immerged into LC (Fig. 6) [12]. The LC structure can be stabilized by the photoalignment layer without applied voltage. The *s*-polarized light can be coupled and it comes from the waveguide, going into a collimated beam inside the LC bulk for further processing, while the *p*-polarized light can be guided by matching polarization maintaining the LC waveguide [28]. We have developed a polarization-independent LC photonic device that can convert both polarization components, out-coupled from a polarization-independent waveguide to one polarization for further processing of light by a polarization-dependent LC structure for routing or other purposes. This new design

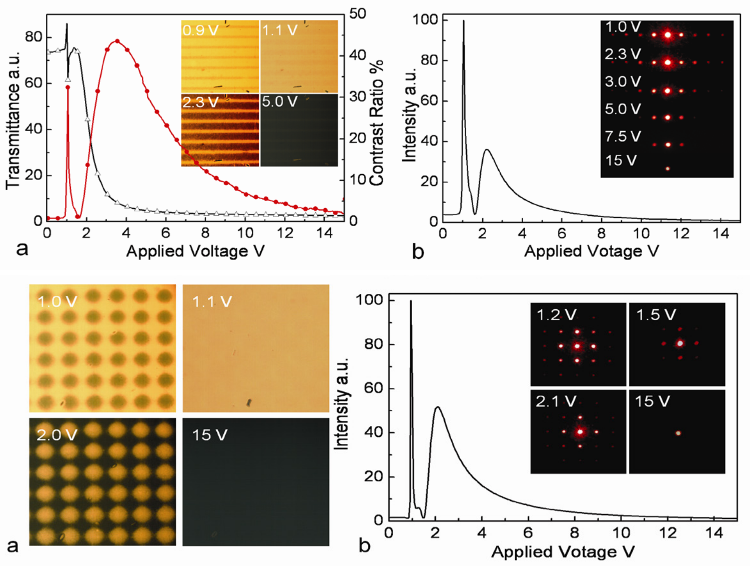

Fig. 5. Diffraction from periodically photoaligned homogeneous/twisted LC structures.
Top: LC switchable 1D diffraction grating.
a) Transmittance–voltage curve (TVC) of the cell (*black line*) and contrast ratio between voltage-dependent intensity of the 1st and 0th orders (*red line*);
b) intensity of the 1st order *vs*. driving voltage.
Bottom: LC switchable 2D diffraction grating.
a) Four states of 2D TN-PA cell under different applied voltages;
b) intensity of the 1st order *vs*. driving voltage.

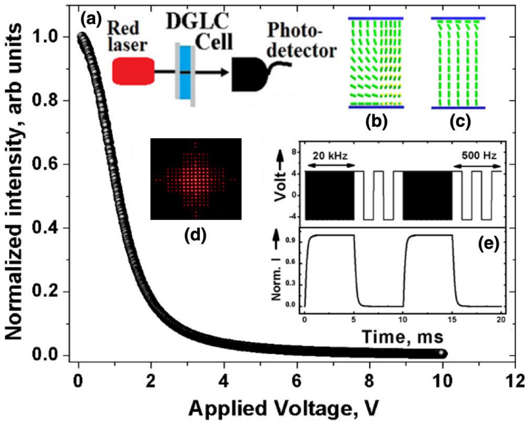

Fig. 6. Intensity *vs*. voltage curve (IVC) obtained by detection of light intensity of 1st order equal-intensity points.
(a) Experimental setup for measuring the IVC.
(b) Molecular alignment in the absence of an electric field; when a low-frequency high electric field was applied, the LC molecules were turned to the molecular state shown in (c).
(d) Diffraction pattern of the dual-frequency LC Dammann grating in the diffractive state.
(e) Electro-optical response of the Dammann grating (*bottom*) when a dual-frequency signal (*top*) was applied [26].

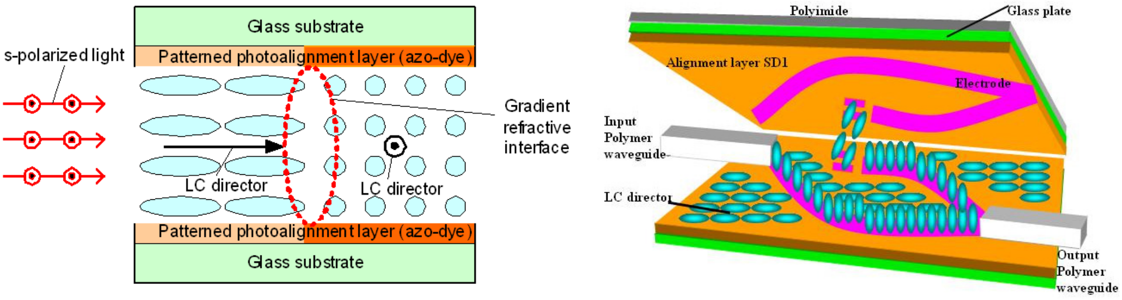

Fig. 7. Refractive interface for *s*-polarized light by nematic LC in the bulk of an LC cell [12].

consists of polarization-maintaining LC waveguides, an LC polarization-dependent passive lens, and an active half-wave plate (HWP) [12].

Based on the outstanding ORW properties of the photoalignment material, a binary-phase LC circular Dammann grating, with two mutually orthogonal light-induced alignments in neighboring alignment domains, was proposed to generate annular patterns with an equal-intensity distribution in the far field [29]. A simple mask-free real-time optical tuning of the LC circular Dammann grating was achieved by mere control of the polarization of ultraviolet exposure light, as well as the energy dose, as shown in Fig. 8. The proposed LC circular Dammann gratings with high efficiencies and desirable uniformities exhibited outstanding optical and electrical tunabilities.

Patterned micro-polarizer array with the photoalignment technology for image sensors

A thin patterned micro-polarizer array, generated by the photoalignment method for complementary metal–oxide–semiconductor (CMOS) image sensors, can be designed for the simultaneous detection of all four Stokes parameters of an output optical image (Fig. 9) [12]. A 2-μm pitch can be achieved by using UV light to rotate the four micro-polarizer elements. The experimental results have proved the concept of high-performance

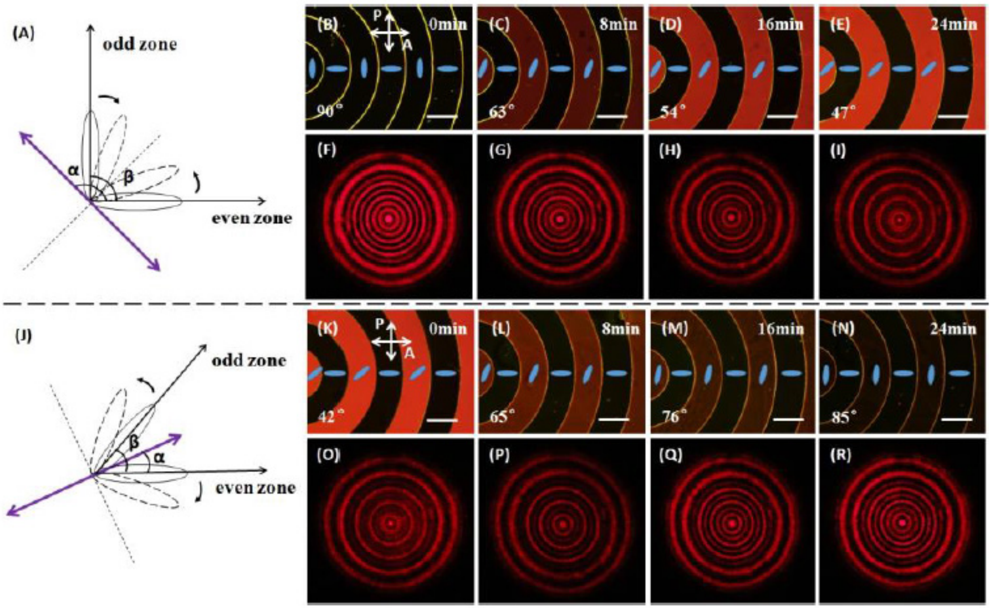

Fig. 8. Schematic diagrams of optical tuning of the β angle between the alignments in even zones and odd zones, micrographs under crossed polarizers, and corresponding diffraction patterns. Scale bars represent 200 μm. Respective optical tuning process for (A) reducing and (J) enlarging the β angle between the LC directors in even zones and odd zones by using linearly polarized UV light (*denoted by purple double-headed arrow*). (B–E) Micrographs for angle β, decreasing from 90° to 47°, with the increasing exposure time. (F–I) Corresponding diffraction patterns with even diffraction orders fading out. (K–N) Micrographs for angle β, increasing from 42° to 85°, with the increasing exposure time. (O–R) Corresponding diffraction patterns with even diffraction orders fading in [29].

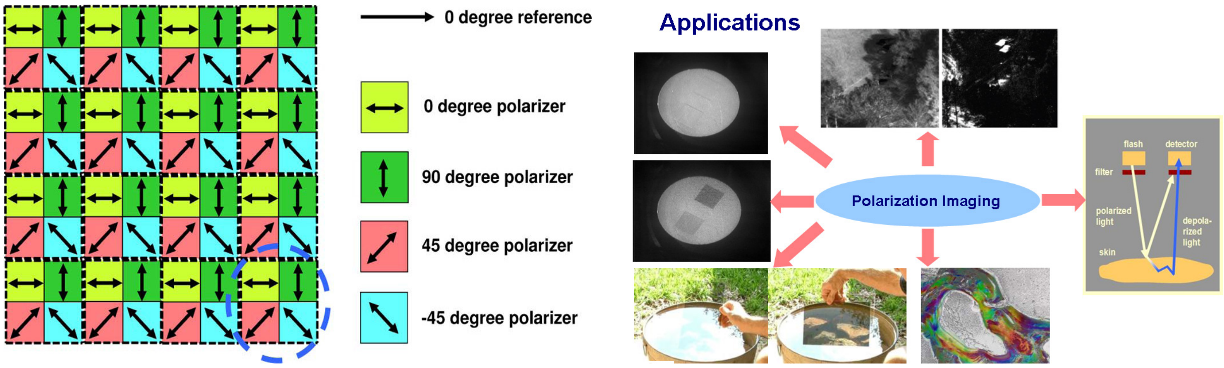

Fig. 9. Patterned micro-polarizer array for complementary metal–oxide–semiconductor (CMOS) image sensors with simultaneous detection of all four Stokes parameters of an output optical image, including “invisible objects” (constant transmission or reflection and no color) [12].

photoaligned LC micro-polarizer arrays, with a high transmittance of ~80% and extinction ratio as high as ~3200 (35 dB).

The micro-polarizer array technology with a high transmittance and extinction ratio, exploiting the “guest–host” LC mode, can be used for visible imaging polarimetry [12, 30]. This high-resolution thin micro-polarizer array, with a 5 × 5 μ pixel pitch and 0.95 μ thickness, was made by the “host” nematic LC molecules, photoaligned by the sulfonic azo dye SD1. The averaged major principal transmittance, polarization efficiency, and order parameter are 80.3%, 0.863, and 0.848, respectively, for the 400–700 nm spectral range. The proposed production technology completely removes the need for any selective etching during the manufacturing/integration process of the micro-polarizer array. It is fully CMOS-compatible, simple, and cost-effective, requiring only spin-coating followed by a single ultraviolet exposure through a “photoalignment master.” It is well adjusted for low-cost polarization imaging applications.

Electrically tunable liquid crystal q-plates

The photoalignment technology is used to create LC q-plates, tuned by electricity with various topological charges for generating optical vortex beams with definite orbital angular momentum (OAM) per photon [31–34]. Several tests have been conducted on the q-plates, including OAM tomography, showing excellent optical performance. These devices can be used in general and quantum optics. The azo dye materials showed a very high-resolution capability of LC alignment in these experiments (Fig. 10).

Electrically switchable liquid crystal Fresnel lens

A LC Fresnel lens based on alternate TN and PA regions (Fig. 11) was made by a two-step photoalignment process [35–38]. The LC Fresnel lens manifested two identical focal lengths because of the TN and PA alignment domains, giving rise to the double light intensity at the focal point, and thus offered double efficiency of the conventional Fresnel zone plates.

A method of production of a LC Fresnel lens, based on a single alignment layer with patterned planar-aligned regions, was disclosed by Xiaoqian Wang *et al.* [39]. The binary-phase LC Fresnel lens demonstrated a diffraction efficiency of 39% at the focal point. Due to the mutually orthogonal alignment in neighboring domains (Fig. 12), the lens is polarization-independent, which is indeed a merit in the viewpoint of efficient energy use.

A polarization-independent Fresnel lens, based on a patterned hybrid aligned nematic dual-frequency LC, was demonstrated [40]. The LC Fresnel lens was made by assembling two glass substrates with different alignment materials. One substrate was coated with a homeotropic alignment layer, and the other was coated with an in-plane patterned alignment layer, wherein the easy axes in every two adjacent alignment domains were mutually orthogonal, as shown in Fig. 13. Due to the outstanding electro-optical properties of the dual-frequency LC, the proposed Fresnel lens exhibited fast-switching time under alternate high frequency and low-frequency electric fields.

Liquid crystal optical elements with integrated Pancharatnam–Berry phases

A polarization-dependent diffractive bifocal vortex lens based on the Pancharatnam–Berry phase was experimentally demonstrated [41–46]. The phase expression of the Pancharatnam–Berry phase optical vortex lens (PBOVL) comprised of two terms, i.e., a Pancharatnam–Berry lens term and a q-plate term. The non-separable spin angular momentum (SAM) and OAM photon states were established when an incident beam passed through the PBOVL, as shown in Fig. 14. Different OAM states at the output of

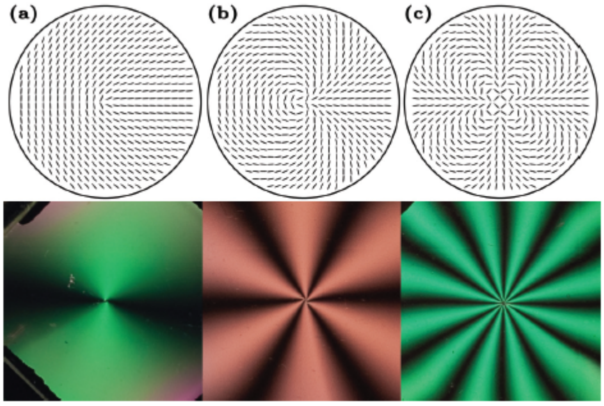

Fig. 10. LC pattern tunable q-plates made by photoalignment with high resolution [33].

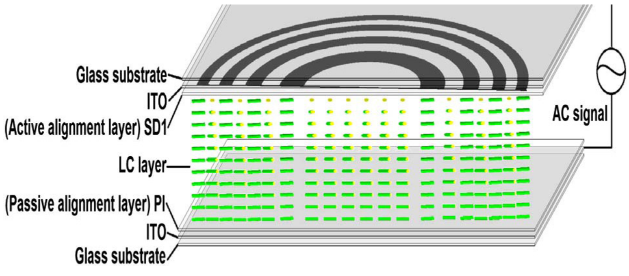

Fig. 11. Configuration of the LC Fresnel lens based on alternate TN and PA regions. One indium tin oxide coated glass substrate was coated with a polyimide layer, while the other substrate was coated with a photoalignment (SD1) layer. The white and black regions represent the TN and PA domains, respectively [35].

the PBOVL could be sorted by the bifocality of the manufactured lens. By using the underlying physics of the Pancharatnam–Berry phase polarization holography, the device was facilely, efficiently, and economically realized. The transmittance and diffraction efficiency of the device was 90% and 91%, respectively.

A LC Pancharatnam–Berry axilens was produced via a digital micro-mirror device (DMD)-based photopatterning system [47]. The polarization-dependent device behaved as an anti-axilens for RHC polarized incident light, for which an optical ring gradually expanded in the transverse direction at the output, and it acted as the axilens for LHC polarized incident light, for which an optical ring was focused with a long focal depth at the output. The modification of the size and sharpness of the diffracted hollow beam was demonstrated by encoding a positive (negative) PB lens term into the director orientation expression of a PB (anti-)axicon, as shown in Fig. 15.

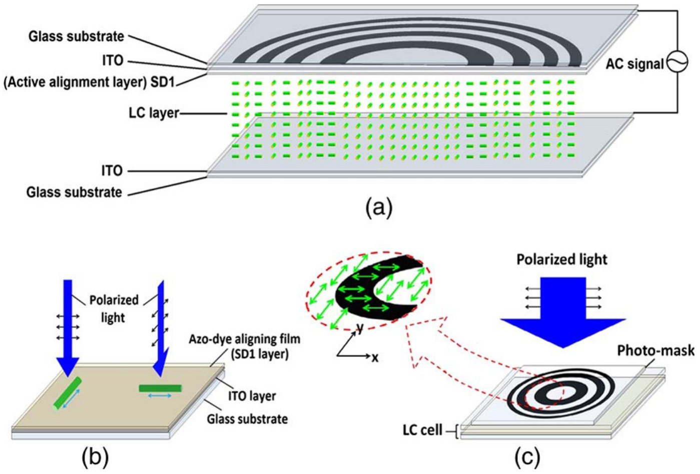

Fig. 12. (a) Configuration of liquid crystal Fresnel lens. (b) Schematic of photoalignment process. The SD1 molecules aligned perpendicular to the polarization of the incident light after sufficient exposure dosage. (c) Photopatterning process with an amplitude photomask. The magnified area in the red dashed circle represents the easy axis distribution in two different alignment domains [39].

A LC beam-splitting lens was made, with spatially separated focuses via the LC photoalignment technology [48–50]. The proposed lens with exotic optical properties was created by integrating a polarization grating with a Pancharatnam–Berry phase LC lens. The two focuses of the proposed lens, i.e., +f and –f, could be spatially separated (Fig. 16). When a linearly polarized incident light successively passed through a conventional convex glass lens with a proper focal length and the fabricated lens, the two emergent light beams exhibited convergent optical behavior and the two focuses were spatially separated. Moreover, by adjusting the distance between the proposed lens and the conventional glass lens, the focal lengths of the lens system could be modulated.

FAST FERROELECTRIC LCD

The ferroelectric liquid crystal (FLC) is the fastest LC mode, which can work with fast-response time and low driving voltages, and is highly suitable for field

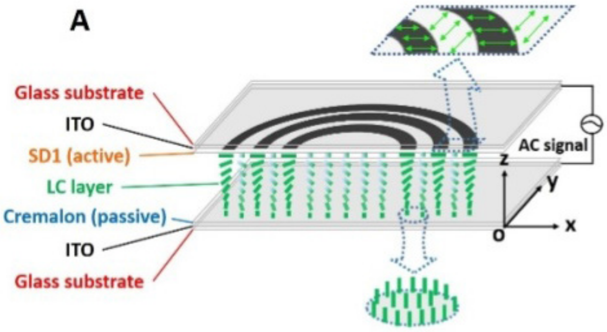

Fig. 13. Configuration of hybrid aligned nematic dual-frequency liquid crystal Fresnel lens. The SD1 molecules under black regions (even zones) and white regions (odd zones) orient in the *X-O-Z* plane and the *Y-O-Z* plane, respectively. The magnified area in the blue dashed square depicts the easy axis distribution in two different alignment domains, and the area in the blue dashed circle represents the homeotropic alignment of LC molecules [40].

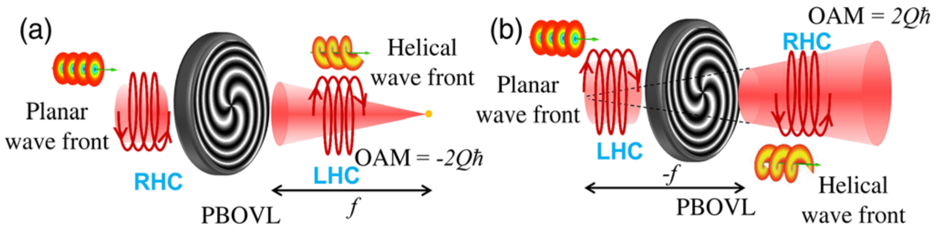

Fig. 14. Coupling of SAM-OAM states at the output of the PBOVL.
(a) For the right-handed circularly (RHC) polarized incident beam, each photon of the focusing output beam possessed an OAM of $-2Q\hbar$ and was left-handed circularly (LHC) polarized with a corresponding SAM of $+\hbar$.
(b) For the LHC polarized incident beam, each photon of the defocusing output beam possessed an OAM of $+2Q\hbar$ and was RHC polarized with a corresponding SAM of $-\hbar$ [41].

sequential applications [12, 51–55]. Fast-switching ferroelectric liquid crystal displays (FLCD) have the potential to become the new generation of the field sequential color (FSC) LCD, which is proved to have a better response time than the usual nematic LC. The best FLC parameters can be obtained on the basis of electrically suppressed helix mode [12].

A reflective display cell has been proposed—suitable for projection displays based on electrically suppressed helix ferroelectric liquid crystal (ESHFLC) with a fast-response time, which is quite suitable for the field sequential display [56, 57]. The pulse width modulation technique is used to control the residual light and provide several grey levels.

The electro-optical performance of the reflective cell at the electric field of 3 V and frequency of 5 kHz was set to achieve a high number of colors. The response time *vs*. the driving frequency, at different driving voltages, is shown in Fig. 17. Even at small driving voltages, the reflective FLC cell still maintains the contrast ratio (CR) enough for the display, CR > 10000 : 1. The response time of the reflective FLC cell at 5 kHz and the electric field of 5 V was around 14 μs. Such a fast-response time allows us to drive the FLC cell even at a very high frequency of 5 kHz (Fig. 17).

Novel photoaligned FLC devices may include FSC FLC with a high resolution, low power consumption and extended color gamut, which can be used in the screens of portable computers, mobile phones, personal digital assistants. The switchable goggles and lenses based on new FLC prototypes can be efficiently applied in the new generations of switchable 2D/3D LCD TV. The FSC FLC micro-display,

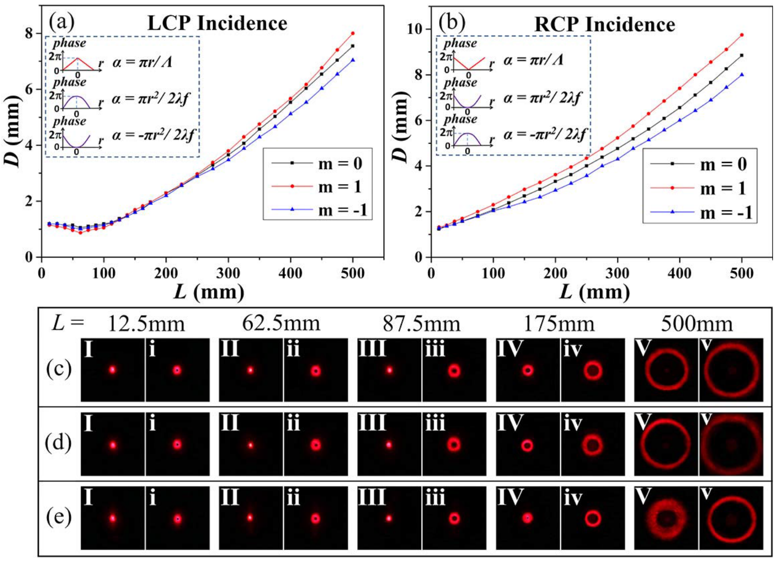

Fig. 15. Comparison of the diffraction properties of three PB axilenses (PBALs). Diagrams of the diffracted ring diameter (D) *vs*. propagation distance (L) for three PBALs under (a) the left-handed circularly polarized (LCP) and (b) the right-handed circularly polarized (RCP) incident beams. The inserts in (a) and (b) show mutually reversed phase profiles for the corresponding director distributions under different circularly polarized beams. The diffraction patterns for (c) PBAL-I (m = 0), (d) PBAL-II (m = 1), and (e) PBAL-III (m = −1) under (**I–V**) LCP and (**i–v**) RCP incident beams at representative distances [47].

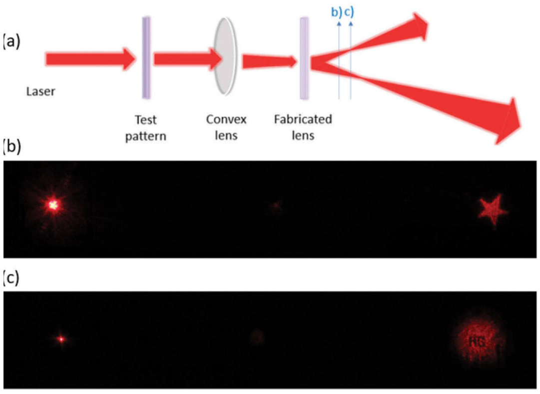

Fig. 16. (a) Schematic optical setup of the system with a screen placed at position (b) when a pentagram is used as the test pattern and (c) when the test pattern is changed to the letters “HG” [48].

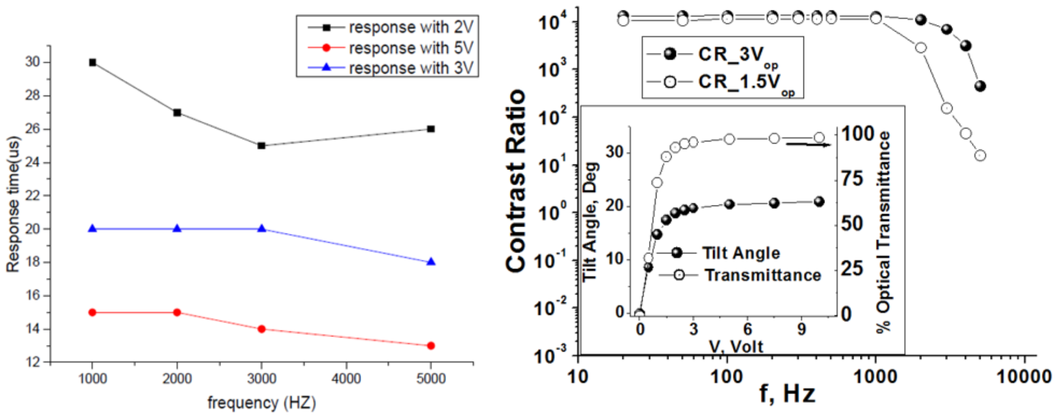

Fig. 17. Left: response time *vs*. driving frequency at different driving voltages [56]. Right: electro-optical response of the photoaligned ESHFLC [12].

which is one of the most advanced technologies for pico-projectors, can be also made on the basis of new materials and electro-optical modes in FLC [12]. The photoalignment technology enables to solve the key problems usually faced in FLCD applications, such as (i) quality of FLC alignment on sufficiently large surface area; (ii) appropriate adjustable anchoring energy and pretilt angle; (iii) low loss in the alignment layers due to their small thickness, *etc*. [12].

Future development of novel photoaligned fast FSC FLCD is aimed at: (i) further fundamental study of the new appropriate electro-optical modes used for switching; (ii) better understanding of the physical mechanisms of FLC interaction with a photoaligned surface of different photosensitive nature to produce a stable alignment with a controllable anchoring energy and pretilt angle over a sufficiently large surface area; (iii) development of new fast-response FLC materials with fast switching and a sufficient number of switchable grey levels (V-shape switching); (iv) implementation of the working prototypes of novel FSC FLC displays; (v) investigation of operation modes to allow the use of efficient addressing of FLCD.

CONCLUSIONS

The LC photoalignment and photopatterning technology for new display and photonic applications is a prominent research area. Such elements have started to appear in displays and on the photonics market. The electro-optical modes are used for light polarization rotation, voltage controllable diffraction, and fast switching of the LC refractive index. The photoalignment technique makes it possible to develop new LC fiber components. Photo-aligning materials are used to align LC in super-thin photonic holes, curved and 3D surfaces, and as cladding layers in micro-ring silicon-based resonators. The prototypes of new efficient LC photonic devices, such as optically rewritable LC E-paper, waveguides, and voltage controllable diffraction gratings are envisaged. The polarization controllers, polarization rotators, VOA, and other passive LC optical elements for fiber communication networks are in development.

We hope that this review can be interesting not only to a wide range of engineers, scientists, and managers, who are willing to develop new LC displays or other LC photonic devices and optical components, but also to researchers in other practically important fields, where the formation of new highly-ordered structures of organic molecules is desirable.

Автор заявляет об отсутствии конфликта интересов.

The author declares no conflicts of interest.

REFERENCES

1. Ichimura K. Photoalignment of Liquid-Crystal Systems. *Chem. Rev.* 2000;100(5):1847-1873.
https://doi.org/10.1021/cr980079e

2. Schadt M., Seiberle H., Schuster A. Optical patterning of multidomain liquid-crystal displays with wide viewing angles. *Nature.* 1996;381(6579):212-215.
https://doi.org/10.1038/381212a0

3. O’Neill M., Kelly S.M. Photoinduced surface alignment for liquid crystal display. *J. Phys. D: Appl. Phys.* 2000;33(10):R67-R84.
https://doi.org/10.1088/0022-3727/33/10/201

4. Gibbons W.M., Shannon P.J., Sun S.-T., Swetlin B.J. Surface-mediated alignment of nematic liquid crystals with polarized laser light. *Nature.* 1991:351(6321):49-50.
https://doi.org/10.1038/351049a0

5. Chatelain P. Sur l’orientation des cristaux liquides par les surfaces frottées. *Bulletin de Minéralogie.* 1943;66(1-6):105-130 (in French).
https://doi.org/10.3406/bulmi.1943.4528

6. Janning J.L. Thin film surface orientation for liquid crystals. *Appl. Phys. Lett.* 1972;21(4):173-174.
https://doi.org/10.1063/1.1654331

7. Chigrinov V.G., Kozenkov V.M., Kwok H.S. *Photoalignment of Liquid Crystalline Materials: Physics and Applications.* Wiley; 2008. 248 p.

8. Yaroshchuk O., Reznikov Y. Photoalignment of liquid crystals: Basics and current trends. *J. Mater. Chem.* 2012;22(2):286-300.
https://doi.org/10.1039/C1JM13485J

9. Nishikawa M., Taheri B., West J.L. Mechanism of unidirectional liquid-crystal alignment on polyimides with linearly polarized ultraviolet light exposure. *Appl. Phys. Lett.* 1998;72:2403-2405.
https://doi.org/10.1063/1.121390

10. Gong S., Kanicki J., Ma L., Zhong J. Ultraviolet-light induced liquid-crystal alignment on polyimide films. *Jpn. J. Appl. Phys.* 1999;38:5996-6004.
https://doi.org/10.1143/JJAP.38.5996

11. Dyadyusha A.G., Marusii T.Ya., Reznikov Yu.A., Khizhnyak A.I., Reshetnyak V.Yu. Orientational effect due to a change in the anisotropy of the interaction between a liquid crystal and a bounding surface. *JETP Lett.* 1992;56:17-21.

12. Chigrinov V.G., Kwok H.S. *Photoalignment of liquid crystals: applications to fast response ferroelectric liquid crystals and rewritable photonic devices.* In: *Progress in Liquid Crystal Science and Technology: in Honor of Shunsuke Kobayashi’s 80th Birthday.* Singapore: World Scientific; 2013. p. 199-226.
https://doi.org/10.1142/9789814417600_0009

13. Chigrinov V.G. *Liquid Crystal Photonics.* Nova Science Publishers; 2014. 204 p. ISBN: 978-1-62948-315-3

14. Xu P., Chigrinov V., Kwok H.S. Optical analysis of a liquid-crystal switch system based on total internal reflection. *J. Opt. Soc. Am. A.* 2008;25(4):866-873. https://doi.org/10.1364/JOSAA.25.000866

15. Muravsky A., Chigrinov V. *Optical switch based on nematic liquid crystals.* IDW'05 Digest; 2005. 223 p.

16. Maksimochkin A.G., Pasechnik S.V., Tsvetkov V.A., Yakovlev D.A., Maksimochkin G.I., Chigrinov V.G. Electrically controlled switching of light beams in the plane of liquid crystal layer. *Opt. Commun.* 2007;270:273-279. https://doi.org/10.1016/j.optcom.2006.09.014

17. Zhuang Z., Suh S.W., Patel J.S. Polarization controller using nematic liquid crystals. *Opt. Lett.* 1999;24:694. https://doi.org/10.1364/OL.24.000694

18. Ertman S., Srivastava A.K., Chigrinov V.G., Chychłowski M.S., Woliński T.R. Patterned alignment of liquid crystal molecules in silica micro-capillaries. *Liq. Cryst.* 2013;40(1):1-6. https://doi.org/10.1080/02678292.2012.725869

19. Du F., Lu Y.-Q., Wu S.-T. Electrically tunable liquid-crystal photonic crystal fiber. *Appl. Phys. Lett.* 2004;85(12):2181-2183. https://doi.org/10.1063/1.1796533

20. Haakestad M.W., Alkeskjold T.T., Nielsen M.D., Scolari L., Riishede J., Engan H.E., Bjarklev A. Electrically tunable photonic bandgap guidance in a liquid-crystal-filled photonic crystal fiber. *IEEE Photonic. Tech. L* 2005;17(4):819-821. https://doi.org/10.1109/LPT.2004.842793

21. Scolari L., Alkeskjold T.T., Riishede J., Bjarklev A., Hermann D.S., Anawati, Nielsen M.D., Bassi P. Continuously tunable devices based on electrical control of dual-frequency liquid crystal filled photonic bandgap fibers. *Opt. Express.* 2005;13(19):7483-7496. https://doi.org/10.1364/OPEX.13.007483

22. Valyukh I., Arwin H., Chigrinov V., Valyukh S. UV-induced in-plane anisotropy in layers of mixture of the azo-dyes SD-1/SDA-2 characterized by spectroscopic ellipsometry. *Phys. Status Solidi C.* 2008;5(5):1274-1277. https://doi.org/10.1002/pssc.200777881

23. Cimrova V., Neher D., Hilderbrandt R., Hegelich M., von der Lieth A., Marowsky G., Hagen R., Kostromine S., Bieringer T. Comparison of the birefringence in an azobenzene-side-chain copolymer induced by pulsed and continuous-wave radiation. *Appl. Phys. Lett.* 2002;81:1228. https://doi.org/10.1063/1.1499766

24. Kiselev A.D., Pasechnik S.V., Shmeliova D.V., Chopik A.P., Semerenko D.A., Dubtsov A.V. Waveguide Propagation of Light in Polymer Porous Films Filled with Nematic Liquid Crystals. *Advances in Condensed Matter Physics.* 2019;1539865. https://doi.org/10.1155/2019/1539865

25. Presnyakov V., Asatryan K., Galstian T., Chigrinov V. Optical polarization grating induced liquid crystal micro-structure using azo-dye command layer. *Opt. Express.* 2006;14:10558-10564. https://doi.org/10.1364/OE.14.010558

26. Wang X.Q., Srivastava A.K., Fan F., Zheng Z.G., Shen D., Chigrinov V.G., Kwok H.S. Electrically/optically tunable photo-aligned hybrid nematic liquid crystal Dammann grating. *Opt. Lett.* 2016;41:5668-5671. https://doi.org/10.1364/OL.41.005668

27. Luo D., Dai H.T., Sun X.W. Polarization tunable circular Dammann grating generated from azo-dye doped nematic liquid crystals. *Proceedings of SPIE.* 2011;7934:79340H. https://doi.org/10.1117/12.874139

28. Luo D., Sun X.W., Dai H.T., Demir H.V. Polarization-dependent circular Dammann grating made of azo-dye-doped liquid crystals. *Appl. Opt.* 2011;50(15):2316-2321. https://doi.org/10.1364/AO.50.002316

29. Wang X., Wu S., Yang W., Yuan C., Li X., Liu Z., Tseng M., Chigrinov V.G., Kwok H., Shen D., Zheng Z. Light-Driven Liquid Crystal Circular Dammann Grating Fabricated by a Micro-Patterned Liquid Crystal Polymer Phase Mask. *Polymers.* 2017;9:380. https://doi.org/10.3390/polym9080380

30. Zhao X., Bermak A., Boussaid F. A low cost CMOS polarimetric ophthalmoscope scheme for cerebral malaria diagnostics. *IFIP Advances in Information and Communication Technology.* 2012;379 AICT:1-9. https://doi.org/10.1007/978-3-642-32770-4_1

31. Slussarenko S., Murauski A., Du T., Chigrinov V., Marrucci L., Santamato E. Tunable liquid crystal q-plates with arbitrary topological charge. *Opt. Express.* 2011;19(5):4085-4090. https://doi.org/10.1364/OE.19.004085

32. Wei B.-Y., Liu S., Chen P., Qi S.-X., Zhang Y., Hu W., Lu Y.-Q., Zhao J.-L. Vortex Airy beams directly generated via liquid crystal q-Airy-plates. *Appl. Phys. Lett.* 2018;112(12):121101. https://doi.org/10.1063/1.5019813

33. Aizawa M., Ota M., Hisano K., Akamatsu N., Sasaki T., Barrett C.J., Shishido A. Direct fabrication of a q-plate array by scanning wave photopolymerization. *J. Opt. Soc. Am. B: Optical Physics.* 2019;36(5):D47-D51. https://doi.org/10.1364/JOSAB.36.000D47

34. Huang Y.-H., Li M.-S., Fuh A.Y.-G. The application of liquid crystal q-plates for modulating Gaussian Beam. *Proceedings of the International Display Workshops.* 2013;1:196-197.

35. Wang X., Srivastava A., Chigrinov V., Kwok H. Switchable Fresnel lens based on micropatterned alignment. *Opt. Lett.* 2013;38:1775-1777. https://doi.org/10.1364/OL.38.001775

36. Lin L.-C., Jau H.-C., Lin T.-H., Fuh A.Y.-G. Highly efficient and polarization-independent Fresnel lens based on dye-doped liquid crystal. *Opt. Express.* 2007;15(6):2900-2906. https://doi.org/10.1364/OE.15.002900

37. Lin L.-C., Cheng K.-T., Liu C.-K., Ting C.-L., Jau H.-C., Lin T.-H., Fuh A.Y.-G. Fresnel lenses based on dye-doped liquid crystals. *Proceedings of SPIE.* 2008;6911:69110I. https://doi.org/10.1117/12.762550

38. Huang Y.-H., Huang S.-W., Chu S.-C., Fuh Y.-G. High-efficiency Fresnel lens fabricated by axially symmetric photoalignment method. *Appl. Optics.* 2012;51(32):7739-7744. https://doi.org/10.1364/AO.51.007739

39. Wang X.Q., Fan F., Du T., Tam A.M., Ma Y., Srivastava A.K., Chigrinov V.G., Kwok H.S. Liquid crystal Fresnel zone lens based on single-side-patterned photoalignment layer. *Appl. Opt.* 2014;53:2026-2029. https://doi.org/10.1364/AO.53.002026

40. Wang X.Q., Yang W.Q., Liu Z., Duan W., Hu W., Zheng Z.G., Shen D., Chigrinov V.G., Kwok H.S. Switchable Fresnel lens based on hybrid photo-aligned dual frequency nematic liquid crystal. *Opt. Mater. Express.* 2017;7:8-15. https://doi.org/10.1364/OME.7.000008

41. Tam A.M.W., Fan F., Du T., Hu W., Zhang W., Zhao C., Wang X., Ching K.L., Li G., Luo H., Chigrinov V.G., Wen S., Kwok H.S. Bifocal Optical-Vortex Lens with Sorting of the Generated Nonseparable Spin-Orbital Angular-Momentum States. *Phys. Rev. Applied.* 2017;7:034010. https://doi.org/10.1103/PhysRevApplied.7.034010

42. Duan W., Chen P., Ge S.-J., Wei B.-Y., Hu W., Lu Y. Helicity-dependent forked vortex lens based on photo-patterned liquid crystals. *Opt. Express.* 2017;25(13):14059-14064.
https://doi.org/10.1364/OE.25.014059

43. He Z., Lee Y.-H., Chen R., Chanda D., Wu S.-T. Switchable Pancharatnam-Berry microlens array with nano-imprinted liquid crystal alignment. *Opt. Lett.* 2018;43(20):5062-5065.
https://doi.org/10.1364/OL.43.005062

44. Zhan T., Xiong J., Lee Y.-H., Wu S.-T. Polarization-independent Pancharatnam-Berry phase lens system. *Opt. Express.* 2018;26(26):35026-35033.
https://doi.org/10.1364/OE.26.035026

45. Duan W., Chen P., Ge S.-J., Liang X., Hu W. A fast-response and helicity-dependent lens enabled by micro-patterned dual-frequency liquid crystals. *Crystals.* 2019;9(2):111.
https://doi.org/10.3390/cryst9020111

46. Li S., Liu Y., Li Y., Liu S., Chen S., Su Y. Fast-response Pancharatnam-Berry phase optical elements based on polymer-stabilized liquid crystal. *Opt. Express.* 2019;27(16):22522-22531.
https://doi.org/10.1364/OE.27.022522

47. Ren J., Wang W., Yang W., Yuan C., Zhou K., Li X., Tam A.M., Meng C., Sun J., Chigrinov V., Kwok H., Wang X., Zheng Z., Shen D. Micro-patterned liquid crystal Pancharatnam–Berry axilens. *Chin. Opt. Lett.* 2018;16:062301.
https://www.osapublishing.org/col/abstract.cfm?uri=col-16-6-062301

48. Zhou Y., Yin Y., Yuan Y., Lin T., Huang H., Yao L., Wang X., Tam A.M.W., Fan F., Wen S. Liquid crystal Pancharatnam–Berry phase lens with spatially separated focuses. *Liq. Cryst.* 2019;46(7):995-1000.
https://doi.org/10.1080/02678292.2018.1550820

49. Ke Y., Liu Y., Zhou J., Liu Y., Luo H., Wen S. Optical integration of Pancharatnam-Berry phase lens and dynamical phase lens. *Appl. Phys. Lett.* 2016;108(10):101102.
https://doi.org/10.1063/1.4943403

50. Chen H.-T., Taylor A.J., Yu N. A review of metasurfaces: Physics and applications. *Rep. Prog. Phys.* 2016;79(7):076401.
https://doi.org/10.1088/0034-4885/79/7/076401

51. Lagerwall S.T. *Ferroelectric and Antiferroelectric Liquid Crystals.* Weinheim: Wiley-VCH; 1999.

52. Favalora G.E., Napoli J., Hall D.M., Dorval R.K., Giovinco M.G., Richmond M.J., Chun W.S. 100 million-voxel volumetric display. *Proceedings of SPIE.* 2002;4712:300-312.
https://doi.org/10.1117/12.480930

53. Nagaraj M., Panarin Y.P., Manna U., Vij J.K., Keith C., Tschierske C. Electric field induced biaxiality and the electro-optic effect in a bent-core nematic liquid crystal. *Appl. Phys. Lett.* 2010;96(1):011106.
https://doi.org/10.1063/1.3280817

54. Kim D.-W., Yu C.-J., Lim Y.-W., Na J.-H., Lee S.-D. Mechanical stability of a flexible ferroelectric liquid crystal display with a periodic array of columnar spacers. *Appl. Phys. Lett.* 2005;87(5):051917.
https://doi.org/10.1063/1.2007856

55. Kumar A., Prakash J., Deshmukh A.D., Haranath D., Silotia P., Biradar A.M. Enhancing the photoluminescence of ferroelectric liquid crystal by doping with ZnS quantum dots. *Appl. Phys. Lett.* 2012;100(13):134101.
https://doi.org/10.1063/1.3698120

56. Shi L., Ma Y., Srivastava A., Chigrinov V., Kwok H.S. *Field Sequential Color Displays based on Reflective Electrically Suppressed Helix Ferroelectric Liquid Crystal.* SID – 2015 International Symposium. 2015; San Jose, CA, USA.

57. Srivastava A.K., Shi L., Kwok H.S. Modern display applications based on ESH ferroelectric liquid crystals. *Proceedings of the International Display Workshops.* 2018;1:62-65.

About the author:

Vladimir G. Chigrinov, Dr. of Sci. (Physics), Professor, Honorary Member of the International Display Society, School of Physics and Optoelectronic Engineering, Foshan University (18, Jiang-Wan-Yi-Lu, Chancheng, Foshan, Guangdong, 528000, P.R. China). E-mail: eechigr@ust.hk. Scopus Author ID: 35601969500, ResearcherID: I-7648-2013, https://orcid.org/0000-0003-0593-2555

Об авторе:

Чигринов Владимир Григорьевич, доктор физико-математических наук, профессор, почетный член Международного дисплейного общества, Школа физики и оптоэлектронного инжиниринга, Фошаньский университет (18, Jiang-Wan-Yi-Lu, Chancheng, Foshan, Guangdong, 528000, P.R. China). E-mail: eechigr@ust.hk. Scopus Author ID: 35601969500, ResearcherID: I-7648-2013, https://orcid.org/0000-0003-0593-2555

Submitted: January 23, 2020; Reviewed: February 28, 2020; Accepted: April 10, 2020.

The text was submitted by the author in English.
Edited for English language and spelling by Enago, an editing brand of Crimson Interactive Inc.

THEORETICAL BASES OF CHEMICAL TECHNOLOGY

ТЕОРЕТИЧЕСКИЕ ОСНОВЫ ХИМИЧЕСКОЙ ТЕХНОЛОГИИ

ISSN 2686-7575 (Online)

https://doi.org/10.32362/2410-6593-2020-15-2-21-29

UDC 66.092.57: (546.263.3-31+546.264-31)

Nickel catalysts for nitrogen–hydrogen mixture purification from carbon oxides

Evgeniy Z. Golosman@, Vasiliy N. Efremov, Anna V. Kashinskaya

NIAP-KATALIZATOR, Novomoskovsk, Tula oblast, 301660 Russia
@Corresponding author, e-mail: evgolosman@yandex.ru

Objectives. *This study is devoted to developing new-generation nickel (Ni) catalysts for the purification of a nitrogen–hydrogen mixture from carbon oxides, which should encompass the best qualities of the NIAP-07-series solid catalysts.*

Methods. *This study used derivatographic and radiographic methods; temperature-programmed recovery, decomposition, and joint temperature-programmed decomposition and recovery; and low-temperature nitrogen adsorption (specific surface determination). The mechanical strength of catalysts was determined using an MP-2C device by crushing granules with an applied load on the end face. The chemical composition and catalytic activity were determined by the methods of TU 2178-003-00209510 Technical Conditions.*

Results. *Many studies regarding Ni–aluminum (Al)–calcium (Ca) methanation catalyst at all stages of its preparation have been conducted. It is demonstrated that Ni hydrocarboxyaluminate, a precursor of the active component of the catalyst, is formed when Ni hydroxocarbonate is mixed with active alumina in the presence of an aqueous solution of ammonia, and its chemical formula is established. Moreover, it was found that the mechanical strength of the catalyst is determined by the amount of industrial Ca aluminate added to the Ni–Al composition. The compositions of catalysts with different contents of the active component have been optimized.*

Conclusions. *The developed catalyst has a low activation temperature and high catalytic activity, thermal stability, and mechanical strength and is resistant to organic and alkaline carbon dioxide absorbers. The catalyst can be produced in the form of a ring, cylindrical tablets, and extrudates of various geometric sizes. The methanation unit at Stavrolen (Budennovsk, Stavropol krai, Russia) has begun commercially operating the catalyst.*

Keywords: *hydrogenation, carbon oxides, nickel catalyst, phase composition, mechanical strength, activation, catalytic activity, industrial use.*

For citation: Golosman E.Z., Efremov V.N., Kashinskaya A.V. Nickel catalysts for nitrogen–hydrogen mixture purification from carbon oxides. *Tonk. Khim. Tekhnol. = Fine Chem. Technol.* 2020;15(2):21-29. https://doi.org/10.32362/2410-6593-2020-15-2-21-29

Никелевые катализаторы для процесса очистки азотоводородной смеси от оксидов углерода

Е.З. Голосман[@], В.Н. Ефремов, А.В. Кашинская

ООО «НИАП-КАТАЛИЗАТОР», Новомосковск, Тульская область, 301660 Россия
[@]Автор для переписки, e-mail: evgolosman@yandex.ru

Цели. *Настоящее исследование посвящено разработке никелевого катализатора нового поколения для очистки азотоводородной смеси от оксидов углерода, который должен аккумулировать лучшие качества контактов серии НИАП-07.*
Методы. *Использованы дериватографический и рентгенографический методы анализа; методы температурно-программированного восстановления, разложения и совместного температурно-программированного разложения и восстановления; низкотемпературная адсорбция азота (определение удельной поверхности). Механическая прочность определялась на приборе МП-2С раздавливанием гранул с приложением нагрузки на торец. Химический состав и каталитическую активность определяли по методикам ТУ 2178-003-00209510.*
Результаты. *Выполнены исследования никельалюмокальциевого катализатора метанирования на всех стадиях его приготовления. Показано, что при смешении гидроксокарбоната никеля с активным оксидом алюминия в присутствии водного раствора аммиака происходит образование гидросокарбоалюмината никеля, являющегося предшественником активного компонента катализатора, и установлена его химическая формула. Обнаружено, что величина механической прочности катализатора определяется количеством технического алюмината кальция, добавляемого в Ni–Al композицию. Оптимизированы составы катализатора, имеющего различное содержание активного компонента.*
Выводы. *Разработанный катализатор имеет пониженную температуру активации, высокую каталитическую активность и термостабильность, большую механическую прочность, устойчивость к воздействию органических и щелочных абсорбентов-поглотителей углекислого газа. Катализатор может изготавливаться в форме кольца, цилиндрических таблеток и экструдатов с различными геометрическими размерами.*
Начата промышленная эксплуатация катализатора в установке метанирования ООО «Ставролен», г. Буденновск, Ставропольский край, Россия.

Ключевые слова: *гидрирование, оксиды углерода, никелевый катализатор, фазовый состав, механическая прочность, активация, каталитическая активность, промышленное внедрение.*

Для цитирования: Голосман Е.З., Ефремов В.Н., Кашинская А.В. Никелевые катализаторы для процесса очистки азотоводородной смеси от оксидов углерода. *Тонкие химические технологии.* 2020;15(2):21-29. https://doi.org/10.32362/2410-6593-2020-15-2-21-29

INTRODUCTION

The fine purification of a nitrogen–hydrogen mixture (synthesis gas) from carbon oxides is used in the large-scale production of synthetic ammonia. The quality of methanation catalysts determines the performance as well as stability of the operation and technical and economic indicators of such industries. Methanation catalysts are produced by a number of foreign companies. In the Russian Federation, methanation catalysts are produced in Novomoskovsk by the catalyst production of *NIAP-CATALIZATOR*.

Methanation catalysts in the form of metal oxides contain nickel (Ni) as the active component, have a high reduction temperature, are manufactured using various carriers, and differ in geometric shape. The NKM-series catalysts manufactured in the Russian Federation (NIAP-07 and TO-2M)[1] are widely used in the chemical and petrochemical industries, among others.

---

[1] *Tekhnicheskie usloviya TU 2178-003-00209510-2006. Katalizatory metanirovaniya* (Technical Conditions TU 2178-003-00209510-2006. Methanation catalysts) (in Russ.).

An increase in the established capacity of the ammonia synthesis unit from 1360 to 1700 t/day led to a decrease in the temperature of the synthesis gas at the inlet of the methanator to 270–290℃, indicating that methanation catalysts must be improved. Such improvement should be implemented through 1) the development of technology that would make it possible to obtain the active component, Ni, in a highly dispersed state; 2) the creation of technology that would enable the preparation of catalysts with a low activation temperature (220–230℃) that can be operated at high space velocities; and 3) the manufacturing of a catalyst that has various geometric shapes (cylindrical tablets, rings, and extrudates with or without an aperture).

This study is devoted to developing new-generation catalyst that encompasses the best qualities of the NIAP-07-series solid catalysts.

The object of the study is a Ni–Al (aluminum)–calcium (Ca) catalyst. Ni hydroxocarbonate (NHC), active alumina, industrial Ca aluminate (talyum), and aqueous ammonia were used as raw materials for its preparation.

MATERIALS AND METHODS

To determine the phase composition and dispersion of crystallites, X-ray diffraction studies were performed using a DRON-3 diffractometer (CuK_α–radiation with a graphite monochromator on a reflected beam). To identify the phases, we used the database of the Joint Committee on Powder Diffraction Standards. Complex thermal studies were carried out using an OD-103 optical derivatograph (linear temperature rise rate of 5℃/min.). The total specific surface area was determined by low-temperature nitrogen adsorption. Total porosity was calculated from true and bulk density data. Bulk density was calculated by the formula

$$\rho = (m_1 - m_2)/V,$$

where m_1 is the mass of the measuring cylinder with an absorber, kg; m_2 is the mass of the graduated cylinder without an absorber, kg; and V is the volume of the cylinder, dm^3.

The mechanical strength was determined using an MP-2C device by crushing granules with an applied load on the end face. The chemical composition and catalytic activity during the process of methanation in a pilot plant at a pressure of 3.0 MPa and a space velocity of $W = 4000\ h^{-1}$ were determined by the methods described in TU 2178-003-00209510. The decomposition and activation processes were studied using temperature-programmed decomposition (TPD) and reduction (TPR) on a thermochromatographic installation.

RESULTS AND DISCUSSION

Catalyst development was based on many years of experience operating methanation catalysts [1–9] (in particular, those in the NIAP-07 [NKM] series) as well as on the results of studies regarding mixed-type catalysts [10–18].

The basis of the new-generation methanation catalyst NIAP-07-07 (NKM-7) is a Ni–Al composition, which is a precursor responsible for catalytic properties. It was found that the most profound interaction between nickel hydroxocarbonate (NHC) and active alumina (γ-Al_2O_3) occurs when the Al_2O_3/NiO ratio is no more than 1.2.

To identify the differences in the synthesis of the Ni–Al composition, X-ray studies of samples 1–4 were carried out, in which the concentration of aqueous ammonia used in the preparation (Table 1) and the non-processed mechanical mixture of NHC+γ-Al_2O_3 differed. To determine the interplanar spacing for all the studied samples, a line of 100% intensity corresponding to the reflection from a plane with a Miller index of 003 for Ni hydroxocarboaluminate (NHCA) was recorded at a speed of 0.25°/min in the angle range $2\theta = 8–14°$.

Table 1. The effect of the concentration of an aqueous solution of ammonia on the interplanar spacing of the Ni-containing phase

Sample №	C_{NH4OH}, %	*d*, Å
Mechanical mixture NHC+γ-Al_2O_3	Unprocessed	5.2
Talcovite ($Ni_6Al_2(OH)_{16}CO_3{\cdot}4H_2O$)	–	7.54
1	0	7.6
2	5.0	7.8
3	15.0	7.8
4	25.0	7.8

According to the data given in card 15-0087 (PCPDF-WIN 1999 database), the Ni-containing phase $Ni_6Al_2(OH)_{16}CO_3 \cdot 4H_2O$ (*talcovite*) has an interplanar spacing of d = 7.54 Å and a hexagonal lattice.

Using data from the X-ray diffraction method of analysis, the interplanar spacing of the formed Ni-containing phase was determined (Table 1).

An X-ray analysis revealed that NHC was absent from the phase composition, and a new Ni-containing compound was recorded. It is worth noting that the use of ammonia during the preparation of an aqueous solution causes the interplanar spacing of the new Ni-containing phase to increase to 7.8 Å, which attests to the fact that, during the preparation at the mixing stage, a chemical interaction occurs between NHC and alumina with the addition of the $[Al(OH)_4]^{-1}$ anion into the NHC structure due to its anion exchange to CO_3^{-2} [19].

An analysis of the obtained data shows that, regardless of the concentration of an aqueous solution of ammonia, the interplanar spacing of this compound remains constant and equal to 7.8 Å (Table 1), allowing us to assume that the dispersion of this Ni-containing phase in the prepared samples will also remain constant. X-ray diffraction studies of activated samples 1–4 showed that the dispersion of Ni in said samples does not change and remains at 60–70 Å. Since the resulting Ni-containing compound is a precursor of the NIAP-07-07 (NKM-7)-brand Ni methanation catalyst prepared through the chemical mixing of the initial raw material components in an aqueous ammonia medium, it is of particular interest to study the composition of this compound. An analysis of the experimental data obtained using derivatographic and radiographic methods of analysis, temperature-programmed recovery, decomposition, and combined recovery allowed us to establish that the structure of the Ni component of the Ni–Al composition after being treated with an aqueous solution of ammonia along with Ni contains the anions $[Al(OH)_4]^{-1}$, CO_3^{-2}, and OH^{-1}. Thus, this compound is NHCA. It was established experimentally that the NHCA composition formed during the preparation of Ni–Al has a structure similar to that of NHC.

To prepare a Ni–Al–Ca catalyst containing 25 (p. 1), 28 (p. 2), 31 (p. 3), and 36 (p. 4) mass % NiO, varying amounts Ca aluminate were added to the Ni–Al composition. Table 2 shows the calculated data of the catalyst mixture's chemical composition. It is worth noting that the minimum amount of Ca aluminate (28%) will have a catalyst mixture containing 36% NiO, and the maximum amount of Ca aluminate (45.5%) will have a catalyst mixture containing 25% NiO.

A mechanical mixture consisting of non-calcined Ni–Al mass, Ca aluminate, and graphite was molded in the form of rings with external diameters of 10 mm and tablets with diameters of 6 mm.

Table 3 presents data related to the phase composition, mechanical strength, and bulk density of the finished catalyst that has passed the hydrothermal treatment (HTT) stage.

With equal values of the mechanical strength of all the studied experimental batches at the input of the tablet machine, after the tablet machine and in the finished catalyst values of the mechanical strength differ (Table 3).

The increase in the mechanical strength of the catalyst after the HTT stage from 15–17 to 64–78 MPa is explained by the fact that the Ca aluminate added

Table 2. Calculated content of the components in the catalyst mixture

Batch №	1	2	3	4
$NiO–Al_2O_3$, mass %	54.5	61	67.6	72
Calcium Aluminate, mass %	45.5	39	32.4	28

Table 3. Phase composition, mechanical strength, and bulk density of the finished catalyst with different contents of $NiO–Al_2O_3$ and Ca aluminate

Batch №	Phase composition	Mechanical strength, MPa	γ, kg/dm³
1	Ni hydroxocarboaluminate, γ-Al_2O_3, C_3AH_6, $Al(OH)_3$, $CaCO_3$, graphite	78	1.05
2		75	1.07
3		67	1.07
4		64	1.08

to the Ni–Al composition acts as a hydraulic binder, which hydrates during hydrothermal treatment, and the hydration products in the form of highly basic Ca aluminate (C_3AH_6–$3CaO \cdot Al_2O_3 \cdot 6H_2O$) and Al hydroxide modifications gibbsite form a mechanically strong catalyst frame. Small pressing forces and the use of the HTT stage contribute to the fact that in the finished catalyst, there is practically no internal microstress that has a negative effect on the mechanical strength during either its activation or future operations.

To determine the minimum activation temperature, studies were carried out using the TPR method. Studies have shown that the activation process of the NIAP-07-07 catalyst is combined with the decomposition of the Ni component (NHCA) and is multistage.

Starting from a temperature of 210–220°C, gibbsite is decomposed to γ-Al_2O_3 and water, and interlayer water is removed from the NHCA. Simultaneously, a certain amount of highly dispersed NiO is formed and reduced to Ni. The process of removing interlayer water is accompanied by the formation of a finely dispersed phase of Ni hydroxoaluminate, which decomposes upon further heating in the hydrogen duct with the release of CO_2 into the gas phase. In the same temperature range (270–370°C), NiO begins to be actively activated. The maximum rate of NiO activation at this stage is achieved at 330°C. The bulk of NiO is reduced when the temperature is 380–650°C.

Table 4 shows results of catalytic activity in the methanation reaction of the studied catalysts with different contents of the active component and also, for comparison, the catalytic activity of the NIAP-07-01 catalyst containing 39% NiO, which is used as a standard sample to evaluate the correct operation of the installation. The CO content in the nitrogen–hydrogen mixture at the inlet to the methanation reactor was 0.65–0.72 vol %, which is 2–3 times more than its content before being added to an industrial methanator.

An analysis of the presented experimental data on the catalytic activity of the studied catalysts shows that after activation at 210°C, the regulatory value of CO (<10 ppm) in the purified gas is not reached. However, a mere 10°C increase in the activation temperature caused the catalysts to exhibit identical catalytic activity regardless of the content of the active component. The temperature of the CO slip in the purified gas is 214°C. A further increase in the activation temperature to 230°C leads to an increase in catalytic activity only in catalyst samples with a high content (36–39 mass %) of the active component. It must be noted that the activation of the studied catalysts at 220–230°C makes it possible to achieve high values of catalytic activity sufficient for their industrial operation.

Thus, the conducted studies have confirmed that the NIAP-07-07 catalyst begins to be activated at 220°C, which is more than 100°C cooler than the methanation catalysts used for industrial conditions.

Table 4. The catalytic activity of Ni catalysts during the methanation process

Activation temperature, °C	**The residual CO content in the purified gas, ppm**				**CO content in the purified gas, vol %**
	NIAP-07-01	**NIAP-07-07**			
	mass % NiO				
	39	**25**	**31**	**36**	
After 210	>10	>10	>10	>10	0.70
After 220	0.00	0.00	0.00	0.00	0.70
215	0.00	0.00	0.00	0.00	
214	>10	>10	>10	>10	
After 230	0.00	0.00	0.00	0.00	0.72
215	0.00	0.00	0.00	0.00	
214	0.00	0.00	0.00	0.00	
213	0.00	>10	0.00	0.00	
208	0.00	–	0.00	0.00	
207	>10	–	>10	0.00	
202	–	–	–	0.00	
201	–	–	–	>10	

Table 4. Continued

Activation temperature, °C	The residual CO content in the purified gas, ppm				CO content in the purified gas, vol %
	NIAP-07-01	NIAP-07-07			
	mass % NiO				
	39	25	31	36	
After 550	0.00	0.00	0.00	0.00	0.65
176	0.00	0.00	0.00	0.00	
175	0.00	>10	0.00	0.00	
171	0.00	–	0.00	0.00	
170	0.00	–	>10	0.00	
167	0.00	–	–	0.00	
166	0.00	–	–	>10	
154	0.00	–	–	–	
153	>10	–	–	–	

It can also be noted that, even with an active component content of 25–31 mass %, the developed catalysts will ensure stable long-term operation in compliance with the regulatory values of the methanation stage since the working temperature of the methanator is 300–320°C.

The activation process at 550°C led to a significant increase in catalytic activity for all samples studied. One can note that the catalytic activity tends to increase as the content of the active component increases. In addition, it was found that the developed catalysts practically retain their catalytic activity at 165–175°C even after overheating at 650°C for 30 h, which confirms their high thermal stability.

In ammonia synthesis units, the converted gas is purified from CO_2 in absorbers using absorbers such as Beinfield and Karsol alkaline solutions as well as organic absorbers in the form of aqueous solutions of monoethanolamine and activated methyldiethanolamine [20, 21]. Due to technological violations, the absorption of absorbents from the stage of purification of the converted gas from CO_2 to the methanation reactor can occur. In most cases, for Ni–Al catalysts, a decrease in catalyst activity and an increase in the gas-dynamic resistance of a methanation reactor occur [22]. As a result of these studies, it was established that the developed catalysts remain highly stable when exposed to these absorbents at 280–320°C [23, 24].

In 2017, an NIAP-07-07 catalyst with a lower activation temperature was loaded into the methanator of the CO methanation unit of the Pyrogas Separation and Benzene Production workshop at *Stavrolen* (Budennovsk, Stavropol krai, Russia). The catalyst was activated by process gas. After heating, the temperature in the methanator was increased to 220°C, and the CO content at the inlet of the reactor was increased to 0.7–0.8 vol % with a load of 4000–6000 m^3/h. After the methanator began operating (inlet temperature: 235°C; temperature in the catalysis zone: 255°C), the total residual content of CO and CO_2 in the purified methane–hydrogen fraction was less than 1 ppm. The catalyst provides the necessary degree of purification from oxygen-containing compounds at a load of feedstock of up to 16 000 m^3/h.

CONCLUSIONS

It was established that, under the selected conditions for preparing a mechanical mixture of HNC and active alumina with a liquid reagent, a chemical interaction occurs between the two and NHCA is formed as a result of this chemical reaction. The compositions of the catalyst with various amounts of the active component were optimized, and the temperature regions of the active phase precursor's activation process were determined. The catalyst has a low activation temperature and high catalytic activity, thermal stability, and mechanical strength. It can be created from the same catalyst mixture by tableting or extrusion in the form of granules of various geometric shapes and sizes. As a result, the catalyst has been used for industrial purposes.

The authors declare no conflicts of interest.

REFERENCES

1. Mel'nikov E.Ya. (Ed.). *Spravochnik azotchika* (Nitric directory). Moscow: Chemistry; 1986. 512 p. (in Russ.).

2. Semenova T.A., Leites I.L. (Eds.). *Ochistka tekhnologicheskikh gazov* (Process gas cleaning). Moscow: Chemistry; 1977. 488 p. (in Russ.).

3. Semenov V.P. (Ed.). *Proizvodstvo ammiaka* (Ammonia production.). Moscow: Chemistry; 1985. 368 p. (in Russ.).

4. Semenov V.P. (Ed.). *Spravochnoe rukovodstvo po katalizatoram dlya proizvodstva ammiaka i vodoroda* (Catalysts guide for ammonia and hydrogen production). Leningrad: Chemistry; 1973. 248 p. (in Russ.).

5. Berezina Yu.I., Shumilkina V.A., Semenova T.A., *et al. Katalizatory metanirovaniya. Obzorn. inform. Ser. Azot. Prom.* (Methanation catalysts. A Review. Nitrogen Industry Series). Moscow: NIITEKhim; 1986. 46 p. (in Russ.).

6. *Obzor i analiz raboty reaktorov i katalizatorov na ustanovkakh proizvodstva etilena i pererabotki pirokondensata* (Review and analysis of the operation of reactors and catalysts in plants for the production of ethylene and pyrocondensate processing). Moscow: VNIIOS-NAUKA; 2004. 10 p. (in Russ.).

7. Golosman E. Z. Treatment of process and exhaust gases using industrial cement-containing catalysts. *Khimicheskaya tekhnologiya = Chemical Technology.* 2000;12:25-35 (in Russ.).

8. Vakk E.G., Shuklin G.V., Leites I.L. *Poluchenie tekhnologicheskogo gaza dlya proizvodstva ammiaka, metanola, vodoroda i vysshikh uglevodorodov: teoreticheskie osnovy, tekhnologiya, katalizatory, oborudovanie, sistemy upravleniya* (Obtaining process gas for the production of ammonia, methanol, hydrogen and higher hydrocarbons: theoretical foundations, technology, catalysts, equipment, control systems). Moscow: 2011. 478 p. ISBN 978-5-98801-033-3 (in Russ.).

9. Dimidenko I.M., Yankovskii N.A., Stepanov V.A., Nikitina E.F., Kravchenko B.V. *Ammiak. Voprosy tekhnologii* (Ammonia. Technology issues), N.A. Yankovskii (Ed.). Donetsk: GIK Novaya Pechat'. OOO Lebed'; 2001. 497 p. (in Russ.).

10. Efremov V.N., Danyushevskii V.Ya., Grechenko A.N., Golosman E.Z., Yakerson V.I. Formation of a nickel catalyst with a different ratio of aluminum oxide and calcium aluminate. *Kinetika i Kataliz = Kinetics and Catalysis.* 1979;20(5):1315-1323 (in Russ.).

11. Yakerson V.I., Golosman E.Z. *Katalizatory i tsementy* (Catalysts and cements). Moscow: Khimiya; 1992. 256 p. (in Russ.). ISBN 5-7245-0762-5

12. Afanas'ev S.V. (Ed.). *Promyshlennyi kataliz v gazokhimii* (Industrial catalysis in gas chemistry). Samara: ANO SNTs Publishing House; 2018. 160 p. (in Russ.).

13. Gazimzyanov N.R., Gartman V.L. Features of methanetion catalyst operation at petrochemical and oil refining plants. *Kataliz v Promyshlennosti = Catal. Ind.* 2006;4:44-51 (in Russ.).

14. Dul'nev A.V., Obysov A.V., Dormidontova S.G. Method of producing a methanation catalyst. RF Pat. 2472587. Publ. 20.01.2013 (in Russ.).

15. Obysov A.V., Gartman V.L., Veinbender A.Ya., Sukhoruchkina L.A. Method of preparing nickel-aluminum-chromium catalyst for reduction-oxidation processes, in particular, for carbon monoxide methanation. RF Pat. 2205068. Publ. 27.05.2003 (in Russ.).

16. Rozhdestvenskii V.P., Polyanskii A.B., Antipov A.V., Lyamina L.A. Methane synthesis catalyst. USSR Inventor's Certificate 1287356. 1984 (in Russ.).

СПИСОК ЛИТЕРАТУРЫ

1. Справочник азотчика, под ред. Е.Я. Мельникова. М.: Химия; 1986. 512 с.

2. Очистка технологических газов, под ред. Т.А. Семеновой и И.Л. Лейтеса. М.: Химия; 1977. 488 с.

3. Производство аммиака, под ред. В.П. Семенова. М.: Химия; 1985. 368 с.

4. Справочное руководство по катализаторам для производства аммиака и водорода, под ред. В.П. Семенова. Л.: Химия; 1973. 248 с.

5. Березина Ю.И., Шумилкина В.А., Семенова Т.А. и др. Катализаторы метанирования. Обзорн. информ. Сер. Азотная пром-сть. М.: НИИТЭХим; 1986. 46 с.

6. Обзор и анализ работы реакторов и катализаторов на установках производства этилена и переработки пироконденсата. М.: ООО «ВНИИОС-НАУКА»; 2004. 10 с.

7. Голосман Е.З. Очистка технологических и выбросных газов с использованием промышленных цементсодержащих катализаторов. *Химическая технология.* 2000;12:25-35.

8. Вакк Э.Г., Шуклин Г.В., Лейтес И.Л. Получение технологического газа для производства аммиака, метанола, водорода и высших углеводородов: теоретические основы, технология, катализаторы, оборудование, системы управления: учеб. пособие. М.: 2011. 478 с. ISBN 978-5-98801-033-3

9. Димиденко И.М., Янковский Н.А., Степанов В.А., Никитина Э.Ф., Кравченко Б.В. Аммиак. Вопросы технологии, под общ. ред. Н.А. Янковского. Донецк: ГИК «Новая печать». ООО «Лебедь», 2001. 497 с.

10. Ефремов В.Н., Данюшевский В.Я., Греченко А.Н., Голосман Е. З., Якерсон В.И. Формирование никелевого катализатора с различным соотношением окиси алюминия и алюмината кальция. *Кинетика и катализ.* 1979;20(5):1315-1323.

11. Якерсон В.И., Голосман Е.З. Катализаторы и цементы. М.: Химия; 1992. 256 с. ISBN 5-7245-0762-5

12. Промышленный катализ в газохимии, под ред. С.В. Афанасьева. Самара: АНО «Издательство СНЦ»; 2018. 160 с.

13. Газимзянов Н.Р., Гартман В.Л. Особенности эксплуатации катализаторов метанирования на предприятиях нефтепереработки и нефтехимии. *Катализ в промышленности.* 2006;4:44-51.

14. Дульнев А.В., Обысов А.В., Дормидонтова С.Г. Способ получения катализатора метанирования: пат. 2472587 РФ. Заявка № 2011144743/04; заявл.03.11.2011; опубл. 20.01.2013. Бюл. № 2.

15. Обысов А.В., Гартман В.Л., Вейнбендер А.Я., Сухоручкина Л.А. Способ получения никель-алюмо-хромового катализатора для окислительно-восстановительных процессов, в частности, для метанирования оксидов углерода: патент 2205068 РФ. Заявка № 2002103954/04; заявл. 18.02.2002; опубл. 27.05.2003.

16. Рождественский В.П., Полянский А.Б., Антипов А.В., Лямина Л.А. Катализатор для синтеза метана: пат. 1287356. СССР. 1984.

17. Кладова Н.В., Борисова Т.В., Качкин А.В., Макаренко М.Г. Способ получения катализатора для гидрирования ароматических соединений, для метанирования CO и CO_2: 2186623 пат. РФ. Заявка № 2001106564/04; заявл. 11.03.2001; опубл. 10.08.2002.

18. Голосман Е.З., Ефремов В.Н. Получение и очистка защитных атмосфер на промышленных катализаторах. Deutschland. Saarbucken: Palmarium Academie Publishing; 2016. 68 с. ISBN 978-3-659-72283-7

17. Kladova N.V., Borisova T.V., Kachkin A.V., Makarenko M.G. Method of synthesis of catalyst for hydrogenation of aromatic compounds, for methanation of CO and CO_2. RF Pat. 2186623. Publ. 10.08.2002 (in Russ.).

18. Golosman E.Z., Efremov V.N. *Poluchenie i ochistka zashchitnykh atmosfer na promyshlennykh katalizatorakh* (Obtaining and purification of protective atmosphere on industrial catalysts). Deutschland. Saarbucken: Palmarium Academie Publishing; 2016. 68 p. (in Russ.). ISBN 978-3-659-72283-7

19. Nechugovskii A.I., Grechenko A.N., Golosman E.Z. Study of the interaction of metal hydroxocarbonates with calcium aluminates in an aqueous medium. *Russ. J. Appl. Chem.* 1990;63(8):1747-1751 (in Russ.).

20. Leites I.L., Avetisov A.K., Yazvikova N.V., Suvorkin S.V., Baichtok Yu.K., Dudakova N.B., Deev K.N. Investigation of the physicochemical properties of the modified MDEA absorbent for fine purification of synthesis gas from carbon dioxide in the production of ammonia. *Khim. Prom. Segodnya = Chem. Ind. Today.* 2003;1:34-41 (in Russ.).

21. Avetisov A.K., Kononov S.M., Sokolov A.M., Baitchok Yu.K., Suvorkin S.V., Leitis I.L., Deripasov V.V. Experience of modernization of the absorption cleaning unit of the ammonia synthesis unit AM-70 at Nevinnomysskii azot with the replacement of the MEA solution with a Russian-made MDEA sorbent. *Khim. Prom. Segodnya = Chem. Ind. Today.* 2003;2:22-24 (in Russ.).

22. Nechueva L.G., Berezina Yu.I., Yazvikova N.V., Chudinov M.G., Glagoleva L.I. Nitrogen fertilizer production. *Trudy GIAP = Procc. of GIAP.* 1979;55:37-44 (in Russ.).

23. Kashinskaya A.V., Efremov V.N., Golosman E.Z., Polivanov B. I. *Issledovanie i vnedrenie v promyshlennost' nanostryktyirovannogo nikel'tsementsoderzhashchtgo katalizatora protsessa metanirovaniya* (Research and implementation of a nanostructured Nickel-cement-containing catalyst for the methanation process in industry). All-Russian scientific and technical conference “Problems of science.” Conference proceedings. Part 1. Chemistry and chemical technology. D.I. Mendeleyev Russian State Technical University, Novomoskovsk Institute (branch). Novomoskovsk: 2019. P. 24-36 (in Russ.).

24. Efremov V.N., Golosman E.Z., Kashinskaya A.V., Polivanov B.I., Polushin A.P. About destruction of nickel catalysts of a methanation under the influence of inorganic and organic absorbents CO_2. *Khim. Prom. Segodnya = Chem. Ind. Today.* 2018;4:14-21 (in Russ.).

19. Нечуговский А.И., Греченко А.Н., Голосман Е.З. Изучение взаимодействия гидроксокарбонатов металлов с алюминатами кальция в водной среде. *Журн. прикл. химии.* 1990;63(8):1747-1751.

20. Лейтес И.Л., Аветисов А.К., Язвикова Н.В., Суворкин С.В., Байчток Ю.К., Дудакова Н.Б., Деев К.Н. Исследование физико-химических свойств модифицированного МДЭА-абсорбента для тонкой очистки синтез-газа от диоксида углерода в производстве аммиака. *Хим. пром. сегодня.* 2003;1:34-41.

21. Аветисов А.К., Кононов С.М., Соколов А.М., Байтчок Ю.К., Суворкин С.В., Лейтис И.Л., Дерипасов В.В. Опыт модернизации отделения абсорбционной очистки агрегата синтеза аммиака АМ-70 на ОАО «Невинномысский азот» с заменой МЭА-раствора на МДЭА-сорбент российского производства. *Хим. пром. сегодня.* 2003;2:22-24.

22. Нечуева Л.Г., Березина Ю.И., Язвикова Н.В., Чудинов М.Г., Глаголева Л.И. Производство азотных удобрений. *Труды ГИАП.* 1979;55:37-44.

23. Кашинская А.В., Ефремов В.Н, Голосман Е.З., Поливанов Б.И. Исследование и внедрение в промышленность наноструктурированного никельцементсодержащего катализатора процесса метанирования. Всероссийская научно-техническая конференция «Проблемы науки». Материалы конференции. Часть 1. Химия и химическая технология. ФГБОУ ВО РХТУ им. Д.И. Менделеева, Новомосковский институт (филиал). Новомосковск: 2019. с. 24-36.

24. Ефремов В.Н., Голосман Е.З., Кашинская А.В., Поливанов Б.И., Полушин А.П. О разрушении активированных никелевых катализаторов метанирования под воздействием неорганических сорбентов CO_2. *Хим. пром. сегодня.* 2018;4:14-21.

About the authors:

Evgeniy Z. Golosman, Dr. of Sci. (Chemistry), Main Researcher, NIAP-KATALIZATOR (10, Svyazi ul., Novomoskovsk, Tula oblast, 301660, Russia). E-mail: evgolosman@yandex.ru. https://orcid.org/0000-0002-3805-7884

Vasiliy N. Efremov, Cand. of Sci. (Engineering), Main Specialist on Catalysts, NIAP-KATALIZATOR (10, Svyazi ul., Novomoskovsk, Tula oblast, 301660, Russia). E-mail: vne45@yandex.ru. https://orcid.org/0000-0002-7913-5754

Anna V. Kashinskaya, Head of the Laboratory of Physical and Chemical Research, NIAP-KATALIZATOR (10, Svyazi ul., Novomoskovsk, Tula oblast, 301660, Russia). E-mail: anutka-20005@yandex.ru. https://orcid.org/0000-0002-6629-4983

Об авторах:

Голосман Евгений Зиновьевич, доктор химических наук, главный научный сотрудник, ООО «НИАП-КАТАЛИЗАТОР» (301660, Россия, г. Новомосковск, Тульская область, ул. Связи, д. 10). E-mail: evgolosman@yandex.ru. https://orcid.org/0000-0002-3805-7884

Ефремов Василий Николаевич, кандидат технических наук, главный специалист по катализаторам, ООО «НИАП-КАТАЛИЗАТОР» (301660, Россия, г. Новомосковск, Тульская область, ул. Связи, д. 10). E-mail: vne45@yandex.ru. https://orcid.org/0000-0002-7913-5754

Кашинская Анна Вячеславовна, заведующая лабораторией физико-химических исследований, ООО «НИАП-КАТАЛИЗАТОР» (301660, Россия, г. Новомосковск, Тульская область, ул. Связи, д. 10). E-mail: anutka-20005@yandex.ru. https://orcid.org/0000-0002-6629-4983

Submitted: December 26, 2019; Reviewed: February 18, 2020; Accepted: April 03, 2020.

Translated from Russian into English by H. Moshkov

Edited for English language and spelling by Enago, an editing brand of Crimson Interactive Inc.

ISSN 2686-7575 (Online)
https://doi.org/10.32362/2410-6593-2020-15-2-30-37
UDC 544.332.2:547.494.254

Quantum chemical approach to calculating the enthalpies of the formation of alkali metal xanthates

Yuriy V. Popov[1]**, Aleksandr S. Dolgachev**[2]**, Evgeniy V. Shishkin**[1,@]**, Yuriy L. Zotov**[1]**, Veniamin E. Shishkin**[1]

[1]Volgograd State Technical University, Volgograd, 400005 Russia
[2]Volzhskii Orgsintez, Volzhskii, Volgograd oblast, 404117 Russia
[@]Corresponding author, e-mail: shishkin@vstu.ru

Objectives. *The aim of this work is to study the possibility of the joint use of quantum chemical methods and correlation analysis to determine the formation enthalpies of metal-containing organic substances using the example of alkali metal xanthates, which are of interest as biologically active substances and effective flotation reagents.*
Methods. *Semi-empirical methods of quantum chemical calculating (Modified Neglect of Diatomic Overlap, Austin Model 1, Recife model 1 methods) and linear regression analysis were used.*
Results. *Using the semi-empirical Modified Neglect of Diatomic Overlap, Austin Model 1, and Recife model 1 methods, the enthalpies of formation of 16 potassium and sodium alkyl xanthates were calculated, and the obtained results were compared with experimental data. It was found that the best correlation for potassium and sodium salts of dithiocarbonic acid esters could be observed using the Austin Model 1 method. Using the obtained regression equations, the enthalpies of formation were calculated for 30 xanthates, the organic part of which contained alkyl, cyclic non-aromatic structures, and one or two heteroatoms such as nitrogen, oxygen, and fluorine, and for which there are no experimental data.*
Conclusions. *As a result of the study, an excellent correlation was established between the experimental and the calculated (by the Austin Model 1 method) values of the enthalpies of formation of potassium and sodium alkyl xanthates. The data obtained can be used to calculate the thermal effect of the xanthogenation reactions of alcohols and to design the production of the corresponding xanthates.*

Keywords: *alkali metal xanthates, semi-empirical quantum chemical calculation methods, correlation analysis, formation enthalpy.*

For citation: Popov Yu.V., Dolgachev S.A., Shishkin E.V., Zotov Yu.L., Shishkin V.E. Quantum chemical approach to calculating the enthalpies of the formation of alkali metal xanthates. *Tonk. Khim. Tekhnol. = Fine Chem. Technol.* 2020;15(2):30-37. https://doi.org/10.32362/2410-6593-2020-15-2-30-37

Квантово-химический подход к расчету энтальпий образования ксантогенатов щелочных металлов

Ю.В. Попов[1], А.С. Долгачев[2], Е.В. Шишкин[1,@], Ю.Л. Зотов[1], В.Е. Шишкин[1]

[1]*Волгоградский государственный технический университет, Волгоград, 400005 Россия*
[2]*АО «Волжский Оргсинтез», Волжский, Волгоградская область, 404117 Россия*
[@]*Автор для переписки, e-mail: shishkin@vstu.ru*

Цели. *Целью работы является исследование возможности совместного использования квантово-химических методов и корреляционного анализа для определения энтальпий образования металлосодержащих органических веществ на примере ксантогенатов щелочных металлов, которые представляют интерес как биологически активные вещества и эффективные флотореагенты.*
Методы. *Использованы полуэмпирические методы квантово-химических расчетов Modified Neglect of Diatomic Overlap, Austin Model 1, Recife model 1 и линейный регрессионный анализ.*
Результаты. *С помощью полуэмпирических методов Modified Neglect of Diatomic Overlap, Austin Model 1, Recife model 1 вычислены энтальпии образования 16 алкилксантогенатов калия и натрия, проведено сопоставление полученных результатов с экспериментальными данными. Выяснено, что наилучшая корреляция для калиевых и натриевых солей эфиров дитиоугольной кислоты наблюдается при использовании метода Austin Model 1. С помощью полученных уравнений регрессии вычислены энтальпии образования для 30 ксантогенатов, органическая часть которых содержит алкильные, циклические неароматические структуры и один или два гетероатома, такие как N, O, F, и экспериментальные данные по которым отсутствуют.*
Выводы. *В результате проведенного исследования была установлена превосходная корреляция между экспериментальными и рассчитанными по методу AM1 значениями энтальпий образования алкилксантогенатов калия и натрия. Полученные данные могут быть использованы для расчета теплового эффекта реакций ксантогенирования спиртов и проектирования производств соответствующих ксантогенатов.*

Ключевые слова: *ксантогенаты щелочных металлов, полуэмпирические квантово-химические методы расчета, корреляционный анализ, энтальпия образования.*

Для цитирования: Попов Ю.В., Долгачев А.С., Шишкин Е.В., Зотов Ю.Л., Шишкин В.Е. Квантово-химический подход к расчету энтальпий образования ксантогенатов щелочных металлов. *Тонкие химические технологии.* 2020;15(2):30-37. https://doi.org/10.32362/2410-6593-2020-15-2-30-37

INTRODUCTION

The thermodynamic characteristics of a substance are its most important parameters. Thermodynamic analysis of a chemical process allows one to determine the direction of the reaction, the equilibrium conditions, and the thermal effect of the process. However, the task of determining the thermodynamic characteristics, primarily, the enthalpies of formation of various organic substances, is time-consuming, and for some compounds, it is not feasible at all. Due to the development of quantum chemistry and computer technology, the thermodynamic parameters of many compounds can now be quickly calculated using various methods; however, it is not possible to fully rely on the obtained values, and it is always necessary to verify the results of calculations with experimental data. Earlier studies, using a combination of semi-empirical quantum chemical methods of calculation and correlation analysis, determined the enthalpies of formation of many organic compounds, for example: cyclophanes [1]; nitrogen-containing heterocycles [2]; and derivatives of adamantane [3]. For the calculations, compounds were used that included the most frequently found elements in organic chemistry: carbon, hydrogen, oxygen, nitrogen, and sulfur. At present, many other organic substances are widely used in the national economy, which, in addition to the elements listed above, also include various metals. Calculating the thermodynamic characteristics of these types of substances is challenging. Therefore, research into the possibility of combining quantum chemical methods and correlation analysis to find the formation enthalpies of such compounds is urgently needed.

MATERIALS AND METHODS

As representatives of the studied group of substances, the salts of dithiocarbonic acid O-esters (xanthates of alkali metals) were chosen, represented by the general formula:

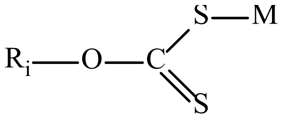

where R_i is the organic part of the molecule, M = Na, K. These compounds are widely used as flotation-reagent collectors [4], and also have a pronounced biological activity [5, 6]. The numbering and structure of xanthates are presented in Table 1.

To identify the correlation between the calculated and experimental values of the enthalpy of formation, 16 compounds were selected: methyl (I, II), ethyl (III, IV), isopropyl (V, VI), propyl (VII, VIII), butyl (IX, X), amyl (XI, XII), hexyl (XIII, XIV) and heptyl (XV, XVI) potassium and sodium xanthates (odd numbers correspond to potassium xanthates, even numbers to sodium). The literature [7–11] contains experimental data on the thermal effect of the xanthogenation reactions of the corresponding alcohols ($\Delta H^0_{\mathrm{r,\,298}}$):

$$\mathrm{ROH + CS_2 + KOH \rightarrow ROC(S)SK + H_2O.}$$

The formation enthalpies of substances I–XVI ($\Delta H^0_{\mathrm{f,\,exp.}}$) were determined using reference data on the participants' enthalpies of formation in the reaction and Hess's law. For these compounds, geometry optimization and calculation of formation enthalpies were also performed using the Modified Neglect of Diatomic Overlap (MNDO), Austin Model 1 (AM1), and Recife Model 1 (RM1) methods in the HyperChem software package. The calculation results are presented in Table 2.

Table 1. List of investigated potassium and sodium xanthates (odd numbers correspond to potassium xanthates, even numbers correspond to sodium xanthates)

No.	Compound	No.	Compound
I, II	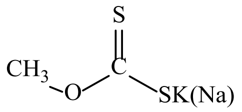	XXIII, XXIV	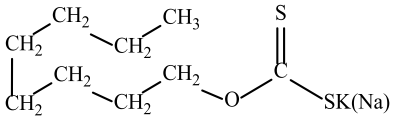
III, IV	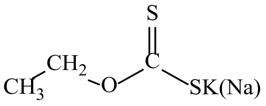	XXV, XXVI	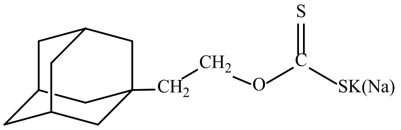
V, VI	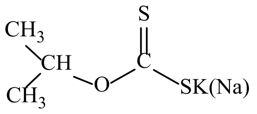	XXVII, XXVIII	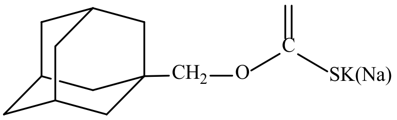
VII, VIII	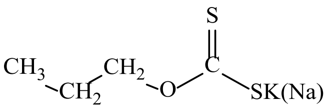	XXIX, XXX	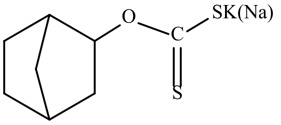
IX, X	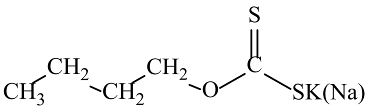	XXXI, XXXII	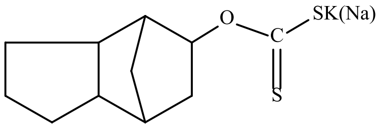
XI, XII	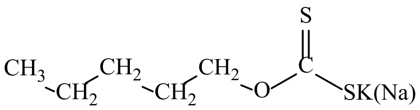	XXXIII, XXXIV	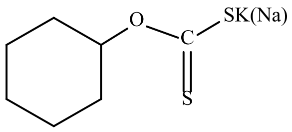

Table 1. Continued

No.	Compound	No.	Compound
XIII, XIV	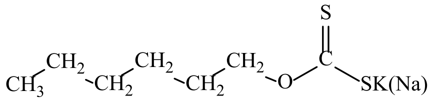	XXXV, XXXVI	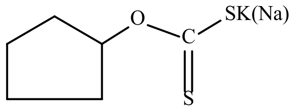
XV, XVI	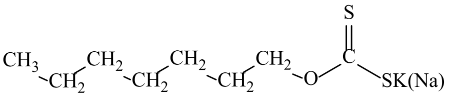	XXXVII, XXXVIII	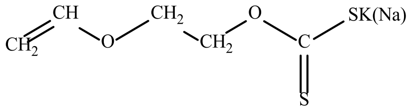
XVII, XVIII	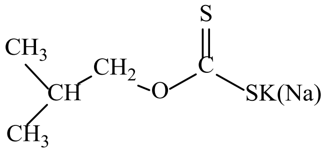	XXXIX, XL	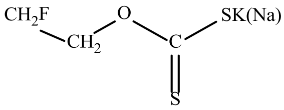
XIX, XX	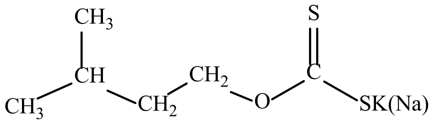	XLI, XLII	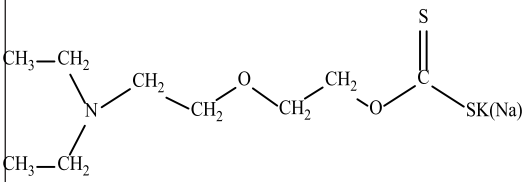
XXI, XXII	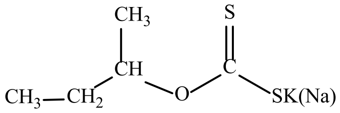	XLIII, XLIV	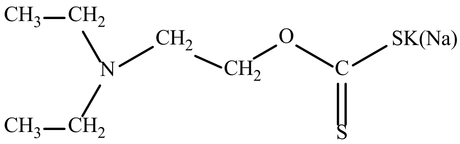
XLV, XLVI	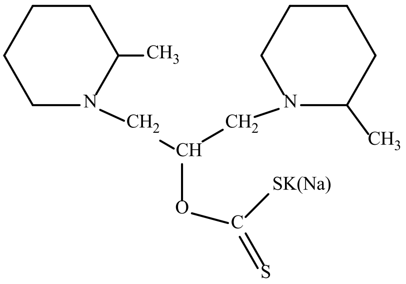		

It was found that a general linear correlation was absent; however, the experimental and calculated data fitted on a straight line separately for potassium and sodium xanthates. Moreover, for each of the calculation methods, the correlation coefficients for the group of sodium xanthates were slightly higher than for the group of potassium xanthates. The highest correlation coefficient in both cases was characteristic of the AM1 method in which r > 0.99, which indicates excellent correlation. The regression equations in this case are:

$$\Delta H^0_{\text{f, exp., K}} = 0.8736 \times \Delta H^0_{\text{f, calc., K}} - 92.2980 \qquad (1)$$

$$\Delta H^0_{\text{f, exp., Na}} = 0.8738 \times \Delta H^0_{\text{f, calc., Na}} - 124.0000 \qquad (2)$$

The obtained dependencies can be used to find the formation enthalpy of those potassium and sodium xanthates, experimental data for which are not available in scientific and technical literature. For further calculations, potassium (odd numbers) and sodium (even numbers) xanthates were selected based on the following alcohols: 2-methylpropan-1-ol (XVII, XVIII), 3-methylbutan-1-ol (XIX, XX), butan-2-ol (XXI, XXII), octan-1-ol (XXIII, XXIV), (1-adamantyl) methanol (XXV, XXVI), 2-(1-adamantyl)-ethan-1-ol (XXVII, XXVIII), bicyclo-[2.2.1]-heptan-2-ol (XXIX, XXX), 2-(vinyloxy)-ethan-1-ol (XXXI, XXXII), 2-fluoroethan-1-ol (XXXIII, XXXIV), 2-(*N,N*-diethylamino)-ethan-1-ol (XXXV, XXXVI), 2-(*N,N*-diethylaminoethoxy)-ethan-1-ol (XXXVII, XXXVIII), cyclopentanol (XXXIX, XL), cyclohexanol (XLI, XLII), 1,3-di-(2-methylpiperidino)-propan-2-ol (XLIII, XLIV), and tricyclo-[5.2.1.0]-decan-9-ol (XLV, XLVI). All these substances are described in the literature [6, 12–19] and are either highly efficient flotation reagents-collectors or exhibit high biological activity.

The results of the calculation of the above xanthates by the AM1 method, and subsequent recalculation of the formation enthalpies according to the regression equations (1) and (2), are given in Table 3.

Table 2. Data of quantum-chemical calculation of formation enthalpy $\Delta H^0_{\text{f, calc.}}$ performed by MNDO, AM1, RM1 methods for xanthates I-XVI and correlation coefficients

No.	$\Delta H^0_{\text{r, 298}}$ **kJ/mol**	$\Delta H^0_{\text{f, exp.}}$ **kJ/mol**	$\Delta H^0_{\text{f, calc.}}$, **kJ/mol**					
			MNDO	**Δ**	**AM1**	**Δ**	**RM1**	**Δ**
I	–45.10	–312.31	–376.94	–64.63	–259.89	52.42	–231.55	80.76
II	–28.35	–297.19	–324.9	–27.71	–210.57	86.62	–175.56	121.63
III	–47.20	–348.21	–399.41	–51.2	–284.41	63.8	–256.46	91.75
IV	–32.79	–335.43	–345.92	–10.49	–235.15	100.28	–200.5	134.93
V	–6.50	–345.3	–405.33	–60.03	–299.78	45.52	–285.9	59.4
VI	–4.97	–345.4	–346.01	–0.61	–250.42	94.98	–230.76	114.64
VII	–52.80	–376.54	–419.27	–42.73	–310.46	66.08	–277.5	99.04
VIII	–36.20	–361.57	–361.57	0	–261.2	100.37	–220.48	141.09
IX	–43.50	–384.14	–438.96	–54.82	–335.14	49	–297.7	86.44
X	–30.92	–373.19	–380.05	–6.86	–289.69	83.5	–241.14	132.05
XI	–35.40	–403.99	–455.74	–51.75	–360.26	43.73	–319.04	84.95
XII	–27.50	–397.72	–396.82	0.9	–315.15	82.57	–259.29	138.43
XIII	–32.20	–428.69	–475.2	–46.51	–384.39	44.3	–337.92	90.77
XIV	–26.10	–424.22	–417.16	7.06	–343.76	80.46	–279.53	144.69
XV	–31.80	–450.75	–494.75	–44	–411.76	38.99	–358.4	92.35
XVI	–24.54	–445.12	–433.24	11.88	–369.12	76	–296.99	148.13
Correlation coefficient			$r_K = 0.9875$ $r_{Na} = 0.9907$		$r_K = 0.9907$ $r_{Na} = 0.9919$		$r_K = 0.9669$ $r_{Na} = 0.9841$	

Table 3. Enthalpies of the formation of compounds XVII-XLVI, calculated ($\Delta H^0_{\text{f, calc.}}$) by the AM1 method and corrected ($\Delta H^0_{\text{f, calc.}}$*) by equations (1) and (2)

No.	$\Delta H^0_{\text{f, calc.}}$, **kJ/mol**	$\Delta H^0_{\text{f, calc.}}$*, **kJ/mol**	**No.**	$\Delta H^0_{\text{f, calc.}}$, **kJ/mol**	$\Delta H^0_{\text{f, calc.}}$*, **kJ/mol**
XVII	–328.39	–379.18	XVIII	–282.02	–370.43
XIX	–359.04	–405.96	XX	–309.78	–394.69
XXI	–325.57	–376.72	XXII	–268.17	–358.33
XXIII	–452.03	–487.19	XXIV	–403.36	–476.46
XXV	–420.30	–459.47	XXVI	–371.44	–448.56
XXVII	–401.41	–442.97	XXVIII	–342.18	–423.00
XXIX	–259.93	–319.37	XXX	–209.58	–307.13

Table 3. Continued

No.	$\Delta H^0_{\text{f, calc.}}$, kJ/mol	$\Delta H^0_{\text{f, calc.}}$*, kJ/mol	No.	$\Delta H^0_{\text{f, calc.}}$, kJ/mol	$\Delta H^0_{\text{f, calc.}}$*, kJ/mol
XXXI	–265.90	–324.59	XXXII	–242.03	–335.49
XXXIII	–359.40	–406.27	XXXIV	–304.94	–390.46
XXXV	–320.61	–372.38	XXXVI	–271.13	–360.91
XXXVII	–335.89	–385.73	XXXVIII	–285.98	–373.89
XXXIX	–484.10	–515.21	XL	–434.06	–503.28
XLI	–270.55	–328.65	XLII	–219.63	–315.91
XLIII	–481.88	–513.27	XLIV	–401.58	–474.90
XLV	–323.05	–374.51	XLVI	–274.31	–363.69

In compiling this list of xanthates, compounds were chosen so that their calculated formation enthalpy lay in the range from −200 to −500 kJ/mol for potassium and from −200 to −450 kJ/mol for sodium. The possibility of applying equations (1) and (2) for xanthates containing heteroatoms in an organic radical is evidenced by previous studies [e.g., 20]. When developing a method for producing potassium diethylaminoethyl xanthate, we evaluated the thermal effect of the reaction under adiabatic conditions. It was found that the change in the enthalpy of xanthogenation of diethylaminoethanol lies in the range from −30 to −45 kJ/mol. In this case, the calculation of the thermal effect of this reaction, taking into account the obtained calculated data, gave the result $\Delta H^0_{\text{r, 298}} = -29.56$ kJ/mol. Given that in reality, along with the main xanthogenation reaction, side exothermic processes occur:

$$6KOH + CS_2 \rightarrow K_2CO_3 + 2K_2S + 3H_2O$$

$$6KOH + 3CS_2 \rightarrow K_2CS_3 + 2K_2S + 3H_2O$$

the calculated value of the change in the enthalpy of diethylaminoethanol xanthogenation can be considered reliable.

CONCLUSIONS

In this work, an excellent correlation was established between the experimental and calculated (using the AM1 method) formation enthalpies of potassium and sodium alkyl xanthates. Using the obtained correlation equations, the formation enthalpies of various xanthates were calculated, the organic part of which contained alkyl, cyclic non-aromatic structures, and one or two heteroatoms such as nitrogen, oxygen, and fluorine. The data obtained can be used to calculate the thermal effect of the xanthogenation reaction of the corresponding alcohols and to design the production of these xanthates.

The authors declare no conflicts of interest.

REFERENCES

1. Zauer E.A. Cyclophanes: Simulation of the formation enthalpy by quantum-chemical methods. *Russ. J. Gen. Chem.* 2017;87:918-922. https://doi.org/10.1134/S1070363217050048

2. Zauer E.A. Enthalpy of formation of five-membered nitrogen-containing aromatic heterocycles. *Russ. J. Gen. Chem.* 2015:85:2268-2276. https://doi.org/10.1134/S1070363215100084

3. Zauer E.A., Zauer O.A. Calculations of the enthalpies of formation of oxygen-containing adamantane derivatives by quantum-chemical methods. *Russ. J. Phys. Chem.* 2009:83;582-586. https://doi.org/10.1134/S0036024409040128

4. Abramov A.A. Flotatsionnye metody obogashcheniya (Flotation methods of enrichment). Moscow: Moscow State Mining University Publ.; 2008. 720 p. (in Russ.).

СПИСОК ЛИТЕРАТУРЫ

1. Zauer E.A. Cyclophanes: Simulation of the formation enthalpy by quantum-chemical methods. *Russ. J. Gen. Chem.* 2017;87:918-922. https://doi.org/10.1134/S1070363217050048

2. Zauer E.A. Enthalpy of formation of five-membered nitrogen-containing aromatic heterocycles. *Russ. J. Gen. Chem.* 2015:85:2268-2276. https://doi.org/10.1134/S1070363215100084

3. Zauer E.A., Zauer O.A. Calculations of the enthalpies of formation of oxygen-containing adamantane derivatives by quantum-chemical methods. *Russ. J. Phys. Chem.* 2009:83;582-586. https://doi.org/10.1134/S0036024409040128

4. Абрамов А.А. Флотационные методы обогащения. М.: Издательство Московского государственного горного университета и др.; 2008. 720 с.

5. Melnikov N. N. *Pestitsidy. Khimiya, tekhnologiya i primenenie* (Pesticides. Chemistry, technology and application). Moscow: Chemistry; 1987. 712 p. (in Russ.).

6. Carta F., Akdemir A., Scozzafava A., Masini E., Supuran C.T. Xanthates and Trithiocarbonates Strongly Inhibit Carbonic Anhydrases and Show Antiglaucoma Effects *in Vivo. J. Med. Chem.* 2013;56(11):4691-4700. https://doi.org/10.1021/jm400414j

7. Waldman A.I., Panfilov B.I., Waldman D.I., Navrotsky V.A. Xanthogenation of alcohols. Message 1. Investigation of the kinetics of the xanthogenation reaction of aliphatic alcohols C1–C7 of normal structure in an aqueous solution of potassium hydroxide. DEP. ONIITEKHIM. Cherkassy, 1984. No. 476 HP-D84 (in Russ.).

8. Waldman, A.I., Panfilov, B.I., Waldman D.I. Xanthogenation of alcohols. Message 2. Investigation of the kinetics of the xanthogenation reaction of aliphatic alcohols C1–C7 of normal structure in an aqueous solution of sodium hydroxide. DEP. ONIITEKHIM. Cherkassy, 1984. No. 477hp-D84 (in Russ.).

9. Waldman A.I., Panfilov B.I., Waldman D.I., Navrotsky V.A. Xanthogenation of alcohols. Message 3. Kinetic regularities of the reaction of xanthogenation of aliphatic alcohols C3–C5 from oxidation in an aqueous solution of alkali metal hydroxide. DEP. ONIITEKHIM. Cherkassy, 1984. No. 478 HP-D84 (in Russ.).

10. Tsarenko S.V., Waldman A.I., Panfilov B.I., Waldman D.I. Calorimetric study of the kinetics of the reaction of xanthogenation of aliphatic alcohols in an aqueous solution of caustic soda. *Izvestiya Vuzov. Seriya khimiya i khimicheskaya tekhnologiya = Russ. J. Chem. Chem. Technol.* 1979;26(1):1054-1058 (in Russ.).

11. Hardin A.P., Waldman A.I., Gnatyuk P.P., Panfilov B.I., Waldman D.I., Lisachenko L.A. Investigation of the kinetics of the process of obtaining sodium isopropylxanthogenate. *Chemical industry.* 1983;28(3):143-144 (in Russ.).

12. Savelyanov V.P., Savelyanova R.T., Utrobin N.P., Rudakova T.V. Method of preparing alkylxanthogenates. USSR Pat. 727641. 15.04.1980 (in Russ.).

13. Tsarenko S.V., Gnatyuk P.P., Zakharova L.A., Nishchenkova N.S., Utrobin N.P. Method of preparing C_5–C_7 alcohol alkaline alkylxanthogenates. USSR Pat. 737397. 30.05.1980 (in Russ.).

14. Hummel K., Sherm A. Xanthates as antitumor agents: USA Pat. 4981869. 01.01.1991

15. Trofimov B.A., Ivanova N.I., Amosova S.V., Leonov S.B., Belkova O.N., Roginskaya L.V., Chebotareva E.G. Potassium vinyloxyethylxanthogenate as collecting agent for flotation of polymetallic ores. USSR Pat. 910615. 07.03.1982 (in Russ.).

16. Larionov S.V., Kosareva L.A. Complexing properties of the trifluoroethyl xanthate ion and volatility of its intracomplex compounds. *Russian Chemical Bulletin.* 1976;25(7):1388-1391 (in Russ.).

17. Bazanova N.M., Gurvich S.M., Livshits A.K. Method for flotation concentration of copper-nickel ores. USSR Pat. 126816. 1960 (in Russ.).

18. Gorgulu A.O., Celikkan H., Arslan M. The Synthesis, Characterization and Electrochemical Behavior of Transition Metal Complexes Containing Nitrogen Heterocyclic Sulphur Donor Ligand. *Acta Chim. Slov.* 2009;56:334-339.

19. Tomioka M., Hasegawa K. Tricyclodecan-9-yl xanthogenate stereoisomers. RF Pat. 2470915. 27.12.2012 (in Russ.).

20. Popov Yu.V., Dolgachev A.S., Shishkin E.V. Synthesis of diethylaminoethyl potassium xanthate *Izvestia VSTU. Chemistry and Technology of Hetero-Organic Monomers and Polymer Materials.* 2015;(4):35-37 (in Russ.).

5. Мельников Н.Н. Пестициды. Химия, технология и применение. М.: Химия; 1987. 712 с.

6. Carta F., Akdemir A., Scozzafava A., Masini E., Supuran C.T. Xanthates and Trithiocarbonates Strongly Inhibit Carbonic Anhydrases and Show Antiglaucoma Effects *in Vivo. J. Med. Chem.* 2013;56(11):4691-4700. https://doi.org/10.1021/jm400414j

7. Вальдман А.И., Панфилов Б.И., Вальдман Д.И., Навроцкий В.А. Ксантогенирование спиртов. Сообщение 1. Исследование кинетики реакции ксантогенирования алифатических спиртов С1–С7 нормального строения в водном растворе гидроксида калия. Деп. ОНИИТЭХИМ. Черкассы, 1984. № 476хп-Д84.

8. Вальдман А.И., Панфилов Б.И., Вальдман Д.И. Ксантогенирование спиртов. Сообщение 2. Исследование кинетики реакции ксантогенирования алифатических спиртов С1–С7 нормального строения в водном растворе гидроксида натрия. Деп. ОНИИТЭХИМ. Черкассы, 1984. № 477хп-Д84.

9. Вальдман А.И., Панфилов Б.И., Вальдман Д.И., Навроцкий В.А. Ксантогенирование спиртов. Сообщение 3. Кинетические закономерности реакции ксантогенирования алифатических спиртов С3–С5 изостроения в водном растворе гидроксида щелочного металла. Деп. ОНИИТЭХИМ. Черкассы, 1984. № 478хп-Д84.

10. Царенко С.В., Вальдман А.И., Панфилов Б.И., Вальдман Д.И. Калориметрическое исследование кинетики реакции ксантогенирования алифатических спиртов в водном растворе едкого натра. *Известия вузов. Серия химия и химическая технология.* 1979;26(1):1054-1058.

11. Хардин А.П., Вальдман А.И., Гнатюк П.П., Панфилов Б.И., Вальдман Д.И., Лисаченко Л.А. Исследование кинетики процесса получения изопропилксантогената натрия. *Химическая промышленность.* 1983;28(3):143-144.

12. Савельянов В.П., Савельянова Р.Т, Утробин Н.П., Рудакова Т.В. Способ получения алкилксантогенатов. А. с. 727641 (1977), Б. И. 1980. № 14.

13. Царенко С.В., Гнатюк П.П., Захарова Л.А., Нищенкова Н.С., Утробин Н.П. Способ получения щелочных алкилксантогенатов спиртов C_5–C_7. А. с. 737397 СССР. Заявка № 2473114; заявл. 13.04.1977; опубл. 30.05.1980. Бюл. № 20.

14. Hummel K., Sherm A. Xanthates as antitumor agents: USA Pat. 4981869. 01.01.1991.

15. Трофимов Б.А., Иванова Н.И., Амосова С.В., Леонов С.Б., Белькова О.Н., Рогинская Л.В., Чеботарева Е.Г. Винилоксиэтилксантогенат калия как собиратель для флотации полиметаллических руд: А. с. 910615 СССР. Заявка № 2967113; заявл. 29.05.1980; опубл. 07.03.1982. Бюл. № 9.

16. Ларионов С.В., Косарева Л.А. Комплексообразующие свойства трифторэтилксантогенат-иона и летучесть его внутрикомплексных соединений. *Известия АН СССР. Серия химическая.* 1976;25(7):1451-1455.

17. Базанова Н.М., Лившиц А.К., Гурвич С.М. Способ флотационного обогащения медно-никелевых руд: А. с. 126816 СССР. Заяка № 628266/22; заявл. 18.05.1959; опубл. 1960. Бюл. № 6.

18. Gorgulu A.O., Celikkan H., Arslan M. The Synthesis, Characterization and Electrochemical Behavior of Transition Metal Complexes Containing Nitrogen Heterocyclic Sulphur Donor Ligand. *Acta Chim. Slov.* 2009;56:334-339.

19. Томиока М., Хасегава К. Стереоизомеры трициклодекан-9-ил ксантогената: Пат. 2470915 РФ. Заявка № 2010103459/04; заявл. 03.07.2008; опубл. 27.12.2012. Бюл. № 36.

20. Попов Ю.В., Долгачев А.С., Шишкин Е.В. Синтез диэтиламиноэтилового ксантогената калия. *Известия ВолгГТУ. Серия «Химия и технология элементоорганических мономеров и полимерных материалов».* 2015;(4):35-37.

About the authors:

Yuriy V. Popov, Dr. of Sci. (Chemistry), Professor, Head of the Department of Organic and Petrochemical Synthesis Technology, Volgograd State Technical University (28, pr. im. V.I. Lenina, Volgograd, 400005, Russia). E-mail: popov@vstu.ru. Scopus Author ID 26028090100, https://orcid.org/0000-0001-5659-028X

Aleksandr S. Dolgachev, Head of the Engineering Center, Volzhskii Orgsintez (100, Aleksandrova ul., Volzhskii, Volgograd oblast, 404117, Russia). E-mail: 30011@zos-v.ru.

Evgeniy V. Shishkin, Dr. of Sci. (Chemistry), Associate Professor, Dean of the Chemical Technology Faculty, Volgograd State Technical University (28, pr. im. V.I. Lenina, Volgograd, 400005, Russia). E-mail: shishkin@vstu.ru. Scopus Author ID 7003414557, https://orcid.org/0000-0002-2994-422X

Yuriy L. Zotov, Dr. of Sci. (Chemistry), Professor, Department of Organic and Petrochemical Synthesis Technology, Volgograd State Technical University (28, pr. im. V.I. Lenina, Volgograd, 400005, Russia). E-mail: ylzotov@mail.ru. Scopus Author ID 7003371961, https://orcid.org/0000-0001-6301-0570

Veniamin E. Shishkin, Dr. of Sci. (Chemistry), Professor, Department of Organic and Petrochemical Synthesis Technology, Volgograd State Technical University (28, pr. im. V.I. Lenina, Volgograd, 400005, Russia). E-mail: shishkin@vstu.ru. Scopus Author ID 7005233691, https://orcid.org/0000-0002-3485-4413

Об авторах:

Попов Юрий Васильевич, доктор химических наук, профессор, заведующий кафедрой технологии органического и нефтехимического синтеза Волгоградского государственного технического университета (400005, Россия, Волгоград, пр-т им. В.И.Ленина, 28). E-mail: popov@vstu.ru. Scopus Author ID 26028090100, https://orcid.org/0000-0001-5659-028X

Долгачев Александр Сергеевич, начальник инженерного центра АО «Волжский Оргсинтез» (404117, Россия, Волгоградская область, г. Волжский, ул. Александрова, 100). E-mail: 30011@zos-v.ru.

Шишкин Евгений Вениаминович, доктор химических наук, профессор кафедры «Технология органического и нефтехимического синтеза», декан химико-технологического факультета Волгоградского государственного технического университета (Россия, 400005, г. Волгоград, проспект им. В.И. Ленина, д. 28). E-mail: shishkin@vstu.ru. Scopus Author ID 7004314557, https://orcid.org/0000-0002-2994-422X

Зотов Юрий Львович, доктор химических наук, профессор кафедры «Технология органического и нефтехимического синтеза» Волгоградского государственного технического университета (Россия, 400005, г. Волгоград, проспект им. В.И. Ленина, д. 28). E-mail: ylzotov@mail.ru. Scopus Author ID 7003371961, https://orcid.org/0000-0001-6301-0570

Шишкин Вениамин Евгеньевич, доктор химических наук, профессор кафедры технологии органического и нефтехимического синтеза Волгоградского государственного технического университета (400005, Россия, Волгоград, пр-т им. В.И.Ленина, 28). E-mail: shishkin@vstu.ru. Scopus Author ID 7005233691, https://orcid.org/0000-0002-3485-4413

Submitted: October 08, 2019; Reviewed: February 03, 2020; Accepted: April 08, 2020.

Translated from Russian into English by S. Durakov

Edited for English language and spelling by Enago, an editing brand of Crimson Interactive Inc.

ISSN 2686-7575 (Online)
https://doi.org/10.32362/2410-6593-2020-15-2-38-46
UDC 544.31:[665.753.2+546.26]

Stacked-cup multiwall carbon nanotubes as components of energy-intensive suspension jet fuels

Larisa S. Karpushenkava@, Gennadii Ya. Kabo, Andrey V. Blokhin

Belarusian State University, Minsk, 220030 Republic of Belarus
@Corresponding author, e-mail: karpushenkava@bsu.by

Objectives. *The addition of high-density carbon materials to jet fuels can lead to a significant increase in the volumetric energy of the fuel combustion. The purpose of the current study was to thermodynamically analyze the possibility of obtaining model hydrocarbon fuels from toluene and T-1 using stacked-cup multiwall carbon nanotubes (MWCNTs).*

Methods. *Bomb combustion calorimetry was used to define the combustion energy of the MWCNTs in the crystalline state. The temperature dependence of the MWCNTs' heat capacity in the range 5–370 K and the fusion parameters were estimated using low-temperature adiabatic calorimetry. The physical density of MWCNTs was measured using the pycnometric method. The sedimentation stability of the mixtures of MWCNTs with liquids was determined using centrifugation at 7000 g. The calculations were carried out in MS Excel.*

Results. *The energy and enthalpy of combustion of a technical sample of MWCNTs in the crystalline state were determined. Based on the smoothed heat capacity values, the standard thermodynamic functions (enthalpy, entropy, and Gibbs reduced energy) of MWCNTs in the crystalline state were obtained in a temperature range of 0–2000 K. The extrapolation of the MWCNTs' heat capacity was carried out at a temperature of up to 2000 K using the heat capacity of crystalline graphite. It has been established that mixtures of MWCNTs with liquids containing more than 33 mass % of MWCNTs are stable during centrifugal sedimentation at 7000 g. For the toluene–MWCNTs and fuel T-1–MWCNTs model systems, the specific and volumetric combustion energies, the adiabatic combustion temperatures, and the conditional final maximum speed of the model rockets with fuel of various compositions were also calculated.*

Conclusions. *The thermodynamic analysis showed that the addition of MWCNTs can significantly increase the volumetric energy intensity of traditional jet fuels, which can in turn improve the operational characteristics of drones and rockets.*

Keywords: *model hydrocarbon fuel, energy intensity, cup multiwall carbon nanotubes, specific energy of combustion, volumetric energy of combustion, adiabatic combustion temperature, specific impulse, conditional final maximum speed, industrial implementation.*

For citation: Karpushenkava L.S., Kabo G.Ya., Blokhin A.V. Stacked-cup multiwall carbon nanotubes as components of energy-intensive suspension jet fuels. *Tonk. Khim. Tekhnol. = Fine Chem. Technol.* 2020;15(2):38-46. https://doi.org/10.32362/2410-6593-2020-15-2-38-46

Многослойные углеродные нанотрубки – компонент энергоемких суспензионных реактивных горючих

Л.С. Карпушенкова@, Г.Я. Кабо, А.В. Блохин

Белорусский государственный университет, Минск, 220030 Республика Беларусь
@Автор для переписки, e-mail: karpushenkava@bsu.by

Цели. *Добавление высокоплотных углеродных материалов в реактивные топлива может привести к значительному увеличению его объемной энергоемкости. Цель работы заключалась в проведении термодинамического анализа возможности получения модельных углеводородных топлив из толуола и Т-1 с многослойными углеродными нанотрубками (МУНТ).*
Методы. *Свойства МУНТ были исследованы при помощи следующих методов: энергия сгорания в кристаллическом состоянии определена методом бомбовой калориметрии, температурная зависимость теплоемкости в интервале 5–370 K – методом адиабатической калориметрии, физическая плотность – пикнометрическим методом, седиментационная устойчивость смесей с жидкостями – центрифугированием при 7000 g. Расчеты проводились в программе MS Excel.*
Результаты. *Определены энергия и энтальпия сгорания технического образца МУНТ в кристаллическом состоянии. На основании сглаженных значений теплоемкости получены стандартные термодинамические функции (энтальпия, энтропия и приведенная энергия Гиббса) МУНТ в кристаллическом состоянии в интервале 0–2000 K. Экстраполяция теплоемкости МУНТ до температуры 2000 K проведена с использованием теплоемкости кристаллического графита. Установлено, что смеси МУНТ с жидкостями, содержащими МУНТ более 33 масс. %, седиментационно устойчивы в центрифуге при 7000 g. Для модельных систем толуол–МУНТ, горючее Т-1–МУНТ вычислены массовые и объемные энергии сгорания, адиабатические температуры горения, условная конечная максимальная скорость модельных ракет с горючим различных составов.*
Выводы. *Термодинамический анализ показал, что добавление МУНТ существенно повышает объемную энергоемкость традиционных реактивных топлив, что должно приводить к улучшению эксплуатационных характеристик летательных аппаратов.*

Ключевые слова: *модельное углеводородное топливо, энергоемкость, многослойные углеродные нанотрубки, массовая теплота сгорания, объемная теплота сгорания, адиабатическая температура горения, удельный импульс, условная конечная максимальная скорость, промышленное внедрение.*

Для цитирования: Карпушенкова Л.С., Кабо Г.Я., Блохин А.В. Многослойные углеродные нанотрубки – компонент энергоемких суспензионных реактивных горючих. *Тонкие химические технологии.* 2020;15(2):38-46. https://doi.org/10.32362/2410-6593-2020-15-2-38-46

INTRODUCTION

The development of energy-intensive chemical fuels for unmanned aerial vehicles and various jet engines is undoubtedly an urgent task. Carbon materials, such as carbon black and C_{60} fullerite, are often used as components of energy-intensive liquid (pasty) and solid (reactive) fuels due to their high physical density, high combustion energy, and the formation of non-condensable products (CO_2) during combustion [1].

This paper presents the results of a study on the thermodynamic properties and density of a technical sample of multiwall carbon nanotubes (MWCNTs, *Vision Development*, Japan). Some of the commercial physicochemical and structural parameters of the investigated MWCNTs are outlined in Table 1.

Table 1. Physicochemical parameters of MWCNTs as provided by the supplier

Parameter	Value
Physical state	Black powder
Average length, m	$\leq(1–2) \times 10^{-6}$
Average inner diameter, m	$\sim 50 \times 10^{-9}$
Outer diameter, m	$(10–80) \times 10^{-9}$
Thermal stability, K	<973

Kabo *et al.* [2, 3] have demonstrated that the density and combustion energy of MWCNTs in terms of 100% carbon content are almost similar to the corresponding parameters of crystalline graphite (Table 2). Moreover, the physical density of MWCNTs is significantly higher than the density of carbon black and fullerite C_{60} (by 16 and 32%, respectively), indicating them as a promising component for the development of energy-intensive fuels in mixtures with hydrocarbons. Fullerite C_{60} has a higher (~ by 10%) specific energy of combustion [4, 5] than graphite and MWCNTs, whereas its physical density is significantly lower than that of graphite by about 30% (Table 2). Fullerite C_{60} is also slightly soluble in hydrocarbons, meaning that the internal cavity of the C_{60} molecules is not filled with liquids, thus presenting a low potential as a component of liquid fuels.

Given our earlier report that liquids with low molecular weight can fill the inner cavity of MWCNTs, while the sorption enthalpy of the liquid components (ionic liquids) is very small [7], this paper presents estimates of the energy efficiency of combustible toluene–MWCNTs and T-1–MWCNTs model systems.

MATERIALS AND METHODS

The density of the MWCNTs was measured in a glass pycnometer with a volume of 0.8876 ± 0.0009 cm^3 using bidistilled water (ρ = 998.3 $kg \cdot m^{-3}$) (292 K) [3] and freshly distilled toluene (ρ = 867.8 $kg \cdot m^{-3}$) [2] as pycnometric liquids. A pycnometer filled with nanotubes and a pycnometric fluid was heated in boiling water and, after cooling to ~293 K without contact with air, was filled to the mark with a pycnometric fluid and weighed. The average physical density of MWCNTs was 2210 ± 22 $kg \cdot m^{-3}$ [2], which practically corresponds to the density of hexagonal graphite 2265 $kg \cdot m^{-3}$ [6]. Moreover, the bulk density of MWCNTs has been reported to be approximately 400 $kg \cdot m^{-3}$ [2].

The combustion enthalpy of a technical sample of MWCNTs was determined in an automated combustion calorimeter [8] with a 326 cm^3 calorimetric bomb and an energy equivalent of 14605 ± 3 $J \cdot K^{-1}$. The MWCNTs samples were dried at 130 and 200°C under vacuum ($P \approx 100$ Pa). According to the results of burning in a calorimetric bomb, the ash content in the MWCNTs was estimated to be 0.88 ± 0.07%, which corresponds to 0.69% of nickel metal used as a synthetic catalyst. It was also shown that metallic nickel cannot be removed from the MWCNTs neither by magnetic separation nor by dissolution in nitric acid within 24 h. According to the results that were obtained after burning the vacuum-dried technical samples of MWCNTs in plastic bags with cotton thread for ignition, the average combustion energy was determined as $\Delta_c U°(298.15\ K) = -(32336 \pm 13)\ kJ \cdot kg^{-1}$ [2].

The heat capacity of a technical sample of MWCNTs in the range of 5–370 K was measured in a TAU-10 adiabatic calorimeter [8]. It has also been shown in [2, 3] that the heat capacity of MWCNTs, graphite, and fullerites C_{60}, C_{70} in a temperature range of 300–350 K differs only by 3%. The extrapolation of the specific heat C_p of the technical sample $MWCNT_{tech}$ from 400 to 2000 K was carried out by the equation:

$$C_p(MWCNT_{tech.}, T(K)) = 0.9931 C_p(graphite, T(K)) + \\ + 0.0069 C_p\ (Ni(cat.)) \times T(K) \qquad (1)$$

The thermodynamic properties of the technical sample of MWCNTs in the range 0–2000 K are presented in Table 3.

RESULTS AND DISCUSSION

Physical and chemical properties of the MWCNTs–liquids (ionic and nonionic) mixtures

In a detailed study of the interaction of ionic and nonionic liquids with MWCNTs [7], it was found that nonionic liquids (toluene and water) penetrate the

Table 2. Combustion energy $-\Delta_c U°(298.15\ K)$ and density ρ of crystalline graphite, MWCNTs, and fullerite C_{60}

Property	Crystalline graphite	MWCNTs	C_{60}
$-\Delta_c U°(298.15\ K)$, $kJ \cdot kg^{-1}$	32764 ± 4[1]	32336 ± 13 [2]	35802 [4]
ρ (298.15 K), $kg \cdot m^{-3}$	2265 [6]	2210 ± 22 [2]	1720 [4]

---

[1] NIST Chemistry Webbook, SRD 69. Available from: webbook.nist.gov/chemistry/ [Accessed March 15, 2019]. https://doi.org/10.18434/T4D303

inner cavity of the MWCNTs when mixed at 293 K and $P = 1$ bar. In comparison, ionic liquids (IL) do not penetrate into the internal cavity of the MWCNTs at atmospheric pressure, but they completely penetrate into a MWCNT under vacuum conditions, thus allowing the determination of the cavity volume. Moreover, the enthalpy of mixing MWCNTs with ILs (e.g., 1-butyl-3-methylimidazolium hexafluorophosphate) does not exceed the sensitivity of the mixing calorimeter [7, 8]. Finally, it was demonstrated that the sedimentation stability of the MWCNT–IL systems during centrifugation at 7000 *g* depends on the components' ratio. In particular, at a mass content of MWCNTs ≥ 0.33 in the mixture, no separation of the systems was observed, implying that systems containing MWCNTs that exceed the bulk density are stable in sedimentation. Furthermore, based on computer simulations [9], it was established that the packing density (φ) of figures of different geometry depends slightly on their configuration and has a mean value of 0.58, which allows the estimation of the formation of the T-1–MWCNTs and toluene–MWCNTs compositions with a mass fraction of up to ω = 0.75.

Certain technical characteristics of the suspension fuel type C_nH_m–MWCNTs

The physicochemical and thermodynamic properties of the suspension fuel type C_nH_m–MWCNTs can be calculated based on the additivity of the corresponding compositions (Tables 4–6).

Table 3. Thermodynamic functions (standard heat capacities, entropies, enthalpies and Gibbs reduced energy) of MWCNTs (99.31 mass % C, 0.69 mass % Ni)

*T**, K	C_p^o, J·kg^{-1}·K^{-1}	$\Delta_0^T S^o$, J·kg^{-1}·K^{-1}	$\Delta_0^T H^o$, kJ·kg^{-1}	Φ^o, J·kg^{-1}·K^{-1}
0	0	0	0	0
50	51.91	28.62	0.9388	9.846
100	158.5	95.64	6.082	34.82
150	290.2	184.0	17.20	69.32
200	437.8	287.5	35.36	110.7
250	591.6	401.7	61.10	157.3
298.15	733.7	518.1	93.04	206.1
300	739.0	522.7	94.40	208.0
370	932.0	697.5	153.0	284.0
400*	932.0	697.5	153.0	284.0
500	1261	1027	296.3	434.3
600	1453	1274	432.3	553.9
700	1598	1510	585.1	673.8
800	1710	1731	750.6	792.4
900	1796	1937	926.0	908.3
1000	1864	2130	1109	1021
1100	1921	2311	1298	1130
1200	1961	2480	1492	1236
1300	2009	2639	1691	1338
1400	2051	2789	1894	1436
1500	2092	2932	2101	1531
1600	2113	3068	2311	1623
1700	2134	3197	2524	1712
1800	2900	3340	2775	1798
1900	3004	3499	3070	1883
2000	2175	3633	3329	1968

*The thermodynamic properties of MWCNTs at 400–2000 K were extrapolated according to equation (1).

Table 4. Physicochemical properties of the fuel components

Component	Composition	M, g·mol^{-1}	ρ, kg·m^{-3}	$-\Delta_c H°(298.15)^*$, kJ·kg^{-1}	$-\Delta_c H°(298.15)^*$, MJ·m^{-3}
MWCNTs [2]	$CNi_{0.0014}$	12.094	2210	32336	71463
Toluene [1]	C_7H_8	92.141	867.1	40963	35519
Combustible T-1 [1]	$C_{12.8}H_{24.12}$	178.05	800	42900	34320
Carbon black [1]	C	12.011	1900	32781	62284

[*] Net calorific value.

Table 5. Lower enthalpies of combustion for the toluene–MWCNTs mixtures in stoichiometric quantities of oxygen and air at 298.15 K and P = 1 bar

ω(MWCNTs), mass fract.	Combustible combustion enthalpy		Fuel combustion enthalpy		
			with oxygen		with air
	$-\Delta_c H°$, MJ·kg^{-1}	$-\Delta_c H°$, MJ·dm^{-3}	$-\Delta_c H°$, MJ·kg^{-1}	$\Delta_c H°^*$, MJ·dm^{-3}	$-\Delta_c H°$, MJ·kg^{-1}
0	40.96	35.52	9.929	10.52	2.825
0.10	40.10	37.02	9.834	10.60	2.805
0.20	39.24	38.73	9.737	10.69	2.785
0.30	38.37	40.69	9.637	10.78	2.764
0.40	37.51	42.97	9.535	10.88	2.743
0.50	36.65	45.65	9.430	10.99	2.721
0.75	34.49	54.95	9.156	11.29	2.663

[*]When calculating the fuel density, the liquid oxygen density was considered to be $\rho(O_2)$ = 1140 kg·m^{-3} [1].

Table 6. Lower enthalpies of combustion for the T-1–MWCNTs mixtures in stoichiometric quantities of oxygen and air at 298.15 K and P = 1 bar

ω(MWCNTs), mass fract.	Combustible combustion enthalpy		Fuel combustion enthalpy		
			with oxygen		with air
	$-\Delta_c H°$, MJ·kg^{-1}	$-\Delta_c H°$, MJ·dm^{-3}	$-\Delta_c H°$, MJ·kg^{-1}	$\Delta_c H°^*$, MJ·dm^{-3}	$-\Delta_c H°$, MJ·kg^{-1}
0	42.90	34.32	9.786	10.17	2.747
10	41.84	35.76	9.708	10.27	2.735
20	40.79	37.40	9.627	10.38	2.722
30	39.73	39.31	9.544	10.50	2.710
40	38.67	41.54	9.457	10.62	2.696
50	37.62	44.19	9.367	10.76	2.682
75	34.98	53.66	9.128	11.15	2.643

[*]When calculating the fuel density, the liquid oxygen density was considered to be $\rho(O_2)$ = 1140 kg·m^{-3} [1].

In contrast, the calculation of the density of the mixtures of liquid fuels and MWCNTs does not obey the rules of additivity. Therefore, the density was determined as the ratio of the mass of the mixture to the sum of the volumes of the components included in the mixture, taking into account the composition.

The conventional adiabatic combustion temperatures (T_{ad}) were determined using the heat capacities of gaseous CO_2, H_2O, N_2, and Ar,[2,3] as follows:

$$-\Delta_c H_{298.15} = \int\limits_{298.15}^{T_{ad}} a_i C_{p,i} dT\,, \qquad (2)$$

where $\Delta H_{298.15}$ is the net calorific value of the fuel in air, a_i represents the mole fractions of the components of the fuel gases in the mixture, and $C_{p,i}$ is the heat capacity of the components in J·mol^{-1}·K^{-1}. The fuel gases consisted of CO_2, H_2O, N_2, and Ar, provided that there was no dissociation and conversion of combustion products. The composition of the air components was obtained from the State Standard[4] and the calculation results are presented in Table 7.

To assess the efficiency of the fuels including MWCNTs, the final gas flow rate (conditional specific impulse (m·s^{-1})) was calculated [10, 11] based on the following formula (3),

$$I_{spec} = W = \sqrt{2(-\Delta_c H) n_t}\,,\ \text{m} \cdot \text{s}^{-1}\,, \qquad (3)$$

where $\Delta_c H$ is the lower enthalpy of fuel combustion with a stoichiometric amount of oxidizing agent (J·kg^{-1}), and n_t is the thermal effective efficiency rocket engine determined by the ratio:

Table 7. Physicochemical characteristics of the combustible suspensions' toluene*–MWCNTs and T-1**–MWCNTs

Property	Mass fraction ω(MWCNTs) in fuel					
	0	**0.20**	**0.30**	**0.40**	**0.50**	**0.75**
toluene*–MWCNTs						
ρ, kg·m^{-3}	867.1	987.1	1060	1146	1246	1593
T_{ad}, K (in O_2)	6227	6302	6343	6387	6433	6565
T_{ad}, K (in the air)	2507	2496	2491	2486	2480	2465
I_{spec}, m·s^{-1}	2004	1990	1983	1975	1967	1946
P_{spec}, s	204.4	202.9	202.2	201.4	200.6	198.4
V_{max}, m·s^{-1}	4615	4816	4928	5049	5181	5574
T-1–MWCNTs**						
ρ, kg·m^{-3}	800	917	989	1074	1175	1534
T_{ad}, K (in O_2)	5738	5870	5944	6025	6114	6378
T_{ad}, K (in the air)	2408	2413	2417	2421	2425	2436
I_{spec}, m·s^{-1}	1977	1969	1984	1959	1954	1940
P_{spec}, s	201.6	200.7	202.3	199.7	199.2	197.8
V_{max}, m·s^{-1}	4553	4776	4950	5037	5186	5634

*toluene: C_7H_8; M = 92.1 g·mol^{-1}; $C°_{298.15}$ = 1693 J·kg^{-1}·K^{-1} [1].
**combustible T-1: $C_{12.8}H_{24.12}$; M = 178.1 g·mol^{-1}; $C°_{298.15}$ = 1921 J·kg^{-1}·K^{-1} [1].

---

[2] NIST Chemistry Webbook, SRD 69. Available from: webbook.nist.gov/chemistry/ [Accessed March 18, 2019] https://doi.org/10.18434/T4D303

[3] IVTANTERMO Database. Available from: http://www.chem.msu.ru/rus/handbook/ivtan/ [Accessed 18.03.2019] (in Russ.).

[4] GOST 4401-81. Standard atmosphere. Parameters. Moscow: Publishing House of Standards; 1981. 179 p. (in Russ.).

$$n_t = 1 - \left(\frac{P_0}{P}\right)^{\frac{k-1}{k}}, \quad (4)$$

where P and P_0 represent the pressure in the combustion chamber and at the nozzle exit, respectively (it is assumed that $P_0/P = 0.01$), and k is the adiabatic exponent, which depends on the molecular masses of the combustion products ($k = C_p/C_v$), provided that $k(T)$ = const. For mixtures of combustion products, the heat capacity was calculated as $C_p = \Sigma a_i C_{p,i}$, where a_i is the mole fraction of the component in the mixture and $C_{p,i}$ is the heat capacity of the component. Then, in the ideal gas approximation, $C_v = C_p - R$ applies.

Moreover, the specific thrust could be calculated by the following formula:

$$P_{\text{spec}} = \frac{I_{\text{spec}}}{g}, \text{ s}, \quad (5)$$

where g is the acceleration of gravity.

The conditional final (maximum) speed of the aircraft (m·s^{-1}) at the time of the combustion completion without taking into account the gravity and aerodynamic drag was calculated by the Tsiolkovsky ratio:

$$V_{\max} = I_{\text{spec}} \ln Z, \quad (6)$$

где $Z = 1 + \frac{m_{\text{fuel}}}{m_{\text{str}}}$; m_{fuel} is the mass of the fuel (kg), and m_{str} is the mass of the structure without fuel (kg). The parameter ln$Z$ was defined for a model rocket with mass ($m_{\text{fuel}} + m_{\text{str}}$) = 1000 kg without MWCNTs (ω = 0) and a constant m_{str} of 100 kg. The volume of the fuel tank (V_t) in this model was 900/ρ_{fuel}. Accordingly, the volume for toluene $V_т'$ was 1.0379 m^3 and that for fuel T-1 $V_т''$ = 1.125 m^3. The dependence of the parameter ln$Z$ on the mass fraction of nanotubes is shown in the following figure.

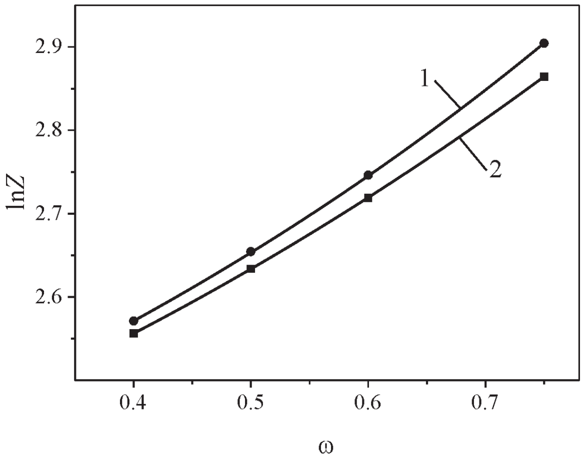

Dependence of the parameter lnZ on the mass fraction of nanotubes:
1) for the mixture T-1–MWCNTs,
2) for the mixture toluene–MWCNTs.

CONCLUSIONS

The calculations indicated that for fuels with MWCNTs, the conditional maximum speed of the model system increases by 24–26% at ω = 0.75, which will probably lead to a corresponding increase in the flight range of the aircraft. The report that catalysts based on carbon nanotubes with metal and oxide nanoparticles can control the burning rate [12], increases the potential of carbon nanotubes as components of energy-intensive fuels and arouses interest in such systems. However, their practical application requires further research, while additional technically important properties, such as viscosity, burning rate, etc., need to be investigated as well.

The authors declare no conflicts of interest.

REFERENCES

1. Sorokin V.A., Frantskevich V.P., Yanovskii L.S., Bakulin V.N., Dubovkin N.F., Kotova V.N. *Energoemkie goryuchie dlya aviatsionnykh i raketnykh dvigatelei* (Energy-intensive fuels for aircraft and rocket engines). Moscow: Fizmatlit; 2009. 400 p. (in Russ.). ISBN 978-5-9221-1091-4

2. Kabo G.J., Paulechka E., Blokhin A.V., Voitkevich O.V., Liavitskaya T., Kabo A.G. Thermodynamic Properties and Similarity of Stacked-Cup Multiwall Carbon Nanotubes and Graphite. *J. Chem. Eng. Data.* 2016;61(11):3849-3857. https://doi.org/10.1021/acs.jced.6b00525

СПИСОК ЛИТЕРАТУРЫ

1. Сорокин В.А., Францкевич В.П., Яновский Л.С., Бакулин В.Н., Дубовкин Н.Ф., Котова В.Н. Энергоемкие горючие для авиационных и ракетных двигателей. М.: Физматлит, 2009. 400 с. ISBN 978-5-9221-1091-4

2. Kabo G.J., Paulechka E., Blokhin A.V., Voitkevich O.V., Liavitskaya T., Kabo A.G. Thermodynamic Properties and Similarity of Stacked-Cup Multiwall Carbon Nanotubes and Graphite. *J. Chem. Eng. Data.* 2016;61(11):3849-3857. https://doi.org/10.1021/acs.jced.6b00525

3. Kabo G.J., Blokhin A.V., Paulechka Y.U., Boitkevich O.V., Levitskaya T.N. Thermodynamic similarity of stacked-cup multiwall carbon nanotubes and graphite. *Sviridovskie Chteniya = Sviridov Readings. Iss. 11*. Minsk: BSU Publing House; 2015. P. 60-67. (in Russ.). URL:
http://elib.bsu.by/handle/123456789/223236

4. Sidorov L.N., Yurovskaya M.A., Borshchevskii A.Ya., Trushkov I.V., Ioffe I.N. *Fullereny: Uchebnoe posobie* (Fullerenes: Study Guide). Moscow: Ekzamen; 2005. 688 p. (in Russ.). ISBN 5-472-00294-X

5. Diky V.V., Kabo G.J. Thermodynamic properties of C_{60} and C_{70} fullerene. *Russ. Chem. Rev*. 2000;69(2):95-104. https://doi.org/10.1070/RC2000v069n02ABEH000535

6. Howe J.Y., Rawn C.J., Jones L.E. Ow H. Improved crystallographic data for graphite. *Powder Diffr.* 2003;18(2):150-154.
https://doi.org/10.1154/1.1536926

7. Shevelyova M.P., Paulechka Y.U., Kabo G.J. Blokhin A.V., Kabo A.G., Gubarevich T.M. Physicochemical Properties of Imidazolium-based Ionic Nanofluids: Density, Heat Capacity, and Enthalpy of Formation. *J. Phys. Chem. C.* 2013;117(9):4782-4790.
https://doi.org/10.1021/jp3059432

8. Kabo G.J., Blokhin A.V., Paulechka E. Roganov G.N., Frenkel M., Yursha I.A., Diky V., Zaitsau D., Bazyleva A., Simirsky V.V., Karpushenkava L.S., Sevruk V.M. Thermodynamic properties of organic substances: Experiment, modeling, and technological applications. *J. Chem. Thermodyn.* 2019;131:225-246.
https://doi.org/10.1016/j.jct.2018.10.025

9. Mizgulin V.V., Kadushnikov R.M., Alievsky D.M., Alievsky V.M. The modeling of dense materials with spherepolyhedra packing method. *Komp'yuternye issledovaniya i modelirovanie = Computer Research and Modeling.* 2012;4(4):757-766 (in Russ.). https://doi.org/10.20537/2076-7633-2012-4-4-757-766

10. Egorychev V.S., Kondrusev V.S. *Topliva khimicheskikh raketnykh dvigatelei* (Fuel chemical rocket engines). Samara: Samara National Research University Publishing House; 2007. 72 p. (in Russ.). ISBN 978-5-7883-0512-7

11. Paushkin Ya.M. *Zhidkie i tverdye khimicheskie raketnye topliva* (Liquid and solid chemical rocket fuels). Moscow: Nauka; 1978. 192 p. (in Russ.).

12. Zhao F., Yi J., Hong W., An T. Yang Y. Preparation, Characterization, and Catalytic Activity of Carbon Nanotubes-Supported Metal or Metal Oxide. In: Energetic Nanomaterials. Synthesis, Characterization and Application, Ch. 10. Amsterdam: Elsevier; 2016. P. 231-284.
https://doi.org/10.1016/B978-0-12-802710-3.00010-6

3. Кабо Г.Я., Блохин А.В., Павлечко Е.В., Войткевич О.В., Левицкая Т.Н. Термодинамическое подобие многослойных конических нанотрубок и графита. *Свиридовские чтения*: сб. ст. Вып. 11. Минск: БГУ, 2015. С. 60-67. URL:
http://elib.bsu.by/handle/123456789/223236

4. Сидоров Л.Н., Юровская М.А., Борщевский А.Я., Трушков И.В., Иоффе И.Н. Фуллерены: Учебное пособие. М.: Экзамен; 2005. 688 с. ISBN 5-472-00294-X

5. Diky V.V., Kabo G.J. Thermodynamic properties of C_{60} and C_{70} fullerene. *Russ. Chem. Rev.* 2000;69(2):95-104.
https://doi.org/10.1070/RC2000v069n02ABEH000535

6. Howe J.Y., Rawn C.J., Jones L.E. Ow H. Improved crystallographic data for graphite. *Powder Diffr.* 2003;18(2):150-154.
https://doi.org/10.1154/1.1536926

7. Shevelyova M.P., Paulechka Y.U., Kabo G.J. Blokhin A.V., Kabo A.G., Gubarevich T.M. Physicochemical Properties of Imidazolium-based Ionic Nanofluids: Density, Heat Capacity, and Enthalpy of Formation. *J. Phys. Chem. C.* 2013;117(9):4782-4790.
https://doi.org/10.1021/jp3059432

8. Kabo G.J., Blokhin A.V., Paulechka E. Roganov G.N., Frenkel M., Yursha I.A., Diky V., Zaitsau D., Bazyleva A., Simirsky V.V., Karpushenkava L.S., Sevruk V.M. Thermodynamic properties of organic substances: Experiment, modeling, and technological applications. *J. Chem. Thermodyn.* 2019;131:225-246.
https://doi.org/10.1016/j.jct.2018.10.025

9. Мизгулин В.В., Кадушников Р.М., Алиевский Д.М. Алиевский В.М. Моделирование плотных материалов методом упаковки сферополиэдров. *Компьютерные исследования и моделирование.* 2012;4(4):757-766.
https://doi.org/10.20537/2076-7633-2012-4-4-757-766

10. Егорычев В.С., Кондрусев В.С. Топлива химических ракетных двигателей. Самара: Изд. СГАУ; 2007. 72 с. ISBN 978-5-7883-0512-7

11. Паушкин Я.М. Жидкие и твердые химические ракетные топлива. М.: Наука; 1978. 192 с.

12. Zhao F., Yi J., Hong W., An T. Yang Y. Preparation, Characterization, and Catalytic Activity of Carbon Nanotubes-Supported Metal or Metal Oxide. In: Energetic Nanomaterials. Synthesis, Characterization and Application, Ch. 10. Amsterdam: Elsevier; 2016. P. 231-284.
https://doi.org/10.1016/B978-0-12-802710-3.00010-6

About the authors:

Larisa S. Karpushenkava, Cand. of Sci. (Chemistry), Associate Professor, Associate Professor of the Department of Physical Chemistry, Belarusian State University (14, Leningradskaya ul., Minsk, 220030, Republic of Belarus). E-mail: karpushenkava@bsu.by. Scopus Author ID 6504468775, ResearcherID AAB-8934-2020, https://orcid.org/0000-0002-8875-5568

Gennadii Ya. Kabo, Dr. of Sci. (Chemistry), Professor, Professor of the Department of Physical Chemistry, Belarusian State University (14, Leningradskaya ul., Minsk, 220030, Republic of Belarus). E-mail: kabo@bsu.by. Scopus Author ID 56261611100

Andrey V. Blokhin, Dr. of Sci. (Chemistry), Professor, Head of the Department of Physical Chemistry, Belarusian State University (14, Leningradskaya ul., Minsk, 220030, Republic of Belarus). E-mail: blokhin@bsu.by. Scopus Author ID 7101971167, ResearcherID AAF-8122-2019, https://orcid.org/0000-0003-4778-5872

Об авторах:

Карпушенкова Лариса Степановна, кандидат химических наук, доцент, доцент кафедры физической химии Белорусского государственного университета (Республика Беларусь, 220030, Минск, ул. Ленинградская, д. 14). E-mail: karpushenkava@bsu.by. Scopus Author ID 6504468775, ResearcherID AAB-8934-2020, https://orcid.org/0000-0002-8875-5568

Кабо Геннадий Яковлевич, доктор химических наук, профессор, профессор кафедры физической химии Белорусского государственного университета (Республика Беларусь, 220030, Минск, ул. Ленинградская, д. 14). E-mail: kabo@bsu.by. Scopus Author ID 56261611100

Блохин Андрей Викторович, доктор химических наук, профессор, заведующий кафедрой физической химии Белорусского государственного университета (Республика Беларусь, 220030, Минск, ул. Ленинградская, д. 14). E-mail: blokhin@bsu.by. Scopus Author ID 7101971167, ResearcherID AAF-8122-2019, https://orcid.org/0000-0003-4778-5872

Submitted: January 30, 2020; Reviewed: March 16, 2020; Accepted: April 11, 2020.

Translated from Russian into English by H. Moshkov

Edited for English language and spelling by Enago, an editing brand of Crimson Interactive Inc.

ISSN 2686-7575 (Online)

https://doi.org/10.32362/2410-6593-2020-15-2-47-55

UDC 661.74, 66.097, 66.091

Esterification of malic acid on various catalysts

Natalia S. Kuzmina[@], Svetlana V. Portnova, Eugen L. Krasnykh

Samara State Technical University, Samara, 443100 Russia
[@]Corresponding author, e-mail: kusminans@yandex.ru

Objectives. *The study aims to identify the optimal choice of an effective catalyst for the esterification of malic acid to produce esters of high purity.*
Methods. *To determine the qualitative and quantitative composition of reaction masses, the following analysis methods were used: mass spectroscopy (using FinniganTrace DSQ device with NIST 2002, Xcalibur 1.31 Sp 5 database) and gas–liquid chromatography (using the Kristall 2000M software and hardware complex).*
Results. *Esters of malic acid and butyl alcohol of normal structure were synthesized using the following catalysts: sulfuric, orthophosphoric, p-toluenesulfonic acid, Amberlyst 36 Dry, Amberlyst 36 Wet, KU-2-FPP, and KIF-T. The obtained products were analyzed by gas–liquid chromatography. The structure of the products was confirmed by mass spectrometry. Schemes for the formation of byproducts are proposed. The yields and purity of the malic acid butyl esters obtained using different catalysts were evaluated. The results show that the heterogeneous catalyst Amberlyst 36 Dry is optimal for obtaining a pure malic acid ester with a maximum yield.*
Conclusions. *The results show that during the esterification of malic acid with butyl alcohol of normal structure, byproducts, such as esters of fumaric and maleic acids, are formed using different catalysts. An accumulation of byproducts occurs as a result of reactions of dehydration of malic acid or its ester. The results also show that the number of byproducts is almost independent of the catalyst, with the exception of sulfuric acid. The Amberlyst 36 Dry catalyst provides an optimal ratio between conversion and selectivity for malic acid dibutyl ester production.*

Keywords: *esterification, esters, malic acid, n-butanol, Amberlyst 36 Dry.*

For citation: Kuzmina N.S., Portnova S.V., Krasnykh E.L. Esterification of malic acid on various catalysts. *Tonk. Khim. Tekhnol. = Fine Chem. Technol.* 2020;15(2):47-55. https://doi.org/10.32362/2410-6593-2020-15-2-47-55

Этерификация яблочной кислоты на различных катализаторах

Н.С. Кузьмина@, С.В. Портнова, Е.Л. Красных

Самарский государственный технический университет, Самара, 443100 Россия
@Автор для переписки, e-mail: kusminans@yandex.ru

Цели. *Обосновать выбор эффективного катализатора этерификации яблочной кислоты для получения сложных эфиров высокой степени чистоты.*
Методы. *Для определения качественного и количественного состава реакционных масс были использованы следующие методы анализа: масс-спектроскопия (на приборе FinniganTrace DSQ с базой NIST 2002, Xcalibur 1.31. Sp 5) и газожидкостная хроматография (на аппаратно-программном комплексе «Кристалл 2000М»).*
Результаты. *Синтезированы сложные эфиры яблочной кислоты и бутилового спирта нормального строения на следующих катализаторах: серная, ортофосфорная, n-толуолсульфокислота, Amberlyst 36 Dry, Amberlyst 36 Wet, КУ-2-ФПП и КИФ-Т. Полученные продукты проанализированы методом газожидкостной хроматографии. Строение продуктов подтверждено масс-спектрометрическим методом. Предложены схемы образования побочных продуктов. Оценены выходы и чистота бутилового эфира яблочной кислоты, полученного на разных катализаторах. Показано, что для получения чистого сложного эфира яблочной кислоты с максимальным выходом оптимальным является гетерогенный катализатор Amberlyst 36 Dry.*
Выводы. *Установлено, что при этерификации яблочной кислоты бутиловым спиртом нормального строения на разных катализаторах образуются побочные продукты – сложные эфиры фумаровой и малеиновой кислот. Накопление побочных продуктов происходит в результате реакций дегидратации яблочной кислоты или его сложного эфира. Показано, что количество побочных продуктов практически не зависит от катализатора, за исключением серной кислоты. Для получения дибутилового эфира яблочной кислоты рекомендуется использовать сульфокатионит Amberlyst 36 Dry, обеспечивающий оптимальное соотношение между конверсией и селективностью.*

Ключевые слова: *этерификация, сложные эфиры, яблочная кислота, н-бутанол, Amberlyst 36 Dry.*

Для цитирования: Кузьмина Н.С., Портнова С.В., Красных Е.Л. Этерификация яблочной кислоты на различных катализаторах. *Тонкие химические технологии.* 2020;15(2):47-55. https://doi.org/10.32362/2410-6593-2020-15-2-47-55

INTRODUCTION

Modern trends within the chemical industry have been aimed at finding processes that are independent from oil and petroleum products. Great interest is shown in materials obtained from renewable sources of raw materials [1], such as alcohols and carboxylic acids.

Today, esters are in high demand in the production of paints, plasticizers, copolymers, various additives to lubricants, and pharmaceuticals. Esters of hydroxycarboxylic acids obtained from renewable natural resources are of particular interest. For example, trisubstituted citric acid esters-trialkylcitrates, obtained by esterification of citric acid with aliphatic alcohols C_2 and C_4, are used as non-toxic plasticizers for PVC products or solvents in the production of food additives, children’s toys, and household packaging [2]. Plasticizers based on citric acid esters are environmentally friendly and have a high plasticizing ability. Another promising industrial product, completely obtained from plant components, is the ester of malic acid and *n*-butyl alcohol. Malic acid is a dibasic oxocarboxylic acid and is used as an additive in the food industry and in medicine. There are known methods for obtaining malic acid from vegetable raw materials, such as unripe apples, sea buckthorn, and cotton leaves as well as and from chemical methods, such as the catalytic hydration of maleic or fumaric acid, which are derived from maleic anhydride.

This process is catalyzed by fumarate hydratase or fumarase. Maleic anhydride, in turn, is obtained by the oxidation of hydrocarbons, primarily butane [3]. Fumaric acid can also be obtained from various enzymatic hydrolysates of cellulose-containing raw materials under the action of a biocatalyst [4]. *n*-Butyl alcohol is used in the paint industry as a solvent as well as in the production of resins, plasticizers, and many other organic compounds. It can be obtained from chemically raw materials or by processing sucrose, starch, or cellulose from agricultural crops [5].

The simplest method for producing esters is direct esterification of acids with alcohols in the presence of a catalyst [6]. Esterification of dicarboxylic acids with alcohols can be performed without a catalyst; however, the reaction proceeds slowly, and high temperatures (200–300°C) are required to achieve sufficient speed [7]. For the esterification of dicarboxylic acids, a process involving mineral acids (sulfuric, hydrochloric, orthophosphoric, boric), alkylsulfonic acids (benzene or *p*-toluene sulfonic acids) and arylsulfochloride as catalysts are used [8−10]. Further, organic titanium compounds are also highly active [11], and recently, heterogeneous catalysts have been used in the production of esters [12–14].

In industrial applications, the liquid phase method of esterification is widely used in periodic- or continuous-motion equipment. The main stages of the liquid phase method are esterification, neutralization of the reaction mass, washing from a homogeneous catalyst, and rectification [15]. However, in order to simplify the design of technology used to obtain esters, the use of heterogeneous catalysts simplifies the process by eliminating the stages of neutralization, washing, and drying, and it also helps to reduce the loss of organic acid. Additionally, heterogeneous catalysts are easily regenerated, allowing them to be used repeatedly. It is also important to reduce the number of generated byproducts, which will reduce energy consumption at the stage of rectification.

Several studies have researched the possibility of obtaining malic acid esters by esterification using homogeneous catalysts [16–18]; however, there are no data on the esterification of malic acid using heterogeneous catalysts. Thus, the aim of this work is to select an effective heterogeneous catalyst for the esterification of malic acid to produce esters of high purity.

MATERIALS AND METHODS

To synthesize esters, racemic DL-malic acid was used with a base substance concentration of at least 99.3%, along with CP grade *n*-butyl alcohol with a purity of at least 99.8%. AR grade benzene was used as an azeotroping agent. As catalysts, this experiment used concentrated sulfuric acid (98% solution), CP grade orthophosphoric acid with a purity of at least 85%, pure grade *p*-toluenesulfonic acid, KU-2 FPP, KIF-T, and sulfocationic catalysts Amberlyst 36 Dry and Amberlyst 36 Wet.

Before synthesis, *p*-toluenesulfonic acid was purified in a similar method as in [19]. The catalysts KU-2 FPP (moisture content no more than 30%) and KIF-T (moisture content no more than 30–60%) were crushed to the size of 1–2 mm and used without additional drying. Amberlyst 36 Dry (water content no more than from 1.5 to 2%) and Amberlyst 36 Wet (moisture content no more than 53−59%) were also used without additional drying.

Esterification of *n*-butyl alcohol with malic acid proceeded according to the scheme in Reaction 1.

A 250 ml round-bottom flask equipped with a Din–Stark trap and a Liebig condenser was filled with 10 g (0.07 mol) of malic acid, 4× molar excess volume of alcohol (22 ml of *n*-buthanol), 40 ml of benzene, and 1 wt % of the tested catalyst. The resulting mixture was boiled with azeotropic distillation of water until the reaction ended. When using a homogeneous catalyst, the reaction mixture was first washed with a solution of sodium bicarbonate to neutralize the acid, then with distilled water to a neutral pH. When using a heterogeneous catalyst, it was filtered. The resulting reaction mass was distilled at a residual pressure

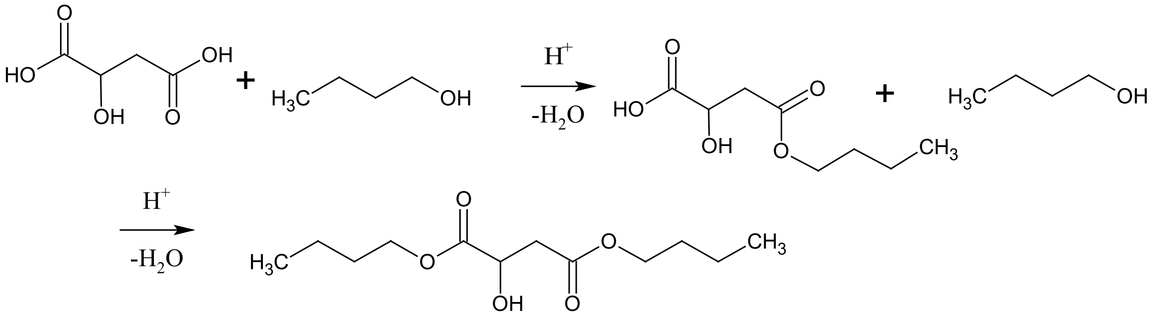

Reaction 1

of 50 mm Hg for separation of benzene and excess butyl alcohol. Pure ester was extracted by fractional distillation at a residual pressure of 13–15 mmHg. The boiling point of dibutyl ester of malic acid is 185–186°C.

RESULTS AND DISCUSSION

The analysis of the reaction mass and the obtained esters was performed using gas–liquid chromatography on the Chromatec Analytic Kristall-2000M chromatograph, equipped with a flame ionization detector and a capillary column with a grafted non-polar phase DB-1, 100 m × 0.2 mm × 0.5 µm. The analysis parameters were as follows:

1) The column temperature was 150°C during the first 20 min, then the column temperature rose up to 260°C with a heating rate of 5°C per minute.
2) The injector temperature was 250°C.
3) The detector temperature was 280°C.
4) The carrier gas was helium, split ratio 1/40.

The sample volume is 1 µl.

A typical chromatogram of malic acid dibutyl ester is shown in Fig. 1.

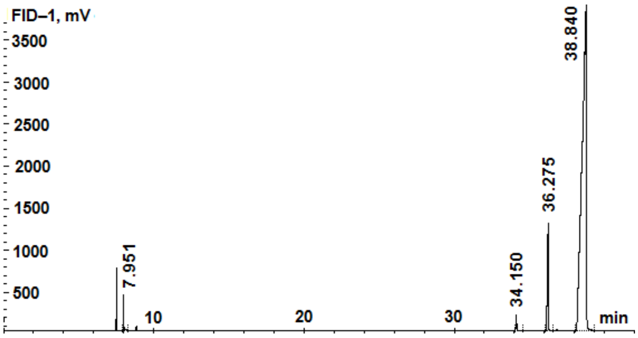

Fig. 1. Chromatogram of malic acid dibutyl ester.

The chromatogram clearly shows two peaks next to the main product. To identify these peaks, an analysis was conducted using a Finnigan Trace DSQ mass spectrometer via electron impact ionization, set at 70 eV, using the National Institute of Standards and Technology (NIST) 2002, Xcalibur 1.31 Sp 5 database[1]. During the analysis, a 30 m long ZB 5MS capillary column with a weak polar phase and an inner diameter of 0.32 mm was used. The injector temperature was set at 250°C, and the transfer line temperature was set at 280°C. The column temperature was initially 80°C during the first 1 min, followed by a temperature elevation rate of 10°C/min until 300°C. The carrier gas was helium, set at a flow rate of 1.3 ml/min.

According to the NIST database, the peak at 34 min was attributed to the maleic acid dibutyl ester (Fig. 2), the peak at 36 min was attributed to the fumaric acid dibutyl ester (Fig. 3), and the main peak at 38 min was attributed to the malic acid butyl ester (Fig. 4).

The formation of maleic and fumaric acid esters is possible by two means. The first option is the esterification of the corresponding unsaturated acids contained as impurities in malic acid, by butanol, as represented in Reaction 2.

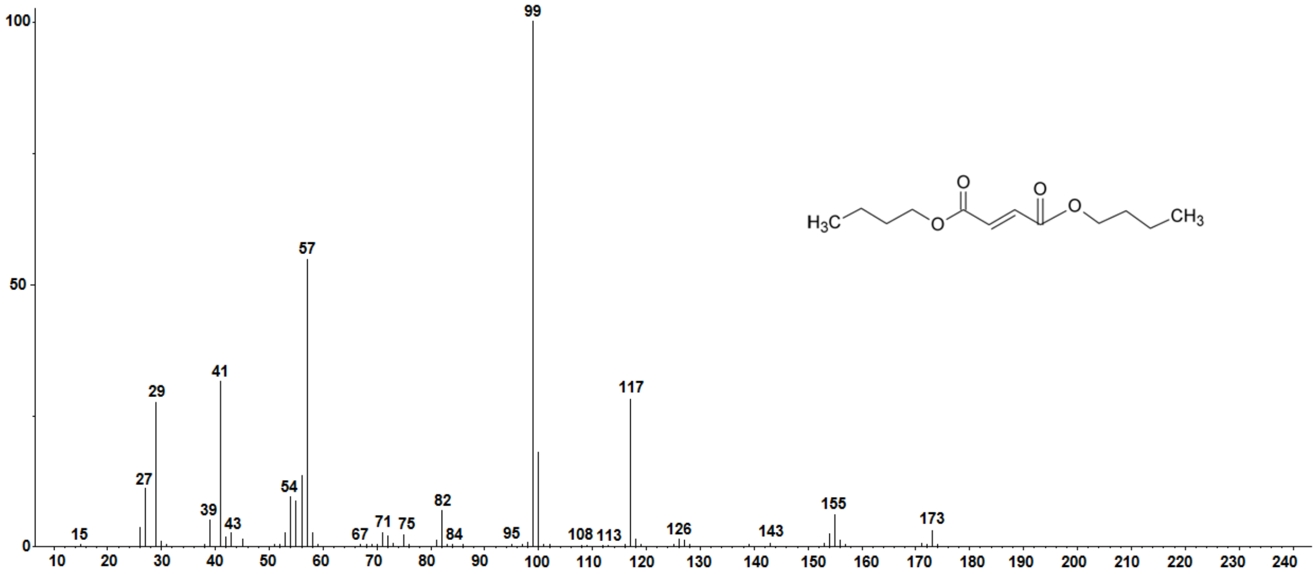

Fig. 2. Mass spectrum of maleic acid dibutyl ester.

---

[1] NIST Chemistry Webbook, SRD 69. Available from: webbook.nist.gov/chemistry/ (Accessed September 20, 2017). https://doi.org/10.18434/T4D303

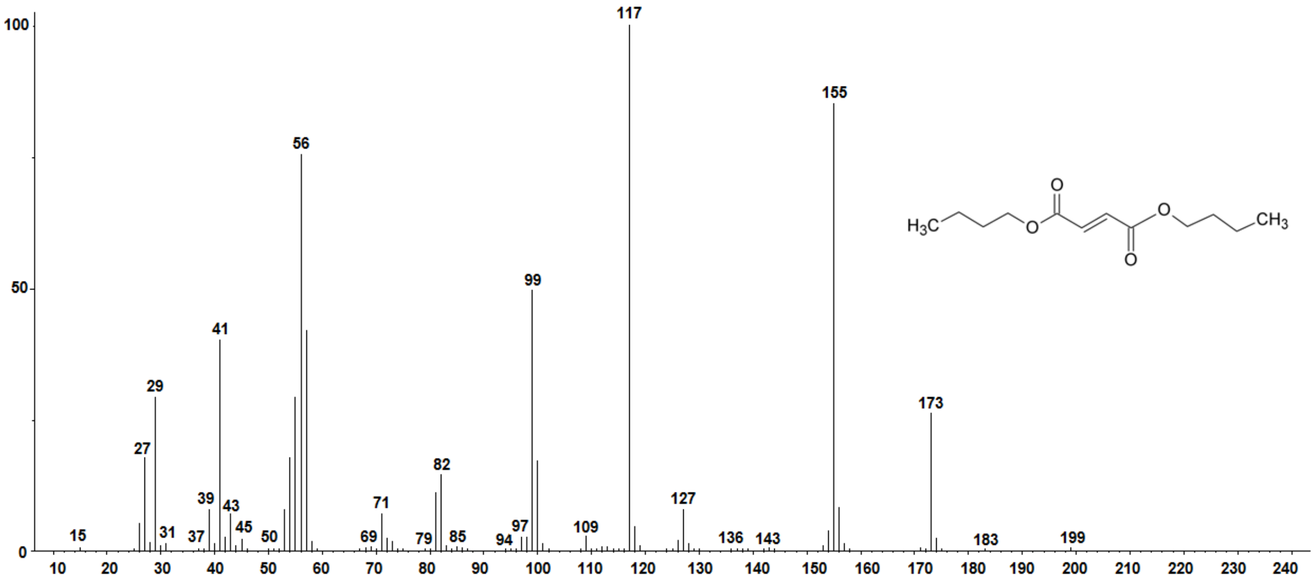

Fig. 3. Mass spectrum of fumaric acid dibutyl ester.

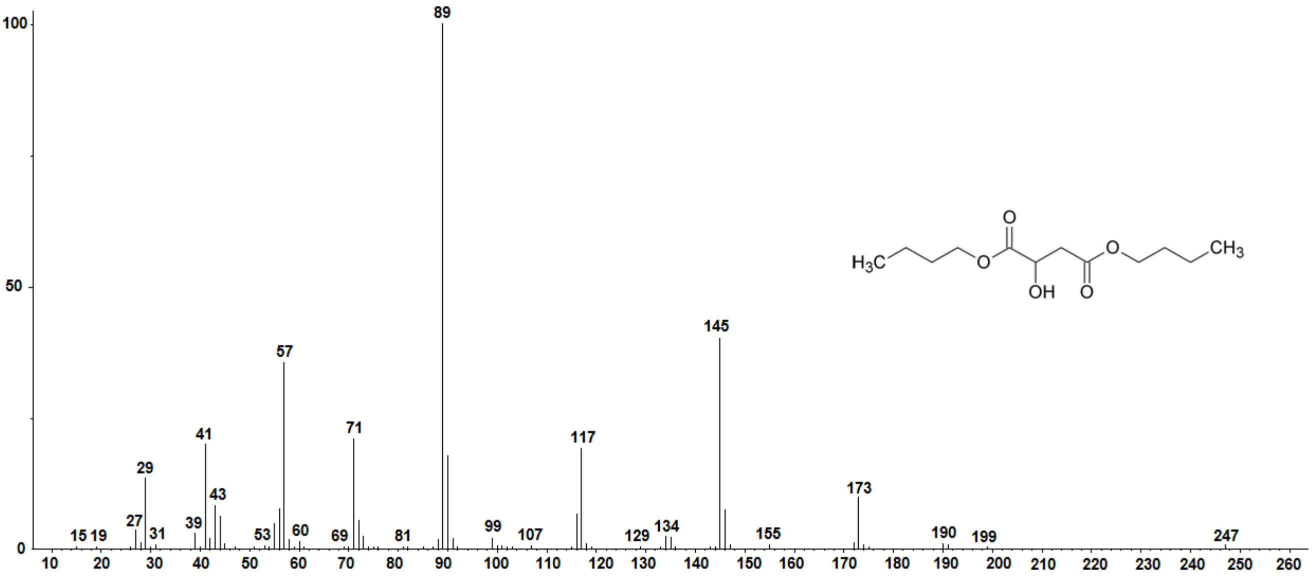

Fig. 4. Mass spectrum of malic acid dibutyl ester.

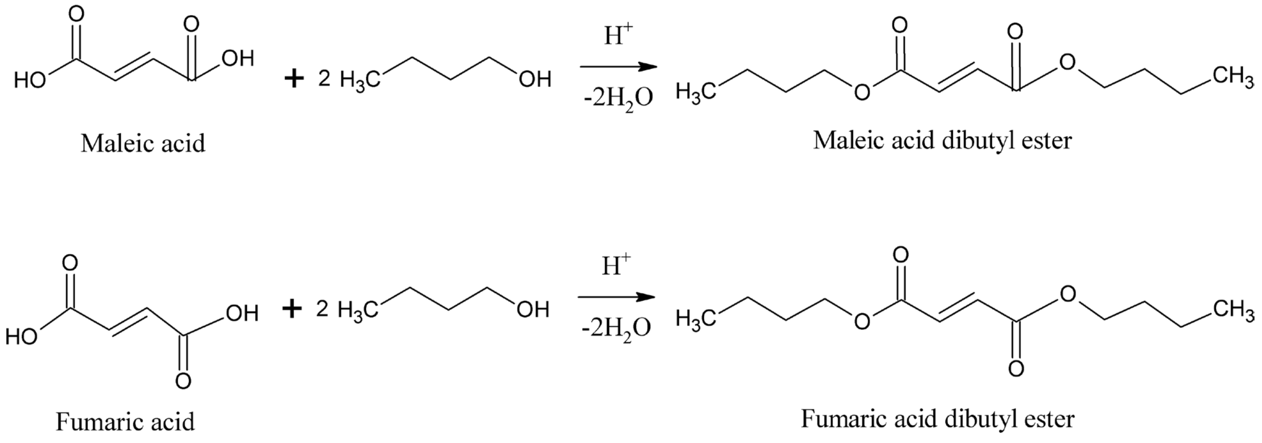

Reaction 2

At the same time, the content of maleic acid dibutyl ester should be significantly higher since this acid is the main impurity in the initial material.

The second option is either the dehydration of malic acid followed by esterification, as shown in Reactions 3 and 2, respectively, or dehydration of the malic acid esters themselves, as shown in Reaction 4. The more likely product in this case is fumaric acid ester.

The yields of butyl ester of malic acid were as follows: 71% for sulfuric acid, 68% for orthophosphoric acid, 56% for *p*-toluenesulfonic acid, 70% for Amberlyst 36 Dry, and 86% for KU-2 FPP. When using the Amberlyst 36 Wet and KIF-T catalysts, the reaction mass was tarred during the synthesis process, so that it was not possible to obtain a pure ester when using these catalysts. Impurities of maleic and fumaric acid esters were present in all the samples and were obtained in different amounts. The amount of maleic acid esters exceeded the content of fumaric acid esters, indicating that their formation occurred in the second option.

To assess the activity of the studied catalysts, several experiments were conducted under identical initial conditions; the temperature was set at 85°C, the amount of catalyst was 1 wt %, and the synthesis time was 80 min. The reaction mass was analyzed, and the conversion of malic acid was calculated. The composition of the final products was also analyzed after isolation and purification, according to the method described above. The results are given in the table.

The results show that the conversion of malic acid, as expected, is maximal on sulfuric acid. The conversion on Amberlyst 36 Dry is comparable to the conversion on p-toluenesulfonic acid. The decrease in malic acid conversion when using Amberlyst 36 Wet is due to the smaller number of active centers than Amberlyst 36 Dry (a limitation of the water content in the catalyst). Orthophosphoric acid, KU-2 FPP, and KIF-T had the least catalytic activity in the reaction of malic acid esterification during the considered time period.

When the finished products were isolated, the content of byproducts did not change significantly. The table shows that using sulfuric acid as a catalyst yields the highest percentage of impurities. When using the other catalysts, except for Amberlyst 36 Wet and KIF-T, the concentration of maleic and fumaric acid esters is approximately the same level and is

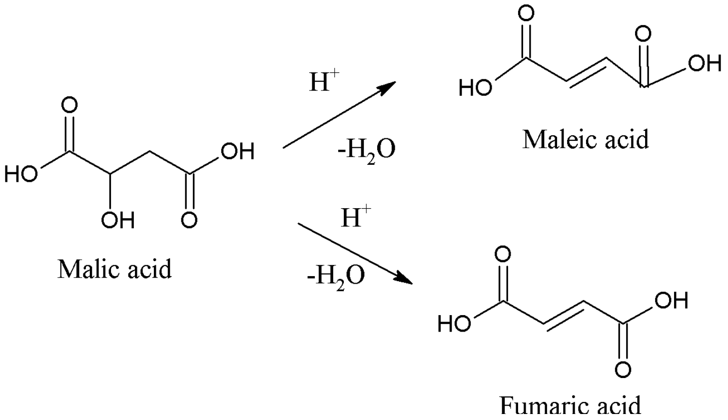

Reaction 3

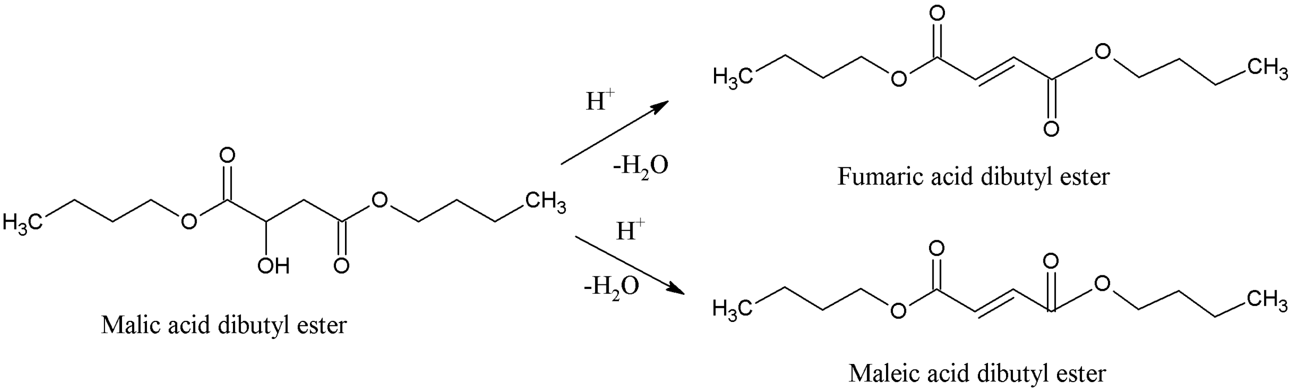

Reaction 4

Analysis of reaction mass and product on different catalysts

Catalyst	Conversion of malic acid at 80 minutes, %	Concentration of the product after purification, %		
		Byproducts	Fumaric acid dibutyl ester	Main product
Sulfuric acid	95.0	0.9	12.6	86.5
Orthophosphoric acid	15.9	0.05	1.15	98.8
p-Toluenesulfonic acid	45.4	0.2	1.1	98.7
Amberlyst 36 Dry	47.1	0.05	1.25	98.7
Amberlyst 36 Wet	30.8	Tarring of the reaction mass		
KU-2-FPP	14.3	0.06	1.24	98.7
KIF-T	5.98	Tarring of the reaction mass		

1.2–1.3 wt %. Regarding Amberlyst 36 Wet and KIF-T, the tarring of the reaction mass may be associated with higher catalytic activity in the dehydration reaction and possible oligomerization of unsaturated acids, although the main parameters, i.e., total static exchange capacity and surface area, of Amberlyst 36 Wet and Amberlyst 36 Dry are almost equal.

Overall, these results show that, among the catalysts tested in this study, Amberlyst 36 Dry yields higher conversion and selectivity in the malic acid esterification process.

CONCLUSIONS

The results of this study show that during the esterification of malic acid with butyl alcohol of normal structure, byproducts, such as esters of fumaric and maleic acids, are formed using different catalysts. The accumulation of byproducts occurs as a result of reactions of dehydration of malic acid or its ester. This study shows that the number of byproducts is almost independent of the catalyst, except for sulfuric acid. In order to obtain the dibutyl ester of malic acid, Amberlyst 36 Dry was shown provide an optimal ratio between conversion and selectivity.

Acknowledgments

The work was carried out with the financial support of the Russian Foundation for Basic Research in the framework of scientific project No. 18-08-00574a.

The authors declare no conflicts of interest.

REFERENCES

1. Kuznetsov B.N. Urgent Directions of Chemical Processing of Renewable Plant Biomass. *Khimiya v interesakh ustoichivogo razvitiya = Chem. Sust. Dev.* 2011;19(1):77-85 (in Russ.).

2. Sushkova S. V., Levanova S. V., Glazko I. L., Alexandrov A. Yu. Esterification of citric adic with aliphatic alcohols C_2-C_5. *Tonk. Khim. Tekhnol. = Fine Chem. Technol.* 2017;12(3):28-32 (in Russ.).
https://doi.org/10.32362/2410-6593-2017-12-3-28-32

3. Hermann B.G., Patel M. Today's and tomorrow's bio-based bulk chemicals from white biotechnology. *Appl. Biochem. Biotechnol.* 2007;136(3):361-388.
https://doi.org/10.1007/s12010-007-9031-9

4. Senko O.V., Stepanov N.A., Maslova O.V., Lyagin I.V., Efremenko E.N. Resource-saving biotechnology of fumaric acid production from renewable sources. *Vestnik KuzGTU.* 2013;1(95): 111-113 (in Russ.).

5. Santiago Malmierca, Rebeca Díez-Antolínez, Ana Isabel Paniagua, and Mariano Martín. Technoeconomic Study of Biobutanol AB Production. 1. Biomass Pretreatment and Hydrolysis. *Ind. Eng. Chem. Res.* 2017;56(6):1518-1524.
https://doi.org/10.1021/acs.iecr.6b02943

СПИСОК ЛИТЕРАТУРЫ

1. Кузнецов Б.Н. Актуальные направления химической переработки возобновляемой растительной биомассы. *Химия уст. разв.* 2011;19(1):77-85.

2. Сушкова С.В., Леванова С.В., Глазко И.Л., Александров А.Ю. Этерификация лимонной кислоты алифатическими спиртами C_2–C_5. *Тонкие химические технологии.* 2017;12(3):28-32.
https://doi.org/10.32362/2410-6593-2017-12-3-28-32

3. Hermann, B.G., Patel, M. Today's and tomorrow's bio-based bulk chemicals from white biotechnology. *Appl. Biochem. Biotechnol.* 2007;136(3):361-388.
https://doi.org/10.1007/s12010-007-9031-9

4. Сенько О.В., Степанов Н.А., Маслова О.В., Лягин И.В., Ефременко Е.Н. Ресурсосберегающая биотехнология получения фумаровой кислоты из возобновляемого растительного сырья. *Вестник КузГТУ.* 2013;1(95):111-113.

5. Santiago Malmierca, Rebeca Díez-Antolínez, Ana Isabel Paniagua, and Mariano Martín. Technoeconomic Study of Biobutanol AB Production. 1. Biomass Pretreatment and Hydrolysis. *Ind. Eng. Chem. Res.* 2017;56(6):1518-1524.
https://doi.org/10.1021/acs.iecr.6b02943

6. Barshtein R.S., Kirilovich V.M., Nosovskii Yu.E. *Plastifikatory dlya polimerov* (Plasticizers for polymers). Moscow: Khimiya; 1982. 200 p. (in Russ.).

7. Lebedev N.N. *Khimiya i tekhnologiya osnovnogo organicheskogo i neftekhimicheskogo sinteza: Uchebnik dlya vuzov* (Chemistry and technology of basic organic and petrochemical synthesis: Textbook for high schools). Moscow: Khimiya; 1988. 592 p. (in Russ.). ISBN: 5-7245-0008-6

8. Lipp S.V., Krasnyh E.L., Sokolov A.B., Glazko I.L., Levanova S.V. Synthesis of C_2-C_6 dicarboxylic acid esters and C_5-C_6 alcohols. *Khim. Prom. Segodnya = Chem. Ind. Today.* 2010;8:26-31 (in Russ.).

9. Melnyk S., Melnyk Yu., Nykulyshyn I., Shevchuk L. Research into esterification of mixture of lower dicarboxylic acids by 2-ethylhexan-1-ol in the presence of *p*-toluensulfonic acid. *Eastern-European Journal of Enterprise Technologies.* 2017;6/6(90):10-16. https://doi.org/10.15587/1729-4061.2017.114324

10. Houston T.A., Wilkinson B.L., Blanchfield J.T. Boric Acid Catalyzed Chemoselective Esterification of α-Hydroxycarboxylic Acids. *Org. Lett.* 2004;6(5):679-681. https://doi.org/10.1021/ol036123g

11. Nafikova R.F., Rahmatullina Z.F., Rahimkulova A.A., Rahimkulov A.G., Rahmatullina F.T. The reception of the ftalate plastificator with the use of the indigorests of the butyl alcohol. *Bashkirskii Khimicheskii Zhurnal = Bashkir Chem. J.* 2006;13(3):60-62 (in Russ.).

12. Samoilov V.O., Ramazanov D.N., Nekhaev A.I., Maksimov A.L. Heterogeneous catalytic conversion of glycerol with *n*-butyl alcohol. *Pet. Chem.* 2016;56(2):125-130. https://doi.org/10.1134/S0965544116010060

13. Gromova V.V., Mamarasulova Z.V. Thermak esterification of penthaerytrite by alyphatic monocarbonic acids. *Bulletin of St PbSIT (TU)*. 2013;20(46):64-67 (in Russ.).

14. Kornilov P.I., Kachalova T.N. 3D design of the plant for obtaining an oxygen-containing additive to automotive gasoline. *Vestnik Kazanskogo tekhnologicheskogo universiteta (Herald of Kazan Technological University).* 2013;16(9):226-227 (in Russ.).

15. Migdal C.A., Rowland R.G. Lubricant compositions containing hydroxyl carboxylic and hydroxyl polycarboxylic acid esters: US Pat. 7696136. 2005/0198894 A 1; prior publ. data 15.09.2005; date of patent 13.04.2010.

16. Xiang Z., Xiaodong L. Circular reaction water phase organic acid esterifying device and organic acid esterifying method thereof: CN Pat. 105884611; prior publ. data 26.05.2016; date of patent 24.08.2016.

17. Houston T.A., Wilkinson B.L., Blanchfield J.T. Boric Acid Catalyzed Chemoselective Esterification of α-Hydroxycarboxylic Acids. *Org. Lett.* 2004;6(5):679-681. https://doi.org/10.1021/ol036123g

18. Ogorodnikov S.K. (Ed.). *Spravochnik neftekhimika* (Petrochemicals Handbook). V. 2. Moscow: Khimiya; 1978. 592 p. (in Russ.).

19. Ageicheva Ya.N., Merzlyakova N.V., Shevtsova I.N. *Sposob ochistki p-toluolsul'fokisloty* (Method of purification of *p*-toluene sulfonic acid): USSR Pat. 1139725 A; 1985.

6. Барштейн Р.С., Кирилович В.М., Носовский Ю.Е. Пластификаторы для полимеров. М.: Химия; 1982. 200 с.

7. Лебедев Н.Н. Химия и технология основного органического и нефтехимического синтеза: Учебник для вузов. М.: Химия; 1988. 592 с. ISBN: 5-7245-0008-6

8. Липп С.В., Красных Е.Л., Соколов А.Б., Глазко И.Л., Леванова С.В. Синтез сложных эфиров дикарбоновых кислот C_2-C_6 и спиртов C_5-C_6. *Хим. Пром. сегодня.* 2010;8:26-31.

9. Melnyk S., Melnyk Yu., Nykulyshyn I., Shevchuk L. Research into esterification of mixture of lower dicarboxylic acids by 2-ethylhexan-1-ol in the presence of *p*-toluensulfonic acid. *Eastern-European Journal of Enterprise Technologies.* 2017;6,6(90):10-16. https://doi.org/10.15587/1729-4061.2017.114324

10. Houston T.A., Wilkinson B.L., Blanchfield J.T. Boric Acid Catalyzed Chemoselective Esterification of α-Hydroxycarboxylic Acids. *Org. Lett.* 2004;6(5):679-681. https://doi.org/10.1021/ol036123g

11. Нафикова Р.Ф., Рахматуллина Ж.Ф., Рахимкулова А.А., Рахимкулов А.Г., Рахматуллина Ф.Т. Получение фталатного пластификатора с использованием кубовых остатков бутиловых спиртов. *Башкирский химический журнал.* 2006;13(3):60-62.

12. Samoilov V.O., Ramazanov D.N., Nekhaev A.I., Maksimov A.L. Heterogeneous catalytic conversion of glycerol with *n*-butyl alcohol. *Pet. Chem.* 2016;56(2):125-130. https://doi.org/10.1134/S0965544116010060

13. Громова В.В., Мамарасулова З.В. Термическая этерификация пентаэритрита алифатическими монокарбоновыми кислотами. *Известия СПбГТИ (ТУ)*. 2013;20(46):64-67.

14. Корнилов П.И., Качалова Т.Н. 3D проектирование установки получения кислородсодержащей добавки к автомобильному бензину. *Вестник Казанского технологического университета.* 2013;16(9):226-227.

15. Migdal C.A., Rowland R.G. Lubricant compositions containing hydroxyl carboxylic and hydroxyl polycarboxylic acid esters: US Pat. 7696136. 2005/0198894 A 1; prior publ. data 15.09.2005; date of patent 13.04.2010.

16. Xiang Z., Xiaodong L. Circular reaction water phase organic acid esterifying device and organic acid esterifying method thereof: CN Pat. 105884611; prior publ. data 26.05.2016; date of patent 24.08.2016.

17. Houston T.A., Wilkinson B.L., Blanchfield J.T. Boric Acid Catalyzed Chemoselective Esterification of α-Hydroxycarboxylic Acids. *Org. Lett.* 2004;6(5):679-681. https://doi.org/10.1021/ol036123g

18. Справочник нефтехимика: в 2-х т. Т. 2, под ред. С.К. Огородникова. Л.: Химия; 1978. 592 с.

19. Агейчева Я.Н., Мерзлякова Н.В., Шевцова И.Н. Способ очистки *n*-толуолсульфокислоты: а.с. 1139725 А СССР. № 3491193/23-04; заявл. 08.09.1982; опубл. 15.02.1985. Бюл. № 6.

About the authors:

Natalia S. Kuzmina, Engineer, Technology of Organic and Petrochemical Synthesis Department, Samara State Technical University (244, Molodogvardeiskaya ul., Samara, 443100, Russia). E-mail: kusminans@yandex.ru. https://orcid.org/0000-0002-5951-5653

Svetlana V. Portnova, Cand. of Sci. (Chemistry), Associate Professor, Technology of Organic and Petrochemical Synthesis Department, Samara State Technical University (244, Molodogvardeiskaya ul., Samara, 443100, Russia). Scopus Author ID: 42062133500, Researcher ID: D-5622-2014, https://orcid.org/0000-0003-2595-0654

Eugen L. Krasnykh, Dr. of Sci. (Chemistry), Head of the Technology of Organic and Petrochemical Synthesis Department, Samara State Technical University (244, Molodogvardeiskaya ul., Samara, 443100, Russia). Scopus Author ID: 6602271562, Researcher ID: I-6314-2013, https://orcid.org/0000-0002-3886-1450

Об авторах:

Кузьмина Наталья Сергеевна, инженер кафедры «Технология органического и нефтехимического синтеза» ФГБОУ ВО «Самарский государственный технический университет» (443100, г. Самара, ул. Молодогвардейская, д. 244). E-mail: kusminans@yandex.ru. https://orcid.org/0000-0002-5951-5653

Портнова Светлана Валериевна, кандидат химических наук, доцент кафедры «Технология органического и нефтехимического синтеза» ФГБОУ ВО «Самарский государственный технический университет» (443100, г. Самара, ул. Молодогвардейская, д. 244). Scopus Author ID: 42062133500, Researcher ID: D-5622-2014, https://orcid.org/0000-0003-2595-0654

Красных Евгений Леонидович, доктор химических наук, заведующий кафедрой «Технология органического и нефтехимического синтеза» ФГБОУ ВО «Самарский государственный технический университет» (443100, г. Самара, ул. Молодогвардейская, д. 244). Scopus Author ID: 6602271562, Researcher ID: I-6314-2013, https://orcid.org/0000-0002-3886-1450

Submitted: December 12, 2019; Reviewed: March 02, 2020; Accepted: April 06, 2020.

Translated from Russian into English by N. Isaeva

Edited for English language and spelling by Enago, an editing brand of Crimson Interactive Inc.

ISSN 2686-7575 (Online)

https://doi.org/10.32362/2410-6593-2020-15-2-56-66

UDC 665.775.4

Investigation of modified bitumen binders via Fourier-transform infrared spectroscopy

Irina V. Gordeeva[1,@], Dmitry A. Melnikov[2], Victoria N. Gorbatova[1], Dmitry S. Reznichenko[2,3], Yulia A. Naumova[3]

[1]N.N. Semenov Federal Research Center of Chemical Physics, Russian Academy of Sciences, Moscow, 119991 Russia
[2]Research Institute of Elastomeric Materials and Products, Moscow, 111024 Russia
[3]MIREA – Russian Technological University, Moscow, 119454 Russia
[@]Corresponding author, e-mail: irinavolchenko90@yandex.ru

Objectives. *This study evaluates the effect of the modification process on the group composition of bitumen and bitumen binders containing rubber powder and hybrid modifier that is based on styrene–butadiene thermoplastic elastomer and rubber crumb. The aim of the study was to determine the presence or absence of functional groups that reflect the direction of physicochemical processes during the preparation of a hybrid modifier in rotary dispersers and during the modification of bitumen binders.*

Methods. *Rubber powder and hybrid modifier were obtained by high-temperature shear grinding using a rotary disperser. Bitumen and modified bitumen binders were investigated via Fourier-transform infrared spectroscopy. Using the method of spectral subtraction, it was determined that during the process of manufacturing modified bitumen binders, structural changes occur in both bitumen and modifiers. During this study, the extraction of modifiers (rubber powder and hybrid modifier) in toluene was performed.*

Results. *The quantitative analysis of changes in the group composition of modifiers before and after the modification procedure was carried out. The active polymer and structural indices were determined. The general trend of the change in the active polymer and structural indices was noted for the initial spectra of the rubber powder and hybrid modifier, and their spectra were obtained after the procedure of subtraction from the spectra of bitumen binders.*

Conclusions. *The interdiffusion of aromatic compounds between the bitumen component and modifier particles was confirmed. On the basis of the results of the extraction of modifiers in toluene, and by taking into account the infrared spectroscopy data, it was determined that during the production of hybrid modifier during the simultaneous grinding of rubber crumb and styrene–butadiene thermoplastic elastomer, there was a chemical interaction between them.*

Keywords: *bitumen, rubber-polymer composites, rubber powders, IR spectroscopy, bituminous binders, hybrid modifier, high-temperature shear grinding, structural index, spectrum subtraction method.*

For citation: Gordeeva I.V., Melnikov D.A., Gorbatova V.N., Reznichenko D.S., Naumova Yu.A. Investigation of modified bitumen binders via Fourier-transform infrared spectroscopy. *Tonk. Khim. Tekhnol. = Fine Chem. Technol.* 2020;15(2):56-66. https://doi.org/10.32362/2410-6593-2020-15-2-56-66

Исследование влияния процесса модификации на групповой состав битума и модификаторов методом Фурье-ИК-спектроскопии

И.В. Гордеева[1,@], Д.А. Мельников[2], В.Н. Горбатова[1], Д.С. Резниченко[2,3], Ю.А. Наумова[3]

[1]*Федеральный исследовательский центр химической физики им. Н.Н. Семенова, Российская академия наук, Москва, 119991 Россия*
[2]*Научно-исследовательский институт эластомерных материалов и изделий, Москва, 111024 Россия*
[3]*МИРЭА – Российский технологический университет, Москва, 119454 Россия*
[@]*Автор для переписки, e-mail: irinavolchenko90@yandex.ru*

Цели. *В статье проанализировано влияние процесса модификации на групповой состав битума и битумных вяжущих, содержащих резиновый порошок и гибридный модификатор на основе бутадиен-стирольного термоэластопласта и резиновой крошки. Целью исследования было определение наличия или отсутствия функциональных групп, отражающих направленность физико-химических процессов при получении гибридного модификатора в роторных диспергаторах и при модификации битумных вяжущих.*
Методы. *Резиновый порошок и гибридный модификатор получены методом высокотемпературного сдвигового измельчения на роторном диспергаторе. Битумы и модифицированные битумные вяжущие исследованы методом инфракрасной спектроскопии с Фурье преобразованием. С помощью метода вычитания спектров установлено, что в процессе изготовления модифицированных битумных вяжущих происходят структурные изменения как в битуме, так и в модификаторах. В работе также проведена экстракция модификаторов (резинового порошка и гибридного модификатора) в толуоле.*
Результаты. *Проведен количественный анализ изменений, происходящих в групповом составе модификаторов до и после процедуры модификации. Определены активный полимерный и структурный индексы. Отмечена общая тенденция в изменении активного полимерного и структурного индексов для исходных спектров резинового порошка и гибридного модификатора и их спектров, полученных после процедуры вычитания из спектров битумных вяжущих спектра битума.*
Выводы. *Подтверждена взаимодиффузия ароматических соединений между битумной составляющей и частицами модификаторов. На основании результатов экстракции модификаторов в толуоле и с учетом данных ИК-спектроскопии найдено, что в процессе производства гибридного модификатора совместным соизмельчением резиновой крошки и бутадиен-стирольного термоэластопласта между ними происходит химическое взаимодействие.*

Ключевые слова: *битум, резино-полимерные композиты, резиновые порошки, ИК-спектроскопия, битумные вяжущие, гибридный модификатор, высокотемпературное сдвиговое измельчение, структурный индекс, метод вычитания спектров.*

Для цитирования: Гордеева И.В., Мельников Д.А., Горбатова В.Н., Резниченко Д.С., Наумова Ю.А. Исследование влияния процесса модификации на групповой состав битума и модификаторов методом Фурье-ИК спектроскопии. *Тонкие химические технологии.* 2020;15(2):56-66. https://doi.org/10.32362/2410-6593-2020-15-2-56-66

INTRODUCTION

In recent years, both in Russia and around the world, traffic has considerably increased. Therefore, the quality of binder for pavements remains relevant because the contribution of binder to the formation of main coating defects is between 40 and 90% [1]. Moreover, numerous studies [2–5], which have been conducted in different countries, show that unmodified bitumen does not provide the proper quality of road surfaces under the conditions of modern heavy traffic. A prerequisite for creating a high-quality asphalt concrete pavement is to modify bitumen binder [6–8].

Thermoplastic elastomers (TPEs) and rubber powders (RPs) are mainly used as bitumen modifiers; in addition, attempts have been made to create hybrid modifiers (HM) [9–13].

Modifiers, depending on the technology of their addition into bitumen, are divided into two groups:

1) Modifiers that are designed to improve bitumen properties prior to the preparation of the asphalt mix by "wet" modification, which involves the stage of continuous cooking of bitumen at high temperatures (usually higher than 180°C). The modification efficiency in this case is achieved by increasing the degree of dispersion of modifiers in bitumen using high-speed mixers.

2) Modifiers that are designed to improve the performance of the asphalt mix by "dry" modification. In this case, the need for long and energy-intensive stages of obtaining modified bitumen binders is eliminated. Modifiers are introduced into the asphalt mix at the time of its preparation in the asphalt mixer. Such modifiers include RP and HM, which are obtained by high-temperature shear grinding. The modification efficiency is achieved by the fast deagglomeration of RP particles or a hybrid modifier upon contact with hot bitumen [6, 14–16].

The first group includes almost all known modifiers. Hybrid binders are mainly obtained by the "wet" method. However, the Federal Research Center of Chemical Physics of the Russian Academy of Sciences has developed a unique hybrid modifier that can be introduced by the "dry" approach, which is similar to the introduction of RP (2nd group modifiers). This approach became possible owing to the joint co-grinding of rubber crumb (RC) and styrene–butadiene thermoplastic elastomer (SBTPE) by high-temperature shear grinding (HTSG).

In this study, infrared (IR) spectroscopy was used to study bitumen, modifiers, and modified bitumen binders. This method allows you to record changes in the group composition and structure of bitumen materials in the process of their modification [17–19]. The aim of the study was to determine the functional groups, the presence or absence of which reflects the physicochemical processes occurring upon receipt of hybrid modifier in rotary dispersants and upon the modification of bituminous binders. To achieve this goal, we used the OMNIC software, with which we performed the procedure of subtracting the spectra of bitumen and modifiers from the spectra of modified bitumen binders. RP and hybrid modifier were extracted with toluene to establish the presence of chemical interaction between rubber and thermoplastic elastomer in the process of obtaining the hybrid modifier by the HTSG method.

MATERIALS AND METHODS

As initial bitumen, BND 60/90 was used, which is recommended for use in road climatic zones II–V. The actual values of the physicochemical parameters of initial bitumen BND 60/90 (*Slavneft-Yaroslavnefteorgsintez*, Yaroslavl, Russia) are presented in Table 1.

The bitumen modifiers used in this study are rubber powder, which is based on used tires STO 11101543-006-2015 (RP studied), and a hybrid modifier obtained by co-grinding RC (cascade production method) and styrene–butadiene thermoplastic elastomer STO 11101543-008-2015 (GM studied). The main characteristics of dispersed elastomeric modifiers are given in Table 2. These modifiers were obtained by the HTSG method on modern installations in rotary dispersants (patent 2612637 Russian Federation, B29B13/00). The raw material for producing dispersed modifiers was RC with a particle size of >1 mm TU 2511-002-56465277-14 (*Oris Prom*, Dzerzhinsk, Moscow oblast, Russia). To obtain GM, we used a mixture of initial RK and SBTPE of the SBS 30-01 L brand (*Voronezhsintezkauchuk*, Voronezh, Russia).

The composition of bitumen binders studied in this study by IR spectroscopy is presented in Table 3.

The samples of RBB and HBB were obtained by mixing bitumen and modifiers obtained by the HTSG method at 160°C for 10 min at the rotation speed of the mixer blades of 600 rpm.

The effect of the modification process on the group composition of bitumen was studied using a Nicolet™ iS5 FT-IR Spectrometer from *Thermo Scientific*™ (USA) with an iD3 ATR Plate.

RESULTS AND DISCUSSION

Using IR spectroscopy, we obtained the spectra of initial unmodified bitumen BND 60/90, rubber-bitumen, and bitumen binders containing HM, as well as the spectra of modifiers (i.e., RP and hybrid modifier obtained by the HTSG method).

Table 1. Physicochemical characteristics of BND 60/90

Parameters	Norm according to GOST 22245-90	Actual value
Penetration grade of unaged binders, 0.1 mm:		
at 25°C	61–90	74
at 0°C	>20	22
Softening point of unaged binders, °C	>47	49
Ductility, cm:		
at 25°C	>55	88
at 0°C	>3.5	3.7
Fraass breaking point, °C	<–15	–22
Flash point, °C	>230	276
Changing the softening point after hardening, °C	<5	5
Penetration index	–1.0 ÷ +1.0	–0.4

Table 2. Characteristics of disperse modifiers

Parameters	Units	RP studied	HM studied
Average particle size	µm	270	250
Specific surface	m^2/g	0.237	0.312
Bulk density	g/cm^3	0.36 ± 0.5	0.32 ± 0.5
Humidity	% by weight, no more than	4	3.2
Residue on the 0.63-mm sieve	%, no more than	2	2
Agglomeration index	no less than	8	8

Table 3. Compounding composition of the investigated bituminous binders

Sample cipher	Sample	Modifier type	Ratio BND/modifier, mass %
1	Bitumen (BND)	–	100/0
2	Rubber-bituminous binder (RBB)	Rubber powder obtained by high-temperature shear grinding (HTSG)	90/10
3	Hybrid bituminous binder (HBB)	Hybrid modifier obtained by HTSG	

A comparative analysis of the modifying action of the RP and hybrid modifier was carried out by comparing the spectra of bitumen and its modifiers before and after the modification of bitumen. Thus, the spectra of bitumen or the spectra of RP and HM were subtracted from the spectra of modified binders, and the results were compared with the spectra of the initial components of modified bitumen binders.

During the first stage, a change in the composition of bitumen after its modification with RP and hybrid modifier was evaluated. The resulting spectra obtained by subtracting the spectra of the original modifiers from the spectra of modified bitumen binders (samples No. 2 and 3) are shown in Fig. 1.

The qualitative analysis of the spectra is shown in Fig. 1, which demonstrates that the structure of the bitumen component changes during the formation of binders. A considerable change in the group composition of aromatic compounds in bitumen is observed. After bitumen modification with RP (Fig. 1a), the absorption bands of *m*-xylene (753 cm^{-1}) and *p*-xylene (781 cm^{-1}) degenerate, and the bands of aromatic compounds at 1600 cm^{-1} and the band of aromatic triplet of bitumen (746 cm^{-1}) disappear.

The absorption spectrum related to the paraffin–naphthenic fraction (e.g., at 1030 cm^{-1}) is not observed in the spectrum of the bitumen component obtained by subtracting the spectrum of RP from the RBB spectrum. The presence of six-membered aromatic cycles can be detected in bitumen only after modification (peak at 1892 cm^{-1} [20]).

The presence of active radicals on the surface of RP leads to a change in the group composition of oxygen-containing compounds. Thus, the absorption bands of anhydrides and esters degenerate (1771 cm^{-1} and 1752 cm^{-1}, respectively); however, a band appears, which corresponds to the stretching vibrations of the CO group (1243 cm^{-1}, acetates).

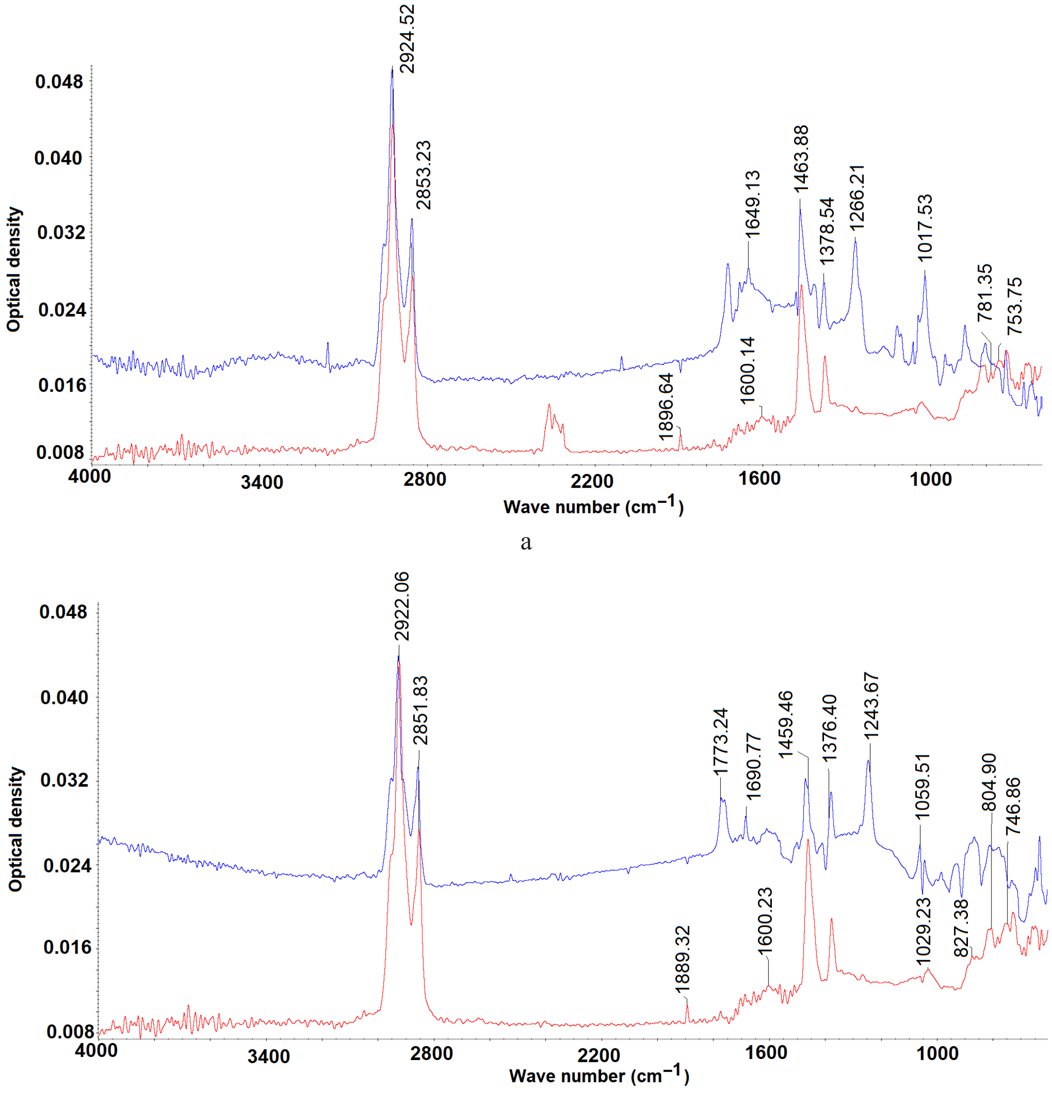

Fig. 1. Spectra of original BND bitumen (red line) and bituminous component (blue line) obtained by subtracting the spectrum of rubber powder (RP) (a) and hybrid modifier HM (b) from the spectrum of the modified bituminous binder.

The nature of changes in the structure of bitumen after modification with a hybrid modifier (Fig. 1b) is similar to the changes caused by the introduction of RP. The group composition of paraffin–naphthenic hydrocarbons changes at 1030 cm^{-1}, when the absorption band present on the spectrum of initial bitumen degenerates in the spectrum of the bitumen component after modification [21].

When using a hybrid modifier, changes are observed at 900–600 cm^{-1}, which are related to aromatic compounds. The degeneration of bands of individual aromatic compounds (746, 753, and 804 cm^{-1}) as well as bands at 1600 cm^{-1} and 1892 cm^{-1}, which characterize five- and six-membered cycles of aromatic compounds [21–23], takes place. Modification with a hybrid modifier leads to the appearance of an absorption band at 1243 cm^{-1} (acetates, phenols).

In the bitumen component of modified binders, both in the case of RP and HM, a band at 1043 cm^{-1} is observed, which corresponds to compounds containing the S=O group ($R–SO^{3-}$-type compounds).

A distinctive feature characteristic of spectra obtained using only HM is the presence of an absorption band at 700 cm^{-1}, which corresponds to the δ(CH) group of the aromatic ring (polystyrene) and to the absence of a band at 1016 cm^{-1}, which indicates the presence in the sample of sulfur compounds in the form of R–SO–R structures.

A similar procedure for comparing the spectra of initial modifiers with the spectra obtained by subtracting the spectrum of bitumen from the spectrum of modified bitumen binders showed that the changes in the set of functional groups according to their assortment and peak intensities are insignificant. The main feature of the spectra of modifiers, both for RP and HM, after contact with bitumen is the appearance of peaks in the low-frequency region corresponding to aromatic compounds (645, 680, 773, 798, 841, 881, 946 cm^{-1}), which confirms the diffusion of aromatic hydrocarbons from the bitumen component into the volume of modifiers [23].

On the basis of the obtained data, the second stage of this study was dedicated to studying the effect of bitumen modification on the physicochemical processes occurring between RC and TPE upon the receipt of a hybrid modifier. To solve this problem, a comparative analysis of the resulting spectra was obtained by subtracting the spectrum of the RP from the spectrum of the hybrid modifier before and after bitumen modification (Fig. 2).

In the spectrum before modification (blue line), shown in Fig. 2, the absorption band of the δ(CH) group of the aromatic ring (styrene) at 700 cm^{-1} and the band characterizing the presence of C=C double bonds (965 cm^{-1}) are observed [22, 23]. After the bitumen modification procedure, the intensity of these peaks considerably decreases, which is associated with the occurrence of diffusion processes during the transition of unsaturated compounds to bitumen.

For the quantitative analysis of the spectra of modified bitumen binders, the method described in [24] was applied. This approach is based on the fact that during modification, the intensity and nature of the peak at 965 cm^{-1}, which is related to *trans*-alkanes, noticeably changes. It was also established that the absorption band at 810 cm^{-1}, which characterizes C–H bonds in aromatic compounds, remains almost unchanged; therefore, it is considered to be a constant value (Fig. 3). The parameter that describes the quantitative changes that occur in the modified bitumen binder and in HM during the modification

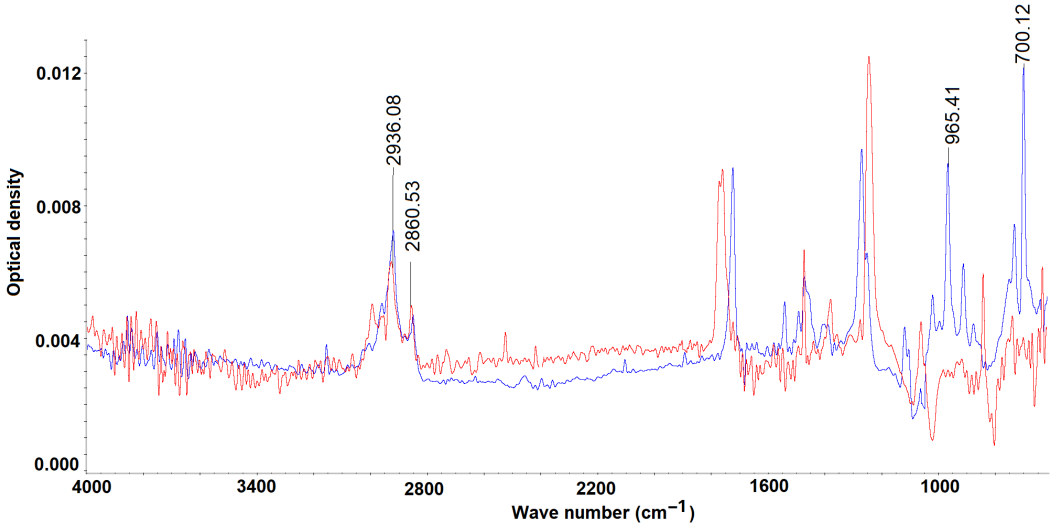

Fig. 2. Spectra obtained by subtracting the RP spectrum from the HM spectrum (blue line for the original modifiers, red line for modifiers after the bitumen modification procedure).

process is the active polymer index (API), which is calculated by the following equation:

$$\mathrm{API} = \frac{S_{965}}{S_{810}},$$

where S_{965} is the peak area at 965 cm^{-1}, and S_{810} is the peak area at 810 cm^{-1}.

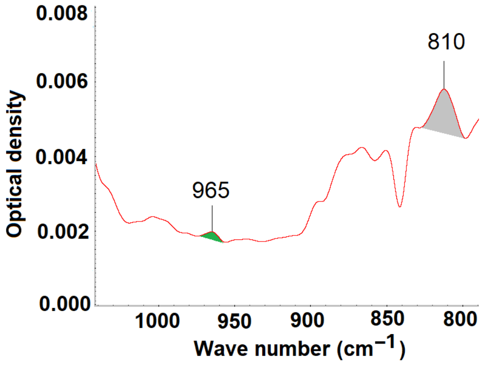

Fig. 3. Determination of peaks for calculating API using HBB as an example.

In [25], for the quantitative analysis of MBB, the structural index (relative optical density) $I_{\mathrm{CH=CH}}$ is used, which equals to the ratio of the peak area at 965 cm^{-1} to the total area of the region between 2000 cm^{-1} and 600 cm^{-1}:

$$I_{\mathrm{CH=CH}} = \frac{S_{965}}{\sum S_{2000-600}}$$

The results of the quantitative analysis of the spectra of modified bitumen binders are presented in Table 4.

The analysis of the data shown in Table 4 allows us to note the general trends in the change in API and $I_{\mathrm{CH=CH}}$ in the initial spectra of RP and hybrid modifier and their spectra obtained after the procedure of subtraction of the spectrum of bitumen from the spectra of bituminous binders. The higher values of these indicators for a hybrid modifier compared to RP are natural and are associated with the presence of the polybutadiene component of SBTPE.

The reverse picture observed in the analysis of the RP and HM spectra after obtaining bituminous binders, which allows us to make an assumption about the possible chemical interactions between RC and TPE during their grinding. When analyzing the spectra of modified bitumen binders, considerably lower numerical values of API and $I_{\mathrm{CH=CH}}$ were obtained. This can occur due to the lower concentrations of modifiers in the binder (bitumen/modifier is 90/10 mass %) and the incorporation of part of the free low molecular weight polymer component of the modifiers into the formed structure of the bitumen binder. A decrease in the structural index $I_{\mathrm{CH=CH}}$ of the hybrid modifier after modification confirms the data from the qualitative analysis shown in Fig. 2. This means that during the manufacturing process of the hybrid modifier, a noticeable physicochemical interaction occurs between the starting components.

To identify the presence of a chemical interaction between RC and TPE during the process of obtaining a hybrid bitumen modifier by the HTSG method, styrene–butadiene thermoplastic elastomer was extracted from the HM sample. The initial RP and hybrid modifier obtained by the HTSG method were placed in toluene and kept there for 14 days. After filtration, the samples were dried and weighed. Samples were dried at constant temperature and humidity. The drying time was determined by achieving a constant mass value of the extracted samples with an accuracy of ±0.001 g. The test results are shown in Table 5.

Table 5 shows that most TPE (>75% for GM 5/95 and >85% for HM 20/80) that are dissolved in toluene are added to hybrid modifier, which confirms the presence of interaction between the polymer and RC during their co-grinding in a rotary disperser.

Table 4. Quantitative analysis of the spectra of MBB and modifiers

Sample	Active polymer index (API)	Structural index $I_{\mathrm{CH=CH}}$
Before modification		
RP	1.466	0.0277
HM	3.245	0.0443
After modification		
RP	0.2400	0.0086
HM	0.2110	0.0052

Table 5. Results of the extraction of RP and thermoplastic with toluene

Parameters	Modifiers/styrene–butadiene thermoplastic elastomer (TPE) content, mass %		
	RP	HM	
	0	5	20
Sample mass, g	0.1207	0.1915	0.1984
Mass of the sample after extraction, g	0.1128	0.1723	0.1543
Mass of substances extracted with toluene, g	0.0079	0.0192	0.0441
Mass fraction of substances extracted with toluene, %	6.54	10.02	22.23
Mass fraction of TPE extracted with toluene, %	–	3.81	17.0

CONCLUSIONS

The use of the method of subtraction of spectra made it possible to evaluate the structural changes occurring in bitumen and its modifiers during the manufacturing of modified bitumen binders. It was determined that using such modification, aromatic hydrocarbons diffuse from the bitumen component to modifier particles. During the modification process, six-membered cyclic aromatic compounds are formed in the bitumen part; the composition of paraffin–naphthenic hydrocarbons is changed, and sulfur compounds are formed and “transferred” from the particles of modifiers to bitumen. Thus, in this study, the phenomenon of interdiffusion between bitumen and modifiers (RP and HM) was confirmed by IR spectroscopy.

The analysis of the results of the extraction of hybrid modifiers in toluene and the IR spectroscopy data allows us to conclude that chemical interaction occurs between RC and thermoplastic elastomer when they are co-milled on a rotary disperser by the HTSG method.

Acknowledgments

The study was supported by the N.N. Semenov Federal Research Center of Chemical Physics of the Russian Academy of Sciences, the project of the state assignment No. 0082-2019-0009 (AAAA-A20-120021390044-2).

The authors declare no conflicts of interest.

REFERENCES

1. Partl M.N., Bahia H.U., Canestrari F., Roche Ch., Benedetto H.D., Piber H., Sybilski D. (eds.) Advances in Interlaboratory Testing and Evaluation of Bituminous Materials: State-of-the-Art Report of the RILEM Technical Committee 206-ATB. Springer; 2013. V. 9. 453 p.

2. Leseur D., Gerard J.-F, Claudy P., Letoffe J.-M., Planche J.-P., Martin D. A structure-related model to describe asphalt linear viscoelasticity. *J. Rheol.* 1996;40:813-856. https://doi.org/10.1122/1.550764

3. Gokhman, L.M. *Bitumy, polimerno-bitumnye vyazhushchie, asfal'tobeton, polimerasfal'tobeton: uchebno-metodicheskoe posobie* (Bitumen, polymer-bitumen binders, asphalt concrete, polymerasphaltobeton: teaching aid). Moscow: EKON-INFORM; 2008. 117 p. (in Russ.).

СПИСОК ЛИТЕРАТУРЫ

1. Partl M.N., Bahia H.U., Canestrari F., Roche Ch., Benedetto H.D., Piber H., Sybilski D. (eds.) Advances in Interlaboratory Testing and Evaluation of Bituminous Materials: State-of-the-Art Report of the RILEM Technical Committee 206-ATB. Springer; 2013. V. 9. 453 p.

2. Leseur D., Gerard J.-F, Claudy P., Letoffe J.-M., Planche J.-P., Martin D. A structure-related model to describe asphalt linear viscoelasticity. *J. Rheol.* 1996;40:813-856. https://doi.org/10.1122/1.550764

3. Гохман Л.М. Битумы, полимерно-битумные вяжущие, асфальтобетон, полимерасфальтобетон: учебно-методическое пособие. М.: ЗАО «ЭКОН-ИНФОРМ»; 2008. 117 с.

4. Soenen H., Lu X., Redelius P. The morphology of SBS modified bitumen in binders and in asphalt mix. In: Advanced Testing and Characterization of Bituminous Materials, London: Taylor & Francis Group; 2009. P. 151-160. ISBN 978-0-415-55854-9

5. Behnood A., Gharehveran M.M. Morphology, rheology, and physical properties of polymer-modified asphalt binders. *Eur. Polym. J.* 2019;112:766-791. https://doi.org/10.1016/j.eurpolymj.2018.10.049

6. Nikolskii V.G., Dudareva T.V., Krasotkina I.A., Zvereva U.G., Bekeshev V.G., Rochev, V.Ya., Kaplan A.M., Chekunaev N.I., Vnukova L.V., Styrikovich N.M., Gordeeva I.V. Development and properties of new nanomodifiers for road coating. *Khimicheskaya Fizika.* 2014;33(7):87-93 (in Russ.). https://doi.org/10.7868/s0207401x14070073

7. Schaur A., Unterberger S., Lackner R. Impact of molecular structure of SBS on thermomechanical properties of polymer modified bitumen. *Eur. Polym. J.* 2017;96:256-265. https://doi.org/10.1016/j.eurpolymj.2017.09.017

8. Loderer C., Partl M.N., Poulikakos L.D. Effect of crumb rubber production technology on performance of modified bitumen. *Constr. Build. Mater.* 2018;191:1159-1171. https://doi.org/10.1016/j.conbuildmat.2018.10.046

9. Biro S., Fazekas B. Asphalt rubber versus other modified bitumens. *Road Mater. Pavement.* 2012. Available from: http://www.ra-foundation.org/wp-content/uploads/2013/02/020-PAP_017.pdf

10. Greene J., Chun S., Nash T., Choubane B. Evaluation and Implementation of PG 76-22 Asphalt Rubber Binder in Florida. *Transport. Res. Rec*. 2015;2524(1);3-10. https://doi.org/10.3141/2524-01

11. Iliopolov S.K., Martirosova I.V., Shcheglov G.A., Chubenko E.N., Cherskov R.M., Haddad L.N. Rubber-polymer bitumen modifier. RF Patent 2266934. Bul. No. 36. 27.12.2005 (in Russ.).

12. Frolov I.N., Yusupova T.N., Ganeeva Yu.M., Barskaya E.E., Romanov G.V. Physical and chemical features of modification of commodity bitumen by mixed olefin thermoplastics. *Neftegazovoe delo.* 2008(2). Available from: http://ogbus.ru/authors/Frolov/Frolov_1.pdf (in Russ.).

13. Senise S., Carrera V., Navarro F.J., Partal P. Thermomechanical and microstructural evaluation of hybrid rubberised bitumen containing a thermoplastic polymer. *Construct. Build. Mater.* 2017;157:873-884. https://doi.org/10.1016/j.conbuildmat.2017.09.126

14. Gordeeva I.V., Nikolskii V.G., Naumova Yu.A. Hybrid modifier on the basis of crushed vulcanizate obtained by the method of high-temperature shear grinding. Collection of papers of the XX Anniversary Scientific-Practical Conference "Rubber Industry: Raw Stocks, Materials, Technologies" Moscow: NIISHP; 2015:217-220 (in Russ.).

15. Zvereva U.G. Rubber-bitumen composites on the basis of bitumen and active rubber powder (APDDR): preparation, structure, rheological properties, application. Diss. of Cand. of Chem. Sci.: 02.00.06. Moscow: 2016. 149 p. (in Russ.).

16. Berlin A.A., Dudareva T.V., Krasotkina I.A., Nikolskii V.G. Disposal of waste tire rubber and active powder of discretely devulcanized rubber. *All materials. Encyclopedic reference book.* 2018;2:27-35 (in Russ.).

17. Zhu C., Zhanga H., Xua G., Wub C. Investigation of the aging behaviors of multi-dimensional nanomaterials modified different bitumens by Fourier transform infrared spectroscopy. *Construct. Build. Mater.* 2018;167:536-542. https://doi.org/10.1016/j.conbuildmat.2018.02.056

4. Soenen H., Lu X., Redelius P. The morphology of SBS modified bitumen in binders and in asphalt mix. In: Advanced Testing and Characterization of Bituminous Materials, London: Taylor & Francis Group; 2009. P. 151-160. ISBN 978-0-415-55854-9

5. Behnood A., Gharehveran M.M. Morphology, rheology, and physical properties of polymer-modified asphalt binders. *Eur. Polym. J.* 2019;112:766-791. https://doi.org/10.1016/j.eurpolymj.2018.10.049

6. Никольский В.Г., Дударева Т.В., Красоткина И.А., Зверева У.Г., Бекешев В.Г., Рочев В.Я., Каплан А.М., Чекунаев Н.И., Внукова Л.В., Стырикович Н.М., Гордеева И.В. Разработка и свойства новых наномодификаторов для дорожного покрытия. *Химическая физика.* 2014;33(7):87-93. https://doi.org/10.7868/s0207401x14070073

7. Schaur A., Unterberger S., Lackner R. Impact of molecular structure of SBS on thermomechanical properties of polymer modified bitumen. *Eur. Polym. J.* 2017;96:256-265. https://doi.org/10.1016/j.eurpolymj.2017.09.017

8. Loderer C., Partl M.N., Poulikakos L.D. Effect of crumb rubber production technology on performance of modified bitumen. *Constr. Build. Mater.* 2018;191:1159-1171. https://doi.org/10.1016/j.conbuildmat.2018.10.046

9. Biro S., Fazekas B. Asphalt rubber versus other modified bitumens. *Road Mater. Pavement.* 2012. URL: http://www.ra-foundation.org/wp-content/uploads/2013/02/020-PAP_017.pdf

10. Greene J., Chun S., Nash T., Choubane B. Evaluation and Implementation of PG 76-22 Asphalt Rubber Binder in Florida. *Transport. Res. Rec*. 2015;2524(1);3-10. https://doi.org/10.3141/2524-01

11. Илиополов С.К., Мардиросова И.В., Щеглов А.Г., Чубенко Е.Н., Черсков Р.М., Хаддад Л.Н. Резиносодержащий полимерный модификатор битума. Патент РФ № 2266934. Бюл. №36. 27.12.2005.

12. Фролов И.Н., Юсупова Т.Н., Ганеева Ю.М., Барская Е.Е., Романов Г.В. Физико-химические особенности модификации товарных битумов смесевыми олефиновыми термопластами. *Нефтегазовое дело.* 2008(2). URL: http://ogbus.ru/authors/Frolov/Frolov_1.pdf

13. Senise S., Carrera V., Navarro F.J., Partal P. Thermomechanical and microstructural evaluation of hybrid rubberised bitumen containing a thermoplastic polymer. *Construct. Build. Mater.* 2017;157:873-884. https://doi.org/10.1016/j.conbuildmat.2017.09.126

14. Гордеева И.В., Никольский В.Г., Наумова Ю.А. Гибридный модификатор на основе измельченного вулканизата, получаемого методом высокотемпературного сдвигового измельчения. Сборник докладов XX Юбилейной научно-практической конференции «Резиновая промышленность: Сырье. Материалы. Технологии». Москва: НИИШП; 2015:217-220.

15. Зверева У.Г. Резинобитумные композиты на основе дорожного битума и активного резинового порошка (АПДДР): получение, структура, реологические свойства, применение. Дисс. кан. хим. наук: 02.00.06. М.: 2016. 149 с.

16. Берлин А.А., Дударева Т.В., Красоткина И.А., Никольский В.Г. Утилизация отходов шинной резины и активный порошок дискретно девулканизованной резины. *Все материалы. Энциклопедический справочник.* 2018;2:27-35.

17. Zhu C., Zhanga H., Xua G., Wub C. Investigation of the aging behaviors of multi-dimensional nanomaterials modified different bitumens by Fourier transform infrared spectroscopy. *Construct. Build. Mater.* 2018;167:536-542. https://doi.org/10.1016/j.conbuildmat.2018.02.056

18. Weigel S., Stephan D. The prediction of bitumen properties based on FTIR and multivariate analysis methods. *Fuel.* 2017;208(15):655-661. https://doi.org/10.1016/j.fuel.2017.07.048

19. Yao H., Dai Q., You Zh. Fourier Transform Infrared Spectroscopy characterization of aging-related properties of original and nano-modified asphalt binders. *Construct. Build. Mater.* 2015;101:1078-1087. https://doi.org/10.1016/j.conbuildmat.2015.10.085

20. Nivitha M.R., Prasad E., Krishnan J.M. Transitions in unmodified and modified bitumen using FTIR spectroscopy. *Mater. Struct.* 2019;52(7):1-11. https://doi.org/10.1617/s11527-018-1308-7

21. Makarov D.B., Agung E.M., Ayupov D.A., Murafa A.V., Faskhutdinov K.A., Khozin V.G., Yakhin R.G. Study of bitumen-polymer binders, modified by mixed thermoplastic elastomer by the method of IR-spectroscopy. *Izvestiya KGASU = News of the KSUAE.* 2015;4(34):280-286. (in Russ.).

22. Bellamy L.J. The Infra-red Spectra of Complex Molecules. Dordrecht: Springer; 1975. https://doi.org/10.1007/978-94-011-6017-9

23. Nakamoto K. Infrared Spectra of Inorganic and Coordination Compounds. New York: John Wiley & Sons, Inc.; 1963.

24. Tang N., Huang W., Xiao F. Chemical and rheological investigation of high-cured crumb rubber-modified asphalt. *Construct. Build. Mater.* 2016;123:847-854. https://doi.org/10.1016/j.conbuildmat.2016.07.131

25. Zhang F., Hu C. The research for structural characteristics and modification mechanism of crumb rubber compound modified asphalts. *Construct. Build. Mater.* 2015;76(1):330-342. https://doi.org/10.1016/j.conbuildmat.2014.12.013

18. Weigel S., Stephan D. The prediction of bitumen properties based on FTIR and multivariate analysis methods. *Fuel.* 2017;208(15):655-661. https://doi.org/10.1016/j.fuel.2017.07.048

19. Yao H., Dai Q., You Zh. Fourier Transform Infrared Spectroscopy characterization of aging-related properties of original and nano-modified asphalt binders. *Construct. Build. Mater.* 2015;101:1078-087. https://doi.org/10.1016/j.conbuildmat.2015.10.085

20. Nivitha M.R., Prasad E., Krishnan J.M. Transitions in unmodified and modified bitumen using FTIR spectroscopy. *Mater. Struct.* 2019;52(7):1-11. https://doi.org/10.1617/s11527-018-1308-7

21. Макаров Д.Б., Ягунд Э.М., Аюпов Д.А., Мурафа А.В., Фасхутдинов К.А., Хозин В.Г., Яхин Р.Г. Изучение битумно-полимерных вяжущих, модифицированных смесевыми термоэластопластами, методом ИК-спектроскопии. *Известия КГАСУ.* 2015;4(34):280-286.

22. Bellamy L.J. The Infra-red Spectra of Complex Molecules. Dordrecht: Springer; 1975. https://doi.org/10.1007/978-94-011-6017-9

23. Накамото К. Инфракрасные спектры неорганических и координационных соединений. М.: Издательство «Мир»; 1966. 411 с.

24. Tang N., Huang W., Xiao F. Chemical and rheological investigation of high-cured crumb rubber-modified asphalt. *Construct. Build. Mater.* 2016;123:847-854. https://doi.org/10.1016/j.conbuildmat.2016.07.131

25. Zhang F., Hu C. The research for structural characteristics and modification mechanism of crumb rubber compound modified asphalts. *Construct. Build. Mater.* 2015;76(1):330-342. https://doi.org/10.1016/j.conbuildmat.2014.12.013

About the authors:

Irina V. Gordeeva, Junior Research Assistant, N.N. Semenov Federal Research Center of Chemical Physics, Russian Academy of Sciences (4, ul. Kosygina, Moscow, 119991, Russia). E-mail: irinavolchenko90@yandex.ru. Scopus Author ID 39261264400, ResearcherID E-6567-2014, https://orcid.org/0000-0002-9879-3701

Dmitry A. Melnikov, Engineer, Research Institute of Elastomeric Materials and Products (2, b. 1, Perovskii proezd, Moscow, 111024, Russia). E-mail: d.melnikov@1lab.niiemi.com. https://orcid.org/0000-0001-7126-3391

Victoria N. Gorbatova, Engineer, N.N. Semenov Federal Research Center of Chemical Physics, Russian Academy of Sciences, (4, ul. Kosygina, Moscow, 119991, Russia). E-mail: vik21477677@yandex.ru. https://orcid.org/0000-0003-1592-345X

Dmitry S. Reznichenko, Cand. of Sci., General Director, Research Institute of Elastomeric Materials and Products (2, b. 1, Perovskii proezd, Moscow, 111024, Russia); Senior Teacher, B.A. Dogadkin Department of Material Physics and Chemistry, Physico-Technological Institute, MIREA – Russian Technological University (1, b. 5, Malaya Pirogovskaya ul., Moscow, 119435, Russia). ResearcherID B-6738-2016, https://orcid.org/0000-0001-8326-667X

Yulia A. Naumova, Dr. of Sci. (Chemistry), Professor, Department of Chemistry and Processing Technology of Elastomers, M.V. Lomonosov Institute of Fine Chemical Technologies, MIREA – Russian Technological University (86, Vernadskogo pr., Moscow, 119571, Russia). E-mail: naumova_yulia@mail.ru. Researher ID C-1077-2018, https://orcid.org/0000-0001-9968-8244

Об авторах:

Гордеева Ирина Владимировна, младший научный сотрудник, Федеральный исследовательский центр химической физики им. Н.Н. Семенова, Российская академия наук (119991, Россия, Москва, ул. Косыгина, д. 4). E-mail: irinavolchenko90@yandex.ru. Scopus Author ID 39261264400, ResearcherID E-6567-2014, https://orcid.org/0000-0002-9879-3701

Мельников Дмитрий Анатольевич, инженер, ООО «Научно-исследовательский институт эластомерных материалов и изделий» (111024, Россия, Москва, Перовский проезд, д. 2, стр. 1). E-mail: d.melnikov@1lab.niiemi.com. https://orcid.org/0000-0001-7126-3391

Горбатова Виктория Николаевна, инженер, Федеральный исследовательский центр химической физики им. Н.Н. Семенова, Российская академия наук (119991, Москва, ул. Косыгина, д. 4). E-mail: vik21477677@yandex.ru. https://orcid.org/0000-0003-1592-345X

Резниченко Дмитрий Сергеевич, кандидат технических наук, генеральный директор, ООО «Научно-исследовательский институт эластомерныхматериалов и изделий» (111024, Россия, Москва, Перовский проезд, д. 2, стр. 1); старший преподаватель, кафедра физики и химии материалов имени Б.А. Догадкина, Физико-технологический институт, ФГБОУ ВО «МИРЭА – Российский технологический университет» (119435, Россия, Москва, улица Малая Пироговская, д. 1, стр. 5). ResearcherID B-6738-2016, https://orcid.org/0000-0001-8326-667X

Наумова Юлия Анатольевна, доктор химических наук, профессор кафедры химии и технологии переработки эластомеров им. Ф.Ф. Кошелева, Институт тонких химических технологий им. М.В. Ломоносова, ФГБОУ ВО «МИРЭА – Российский технологический университет» (119571, Россия, Москва, пр-т Вернадского, д. 86). E-mail: naumova_yulia@mail.ru. ResearherID C-1077-2018, https://orcid.org/0000-0001-9968-8244

Submitted: July 01, 2019; Reviewed: January 31, 2020; Accepted: April 02, 2020.

Translated from Russian into English by H. Moshkov
Edited for English language and spelling by Enago, an editing brand of Crimson Interactive Inc.

ISSN 2686-7575 (Online)
https://doi.org/10.32362/2410-6593-2020-15-2-67-76
UDC 546.77+ 661.877.22

Molybdenum(VI) oxide: New methods of synthesis and properties

Elena E. Nikishina[@], **Elena N. Lebedeva**, **Dmitry V. Drobot**

MIREA – Russian Technological University (M.V. Lomonosov Institute of Fine Chemical Technologies), Moscow, 119571 Russia
[@]Corresponding author, e-mail: helena_nick@mail.ru

Objectives. *The present study aims to develop new methods for the synthesis of molybdenum(VI) oxide, which is a precursor for the synthesis of functional materials, as well as to investigate the physicochemical properties of the resulting oxide phases.*
Methods. *The synthesized phases and the products of their thermolysis were studied by differential thermal analysis, IR spectroscopy, X-ray diffraction analysis, and granulometry.*
Results. *Three methods for the synthesis of molybdenum(VI) oxide were developed, and the physicochemical properties of the oxide phases obtained were studied. The first method consisted in the reaction of molybdenum pentachloride with a 6.0–9.5 mol/L ammonia solution, the second one was the reaction of niobium pentachloride with a sulfuric acid solution, and the third method involved the reaction of ammonium molybdate with nitric acid, affording brown molybdenum(V)* $MoO(OH)_3$ *hydroxide, a bright blue precipitate of molybdenum blue* $MoO_{2.75}$*, and white hydrated oxide* $MoO_3{\cdot}H_2O$*, respectively.*
Conclusions. *A series of thermal and X-ray diffraction analysis demonstrated that in all cases the samples were amorphous phases. Heat treatment at 580 °C of the synthesized phases led to the formation of a rhombic modification of molybdenum trioxide. The lattice parameters and X-ray density were calculated for all thermolysis products. The effect of heat treatment on the particle size of the synthesized samples and their thermolysis products was studied. Particle size analysis demonstrated that particles of different diameters were formed depending on the synthetic method. The smallest particle size (0.3–0.6 µm) was found in molybdenum trioxide, a product of the thermolysis of the sample obtained by the reaction of molybdenum pentachloride with a concentrated ammonium solution.*

Keywords: *molybdenum, oxides, thermal analysis, X-ray diffraction analysis, IR spectroscopy, particle size analysis.*

For citation: Nikishina E.E., Lebedeva E.N., Drobot D.V. Molybdenum(VI) oxide: New methods of synthesis and properties. *Tonk. Khim. Tekhnol. = Fine Chem. Technol.* 2020;15(2):67-76. https://doi.org/10.32362/2410-6593-2020-15-2-67-76

Оксид молибдена(VI): Новые методы синтеза и свойства

Е.Е. Никишина@, Е.Н. Лебедева, Д.В. Дробот

МИРЭА – Российский технологический университет (Институт тонких химических технологий имени М.В. Ломоносова), Москва, 119454 Россия
@Автор для переписки, e-mail: helena_nick@mail.ru

Цели. *Целью работы была разработка новых методов синтеза оксида молибдена(VI), являющегося предшественником для синтеза функциональных материалов на его основе, а также исследование физико-химических свойств полученных фаз.*
Методы. *Синтезированные фазы и продукты их термолиза изучали методами дифференциально-термического анализа, ИК-спектроскопии, рентгенофазового анализа, гранулометрии.*
Результаты. *Разработаны три метода синтеза оксида молибдена(VI) и исследованы физико-химических свойства полученных оксидных фаз. Первый способ заключался во взаимодействии пентахлорида молибдена с раствором аммиака концентрацией 6.0–9.5 моль/л, второй – во взаимодействии пентахлорида ниобия с раствором серной кислоты, третий – во взаимодействии молибдата аммония с азотной кислотой. В первом случае образовался гидроксид молибдена(V)* $MoO(OH)_3$ *бурого цвета, во втором случае наблюдалось образование осадка ярко-синего цвета – молибденовой сини* $MoO_{2.75}$, *в третьем случае образовался гидратированный оксид* $MoO_3{\cdot}H_2O$ *белого цвета.*
Выводы. *Дифференциально-термический и рентгенофазовый анализы показали, что во всех случаях образцы представляют собой аморфные фазы. Термическая обработка (T = 580 °C) синтезированных фаз приводит к образованию триоксида молибдена ромбической модификации. Для всех продуктов термолиза рассчитаны параметры решетки и рентгеновская плотность. Проведено исследование влияния термической обработки на размер частиц синтезированных образцов и продуктов их термолиза. Гранулометрический анализ показал, что в зависимости от способа получения триоксида молибдена, образуются частицы разного диаметра. Наименьший размер частиц (0.3–0.6 мкм) обнаружен у триоксида молибдена – продукта термолиза образца, полученного при взаимодействии пентахлорида молибдена с концентрированным раствором аммиака.*

Ключевые слова: *молибден, оксиды, термический анализ, рентгенофазовый анализ, ИК-спектроскопия, гранулометрический анализ.*

Для цитирования: Никишина Е.Е., Лебедева Е.Н., Дробот Д.В. Оксид молибдена(VI): Новые методы синтеза и свойства. *Тонкие химические технологии.* 2020;15(2):67-76. https://doi.org/10.32362/2410-6593-2020-15-2-67-76

INTRODUCTION

Molybdenum forms compounds having a wide variety of metal oxidation states, which results in oxide phases that are characterized by a rich chemistry. Despite the increased interest in the oxide phases of molybdenum, especially in MoO_2 and MoO_3, the available information about their properties is still scarce. Further study of the oxides of molybdenum is essential for the development of new applications in modern industry. In particular, these compounds are potential candidates for efficient electrochemical energy storage systems due to their unique physical and chemical properties such as conductivity and mechanical and thermal stability [1–4].

Figure 1 shows the phase diagram of the molybdenum–oxygen system.

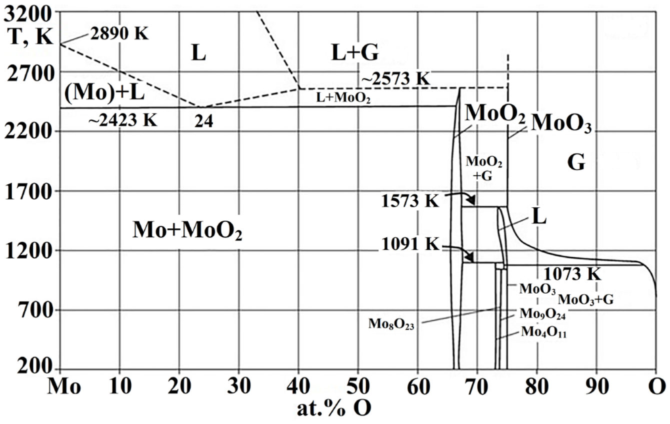

Fig. 1. Phase diagram of the molybdenum–oxygen system [5].

The stable oxides of this system are the α-phase of molybdenum trioxide (MoO_3) and the δ-phase of molybdenum dioxide (MoO_2). Additionally, there are eight phases of intermediate composition between MoO_3 and MoO_2: Mo_4O_{11}, Mo_5O_{14}, Mo_6O_{17}, Mo_7O_{20}, Mo_8O_{23}, Mo_9O_{26}, $Mo_{17}O_{47}$, and $Mo_{18}O_{52}$. These phases have a pronounced nonstoichiometry, and most of them are unstable. For example, the Mo_4O_{11} phase disproportionates into MoO_2 and MoO_3. The bonds in oxides are mainly ionic, but also partially covalent; the volatility of oxides confirms the covalent nature of their bonds [5–8].

Molybdenum(IV) oxide crystallizes in a distorted rutile-type monoclinic lattice (a = 0.5611 nm, b = 0.4856 nm, c = 0.5628 nm). This oxide has a chain structure consisting of MoO_6 octahedra that are connected by common edges and vertices (Fig. 2) [5, 9].

Molybdenum(VI) oxide consists of white, green-tinged, flat rhombic crystals (a = 0.3963 nm, b = 1.3855 nm, c = 0.3696 nm) with a layered structure. In the MoO_3 molecule, the coordination number of molybdenum is six. Its structure, which is similar to that of crystalline ReO_3, is constructed from coordination polyhedra that can be joined by vertices, edges, or both. The unequal number of molybdenum–oxygen bonds connected by vertices and edges leads to a strongly distorted octahedral coordination around the metal centers. Each molybdenum atom is located in the center of a MoO_6 octahedron and surrounded by six oxygen atoms, which are located at the vertices of the octahedron. MoO_3 has several polymorphic modifications (Fig. 3): the most thermodynamically stable phase α-MoO_3 (*Pnma* space group), the metastable modification β-MoO_3, and h-MoO_3. In the α-MoO_3 and h-MoO_3 modifications, the MoO_6 octahedra are linked to each other by both vertices and edges, whereas they are linked only by the vertices in β-MoO_3 [5, 10–12].

The unique layered structure of MoO_3 renders it a promising material for anode and cathode in electrochemical capacitors [4]. Catalytic materials based on MoO_3 have been used in processes such as methanol oxidation, isomerization and hydrogenation of olefins, and oil refining (cracking, hydrotreating, and reforming) [13, 14]. Currently, the production of MoO_3-based materials is carried out via a limited number of methods including chemical deposition, hydrothermal process, sol–gel method, or chemical vapor deposition [15–20], most of which require high temperatures and pressures.

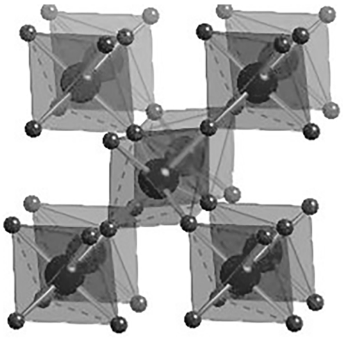

Fig. 2. Structure of molybdenum dioxide. Oxygen atoms are located at the vertices of octahedra, and molybdenum atoms are located in the center of octahedra [5].

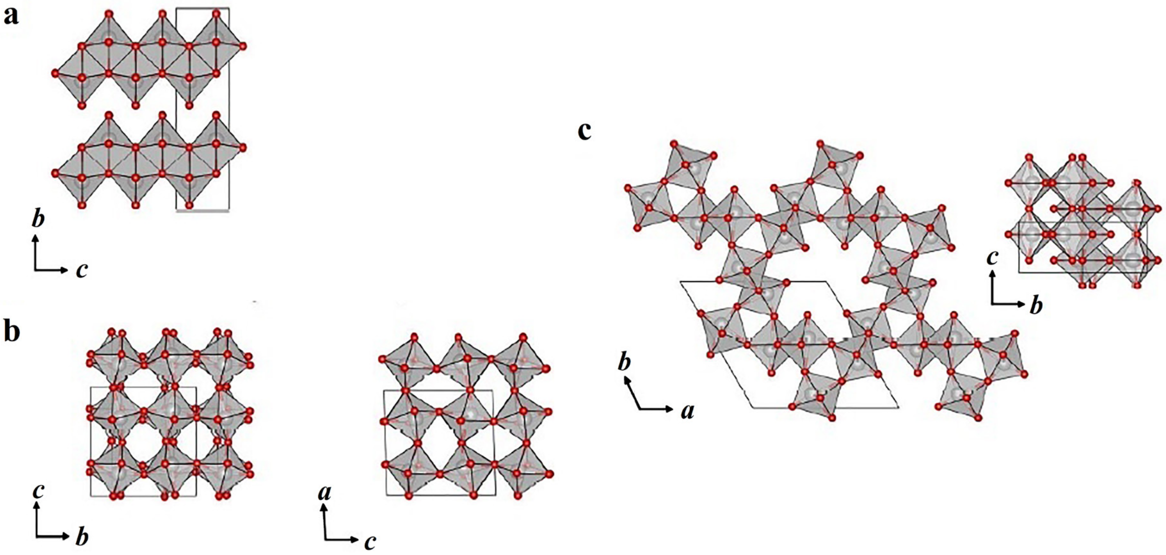

Fig. 3. Structures of polymorph modifications of molybdenum trioxide: a) α-MoO_3, b) β-MoO_3, c) h-MoO_3. In all structures, a unit cell is shown as a thin black line, oxygen atoms are indicated by black spheres, molybdenum atoms are located inside the gray MoO_6 octahedra [12].

The aim of this work is to explore new methods for the synthesis of molybdenum(VI) oxide, which is a precursor for the synthesis of functional materials, as well as to study the physical and chemical properties of the resulting phases.

MATERIALS AND METHODS

The precursors used in this work were molybdenum pentachloride (qualification ACS, *Merck*, Germany), ammonium molybdate (qualification AR, *Merck*, Germany), sulfuric acid (qualification CP, GOST 4204-77, *CHIMMED*, Russia), nitric acid (qualification ACS, GOST 11125-84, *CHIMMED*, Russia), and ammonia solution (qualification ACS 25-5, GOST 24147-80, *CHIMMED*, Russia).

Molybdenum oxide phases were obtained by the three following synthesis methods:

- The first synthesis consisted in the reaction of molybdenum pentachloride with a 6.0–9.5 mol/L ammonia solution. In this case, a brown precipitate was formed, which was indicative of the formation of molybdenum(V) hydroxide $MoO(OH)_3$ according to reaction (1) as follows [21]:

$$MoCl_5 + 5NH_3{\cdot}H_2O \rightarrow MoO(OH)_3 + 5NH_4Cl + H_2O \quad (1)$$

- In the second synthetic procedure, a solution of concentrated sulfuric acid was added to molybdenum pentachloride. During this reaction, the formation of a bright blue precipitate was observed, which corresponds most likely to molybdenum blue. This compound, in which molybdenum exhibits the oxidation states +5 and +6, is usually obtained by reducing molybdenum(VI) to molybdenum(V) [22, 23]. In contrast, we oxidized molybdenum(V) to molybdenum(VI) using sulfuric acid as a strong oxidizer according to reaction (2):

$$4MoCl_5 + 2H_2SO_4 + 9H_2O \rightarrow 4MoO_{2.75} + SO_2 + 20HCl \quad (2)$$

- The third synthesis consisted in the reaction of ammonium molybdate with boiling nitric acid as follows:

$$(NH_4)_2MoO_4 + 2HNO_3 \rightarrow MoO_3{\cdot}nH_2O + 2NH_4NO_3 \quad (3)$$

As a result, a fine white powder was formed.

Differential thermal analysis of the samples was performed on a Q-1500 D derivatograph (F. Paulik, J. Paulik, L. Erdey; *MOM*, Hungary) in air with the simultaneous recording of four curves, namely, differential (DTA), thermal (T), differential thermogravimetric (DTG), and integral weight loss (TG) curves using the software and hardware systems developed by *IP Tetran*, Russia, in the LabVIEW 8.21 environment (*National Instruments*, Austin, Texas, USA). The temperature was measured using a PP-1 platinum/platinum–rhodium thermocouple with an error of ±5°C within a temperature range of 20–1000°C, at a heating rate of 10°C/min, and using α-Al_2O_3 as a reference sample.

X-ray diffraction (XRD) analysis was performed on a Bruker D8 Advance diffractometer using CuK_α radiation, continuous sample rotation (1°/min), and step-by-step (step $2\theta = 0.02°$, exposure 0.5 s/step) mode in the angle range $2\theta = 5$–$80°$. The International Center for Diffraction Data–Joint Committee on Power Diffraction Standards (ICDD–JCPDS) card file was used for phase identification.

The X-ray density was calculated using the formula:

$$\rho_{X-ray} = \frac{M \times Z \times 1.66}{V}, \quad (4)$$

where M is the molecular weight, g/mol; Z is the number of formula units; and V is the volume of the unit cell, Å^3.

In the case of the rhombic modification of molybdenum trioxide ($a \neq b \neq c$, $\alpha = \beta = \gamma = 90°$), the following formula applies:

$$V = a \times b \times c. \quad (5)$$

Infrared (IR) absorption spectra in the area of 3600–400 cm^{-1} were recorded on a Specord M80 spectrometer by using KBr pellets, with an error below 3–4 cm^{-1}.

Granulometric analysis for the determination of the particle size distribution was performed using a DelsaNano laser particle analyzer from *Beckman Coulter*, USA. This device can measure particles dispersed in a liquid in the measurement range from 0.6 nm to 7 µm by diffraction method. The LS series devices use laser light with a wavelength of 780 nm.

Heat treatment of samples was carried out in a laboratory furnace TK-12.1250.H.1Ф equipped with an automatic temperature controller "Thermomatic-N." The error of automatic control at the nominal temperature was ±1°C.

RESULTS AND DISCUSSION

The thermal transformations of the synthesized phases were studied in the temperature range from 20 to 1000°C.

Figure 4 shows the DTA curves of the samples.

The DTA curves demonstrate the occurrence of endothermic effects associated with a dehydration

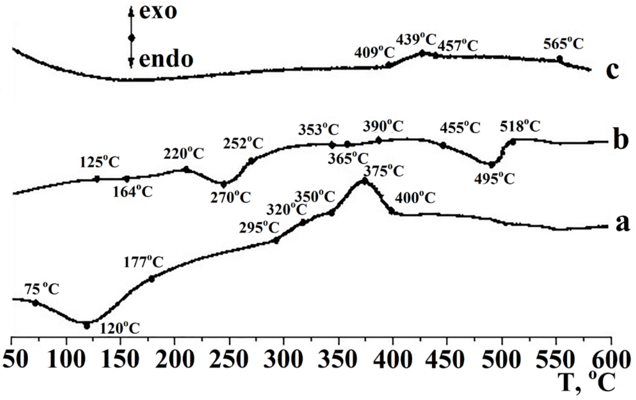

Fig. 4. Differential thermal analysis curves of
a) the sample obtained by the reaction of molybdenum(V) chloride with a concentrated ammonium solution (brown powder),
b) the sample obtained by the reaction of molybdenum(V) chloride with a concentrated sulfuric acid solution (molybdenum blue),
and c) the sample obtained by the reaction between ammonium molybdate and nitric acid.

process. In addition, for the sample obtained by reacting molybdenum(V) chloride with a concentrated sulfuric acid solution, the observed endothermic effects may be associated with the volatilization of reaction byproducts such as SO_2 and HCl. The presence of an exothermic effect at 350–400°C (Fig. 4a) corresponds to the oxidation process of Mo(V) to Mo(VI), which was confirmed by the increase in the mass of the sample during the annealing process. An exothermic effect in the temperature range of 410–460°C for the sample obtained by the reaction between ammonium molybdate and nitric acid (Fig. 4c) can be attributed to the decomposition of the reaction byproduct, i.e., molybdenum oxonitrate $MoO_2(NO_3)_2$, to nitrogen dioxide (NO_2) and molybdenum oxide (MoO_3). This process was accompanied by a decrease in the mass of the sample. Moreover, an exothermic effect in the temperature range of 555–565°C can be assigned to the crystallization of amorphous molybdenum trioxide.

At temperatures above 600°C, a significant decrease in mass was observed for all samples due to evaporation of molybdenum(VI) oxide. According to the literature, this compound begins to evaporate below its melting point (in the range of 600–795°C). Thus, a noticeable increase in pressure occurs at the melting temperature (795°C) [24].

On the basis of the IR spectroscopy and XRD results, we decided to anneal the samples at 580°C because the mass of the samples remains constant at this temperature, and the evaporation process has not yet begun.

Similar absorption bands are observed in the IR spectra of the three samples. In particular, the residual absorption band in the region of 3600–3000 cm^{-1}, with a maximum at ~3465 cm^{-1}, is attributable to valence vibrations of hydroxo groups and water (Fig. 5) [25]. The absorption band at 993–987 cm^{-1} corresponds to the Mo=O bonds. This band is characteristic of crystalline MoO_3, in which each molybdenum atom is surrounded by six oxygen atoms, thus forming a MoO_6 octahedron [26]. The absorption bands in the 880–860 cm^{-1} region correspond to symmetrical Mo–O–Mo vibrations, and the absorption band at 820 cm^{-1} corresponds to asymmetric Mo–O–Mo vibrations of molybdenum trioxide, in which the oxygen atom bridges two MoO_6 octahedra [27]. The absorption band at 623–583 cm^{-1} corresponds to Mo_3–O vibrations. In this case, the oxygen atom is shared between three MoO_6 octahedra [27, 28].

Then, the samples were subjected to isothermal annealing at 580°C for 15 hours. The annealing temperature was selected according to the results of differential thermal analysis; at 580°C, the loss of mass was completed. The resulting phases were gray-green powders.

To identify the obtained phases, the synthesized samples and their thermolysis products were subjected to an XRD analysis at 580°C. All the synthesized samples were amorphous phases.

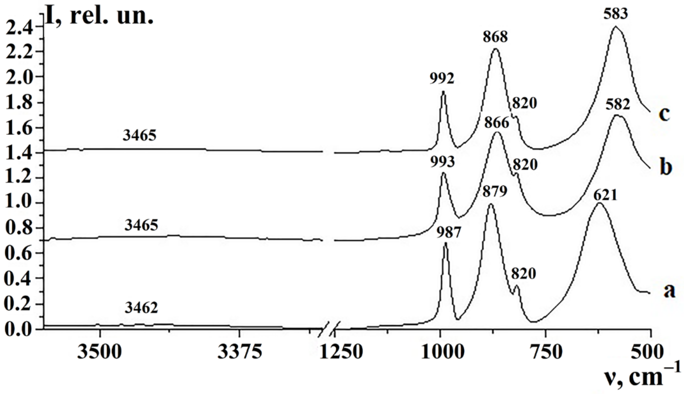

Fig. 5. IR spectra of the products of the thermal decomposition of
a) the sample obtained by the reaction of molybdenum(V) chloride with a concentrated ammonia solution (brown powder),
b) the sample obtained by the reaction of molybdenum(V) chloride with a concentrated sulfuric acid solution (molybdenum blue),
and c) the sample obtained by the reaction between ammonium molybdate and nitric acid.

The XRD patterns of the thermal decomposition products (T = 580°C) are shown in Fig. 6. In all cases, the formation of a rhombic modification of molybdenum oxide MoO_3 can be observed. The unit cell parameters and X-ray density are summarized in table.

The influence of heat treatment on the particle size of the synthesized samples and their thermolysis products at 580°C was studied. Figure 7a shows the particle size distribution of the sample obtained by reacting molybdenum pentachloride with an ammonia solution. The main fraction corresponds to a particle size of 0.7–1.2 µm (~90%). Upon heat treatment of this sample, molybdenum trioxide having particles of 0.3–0.6 µm (~95%) was obtained (Fig. 7b). Unfortunately, the determination of the particle size of the sample obtained by reaction of molybdenum pentachloride with a sulfuric acid solution was hindered by its solubility in water.

Figure 8 shows the particle size distribution of the thermolysis product of this sample. The main fraction corresponds to a particle size of 0.6–0.9 µm (~95%).

Figure 9a shows the particle size distribution of a sample obtained by reacting ammonium molybdate with a nitric acid solution. The main fraction corresponds to particles with a size of 3.0–5.0 µm (~90%). During heat treatment of the sample, molybdenum trioxide having two particle fractions, i.e., particles of 0.7–1.0 µm (~80%) and 3.0–6.0 µm (~6%), was obtained (Fig. 9b).

As can be seen from the particle distributions, the smallest particles were formed upon thermolysis of the sample obtained by reacting molybdenum pentachloride with an ammonia solution.

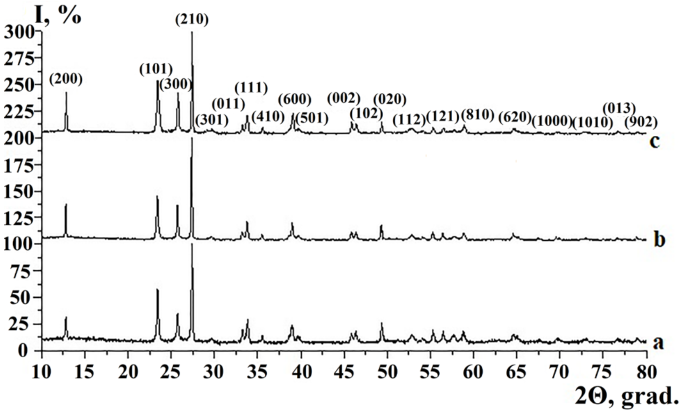

Fig. 6. X-ray diffraction patterns of the products obtained after thermal decomposition at 580°C for 15 hours of a) the sample obtained by the reaction of molybdenum(V) chloride with a concentrated ammonia solution (brown powder), b) the sample obtained by the reaction of molybdenum(V) chloride with a concentrated sulfuric acid solution (molybdenum blue), and c) the sample obtained by the reaction between ammonium molybdate and nitric acid.

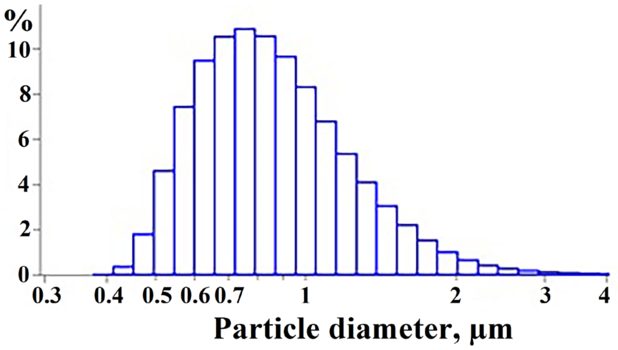

Fig. 8. Particle size distribution of the product of the thermolysis of the sample obtained by the reaction of molybdenum pentachloride with a sulfuric acid solution.

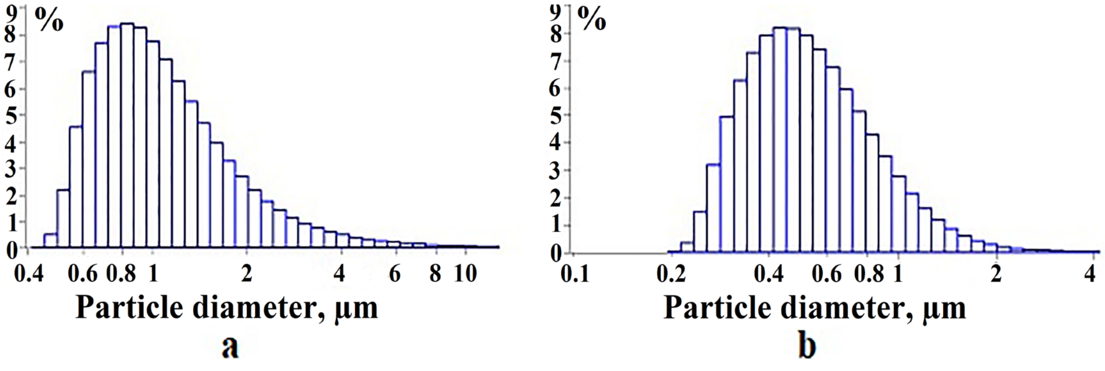

Fig. 7. Particle size distribution of (a) the sample obtained by the reaction of molybdenum pentachloride with an ammonia solution and (b) the product of its heat treatment at T = 580°C.

XRD data of the samples obtained after annealing at 580°C

Lattice parameters of the synthesized samples		ICDD–JCPDS data for MoO_3 (orthorhombic)
Synthesis 1 (molybdenum pentachloride and ammonia solution)	$a = (1.382 \pm 0.001)$ nm $b = (0.3696 \pm 0.0005)$ nm $c = (0.3956 \pm 0.0005)$ nm $V = 202.07 \times 10^{-3}$ nm^3 $\rho_{X\text{-}ray} = 4.73$ g/cm^3	$a = 1.3825$ nm $b = 0.3694$ nm $c = 0.3954$ nm $V = 201.93 \times 10^{-3}$ nm^3 $\rho_{X\text{-}ray} = 4.73$ g/cm^3
Synthesis 2 (molybdenum pentachloride and sulfuric acid)	$a = (1.383 \pm 0.001)$ nm $b = (0.3699 \pm 0.0005)$ nm $c = (0.3960 \pm 0.0005)$ nm $V = 202.70 \times 10^{-3}$ nm^3 $\rho_{X\text{-}ray} = 4.54$ g/cm^3	
Synthesis 3 (ammonium molybdate and nitric acid)	$a = (13.817 \pm 0.01)$ nm $b = (3.694 \pm 0.001)$ nm $c = (3.959 \pm 0.005)$ nm $V = 202.07 \times 10^{-3}$ nm^3 $\rho_{X\text{-}ray} = 4.73$ g/cm^3	

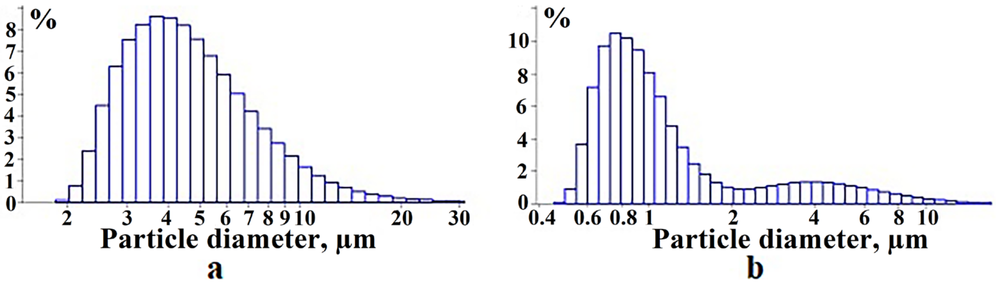

Fig. 9. Particle size distribution of (a) the sample obtained by the reaction of ammonium molybdate with nitric acid and (b) the product of its heat treatment at T = 580°C.

CONCLUSIONS

1. Oxide phases in the molybdenum–oxygen system were synthesized following three procedures. The first method consists in the heterophase reaction of molybdenum pentachloride with a concentrated ammonia solution, the second in the reaction of molybdenum pentachloride with a concentrated sulfuric acid solution, and the third in the reaction of nitric acid with ammonium molybdate.

2. Using various analytical methods including XRD, DTA-DTG, IR spectroscopy, and granulometry, the physicochemical properties of the synthesized samples and their thermolysis products were studied.

3. DTA and XRD analysis demonstrated that in all cases the samples were amorphous phases. Heat treatment at 580°C led to the formation of a rhombic modification of molybdenum trioxide. Lattice parameters and X-ray density were calculated for all thermolysis products.

4. The results of granulometric analysis showed that particles of different diameters were formed depending on the synthetic method. The smallest particle size (0.3–0.6 μm) was found in molybdenum trioxide, a thermolysis product of the sample obtained by reacting molybdenum pentachloride with a concentrated ammonia solution.

Acknowledgments

This work was supported by the Russian Foundation for Basic Research, project No. 18-03-00671.

The authors declare no conflicts of interest.

REFERENCES

1. Miao F., Wu W., Li Q., Miao R., Tao B. Fabrication and Application of Molybdenum Trioxide Nanostructure Materials for Electrochemical Capacitors. *Int. J. Electrochem. Sci.* 2017;12:12060-12073.
https://doi.org/10.20964/2017.12.200

2. Ban D., Xu N., Deng S., Chen J., She J. Low-temperature Synthesis of Large-area Films of Molybdenum Trioxide Microbelts in Air and the Dependence of Their Field Emission Performance on Growth Conditions. *J. Mater. Sci. Technol.* 2010;26(7):584-588.
https://doi.org/10.1016/S1005-0302(10)60089-8

3. Li G., Jiang L., Pang S., Peng H. Zhang Z. Molybdenum Trioxide Nanostructures: The Evolution from Helical Nanosheets to Crosslike Nanoflowers to Nanobelts. *J. Phys. Chem. B.* 2006;110(48):24472-24475.
https://doi.org/10.1021/jp064855v

4. Hu X., Zhang W., Liu X., Meia Y., Huang Y. Nanostructured Mo-based electrode materials for electrochemical energy storage. *Chem. Soc. Rev.* 2015;44(8):2376-2404.
https://doi.org/10.1039/C4CS00350K

5. Predel F. Phase diagram of Mo–O (molybdenum–oxygen) system. In: Predel F. (eds.) Phase Equilibria, Crystallographic and Thermodynamic Data of Binary Alloys. Physical Chemistry. Berlin, Heidelberg: Springer; 2016. V. 12D.

6. Karelin V.A. *Himiya i tekhnologiya molibdena i vol'frama* (Chemistry and technology molybdenum and tungstem). Tomsk: Tomsk Polytechnic University; 2017. 58 p. (in Russ.).

7. Henrich V.E., Cox P.A. The surface science of metal oxides. Cambridge: Cambridge University Press; 1996. 480 p.

8. Kihlborg L. Studies on molybdenum oxides. *Acta Chem. Scand.* 1959;13:954-962.
https://doi.org/10.3891/acta.chem.scand.13-0954

9. Brandt B.G. Skapski A.C. A refinement of the crystal structure of molybdenum dioxide. *Acta Chem. Scand.* 1967;21:661-672.
https://doi.org/10.3891/acta.chem.scand.21-0661

10. Tsuda N., Nasu K., Fujimori A., Siratori K. Electronic conduction in oxides. New York: Springer-Verlag; 1991. 323 p.

11. Kihlbord L. Least squares refinement of the crystal structure of molybdenum. *Arkiv för Kemi.* 1963;21:357-364.

12. Yun J., Jang W., Lee T., Lee Y., Soon A. Aligning the band structures of polymorphic molybdenum oxides and organic emitters in light-emitting diodes. *Phys. Rev. Applied.* 2017;7:024025-1-024025-8.
https://doi.org/10.1103/PhysRevApplied.7.024025

13. Mendes F.M. Weibel D.E., Blum R.P., Middeke J. Preparation and characterization of well-ordered MoO_x films on $Cu_3Au(100)$–oxygen substrate (CAOS). *Catal. Today.* 2008;133(1):187-191.
https://doi.org/10.1016/j.cattod.2007.11.046

14. Tomina N.N., Pimerzin A.A., Moiseev I.K. Sulfide catalysts for hydropurification of oil fractions. *Russ. J. Gen. Chem.* 2009;79(6):1274-1288.
https://doi.org/10.1134/S1070363209060449

15. Méndez-Vivar J. Synthesis of molybdenum oxides by the sol-gel method. *Inorg. Chim. Acta.* 1991;179(1):77-82.
https://doi.org/10.1016/S0020-1693(00)85376-1

16. Ganguly A., George R. Synthesis, characterization and gas sensitivity of MoO_3 nanoparticles. *Bull. Mater. Sci.* 2007;30(2):183-185.
https://doi.org/10.1007/s12034-007-0033-6

СПИСОК ЛИТЕРАТУРЫ

1. Miao F., Wu W., Li Q., Miao R., Tao B. Fabrication and Application of Molybdenum Trioxide Nanostructure Materials for Electrochemical Capacitors. *Int. J. Electrochem. Sci.* 2017;12:12060-12073.
https://doi.org/10.20964/2017.12.200

2. Ban D., Xu N., Deng S., Chen J., She J. Low-temperature Synthesis of Large-area Films of Molybdenum Trioxide Microbelts in Air and the Dependence of Their Field Emission Performance on Growth Conditions. *J. Mater. Sci. Technol.* 2010;26(7):584-588.
https://doi.org/10.1016/S1005-0302(10)60089-8

3. Li G., Jiang L., Pang S., Peng H. Zhang Z. Molybdenum Trioxide Nanostructures: The Evolution from Helical Nanosheets to Crosslike Nanoflowers to Nanobelts. *J. Phys. Chem. B.* 2006;110(48):24472-24475.
https://doi.org/10.1021/jp064855v

4. Hu X., Zhang W., Liu X., Meia Y., Huang Y. Nanostructured Mo-based electrode materials for electrochemical energy storage. *Chem. Soc. Rev.* 2015;44(8):2376-2404.
https://doi.org/10.1039/C4CS00350K

5. Predel F. Phase diagram of Mo–O (molybdenum–oxygen) system. In: Predel F. (eds.) Phase Equilibria, Crystallographic and Thermodynamic Data of Binary Alloys. Physical Chemistry. Berlin, Heidelberg: Springer; 2016. V. 12D.

6. Карелин В.А. Химия и технология молибдена и вольфрама. Томск: изд-во Томского политехнического университета; 2017. 58 с.

7. Henrich V.E., Cox P.A. The surface science of metal oxides. Cambridge: Cambridge University Press; 1996. 480 p.

8. Kihlborg L. Studies on molybdenum oxides. *Acta Chem. Scand.* 1959;13:954-962.
https://doi.org/10.3891/acta.chem.scand.13-0954

9. Brandt B.G., Skapski A.C. A refinement of the crystal structure of molybdenum dioxide. *Acta Chem. Scand.* 1967;21:661-672.
https://doi.org/10.3891/acta.chem.scand.21-0661

10. Tsuda N., Nasu K., Fujimori A., Siratori K. Electronic conduction in oxides. New York: Springer-Verlag; 1991. 323 p.

11. Kihlbord L. Least squares refinement of the crystal structure of molybdenum. *Arkiv för Kemi.* 1963;21:357-364.

12. Yun J., Jang W., Lee T., Lee Y., Soon A. Aligning the band structures of polymorphic molybdenum oxides and organic emitters in light-emitting diodes. *Phys. Rev. Applied.* 2017;7:024025-1-024025-8.
https://doi.org/10.1103/PhysRevApplied.7.024025

13. Mendes F.M. Weibel D.E., Blum R.P., Middeke J. Preparation and characterization of well-ordered MoOx films on $Cu_3Au(100)$–oxygen substrate (CAOS). *Catal. Today.* 2008;133(1):187-191.
https://doi.org/10.1016/j.cattod.2007.11.046

14. Tomina N.N., Pimerzin A.A., Moiseev I.K. Sulfide catalysts for hydropurification of oil fractions. *Russ. J. Gen. Chem.* 2009;79(6):1274-1288.
https://doi.org/10.1134/S1070363209060449

15. Méndez-Vivar J. Synthesis of molybdenum oxides by the sol-gel method. *Inorg. Chim. Acta.* 1991;179(1):77-82.
https://doi.org/10.1016/S0020-1693(00)85376-1

16. Ganguly A., George R. Synthesis, characterization and gas sensitivity of MoO_3 nanoparticles. *Bull. Mater. Sci.* 2007;30(2):183-185.
https://doi.org/10.1007/s12034-007-0033-6

17. Pergament A.L., Malinenko V.P., Aleshina L.A., Kazakova E.L., Kuldin N.A. Electrical switching in thin film structures based on molybdenum oxides. *J. Exp. Phys.* 2014;2014:6 p. https://doi.org/10.1155/2014/951297

18. Chiang T.H., Yeh H.C. The synthesis of α-MoO$_3$ by ethylene glycol. *Materials.* 2013;6(10):4609-4625. https://doi.org/10.3390/ma6104609

19. Parviz D., Kazemeini M., Rashidi A.M., Jozani J. Synthesis and characterization of MoO$_3$ nanostructures by solution combustion method employing morphology and size control. *J. Nanopart. Res.* 2010;12(4):1509-1521. https://doi.org/10.1007/s11051-009-9727-6

20. Siciliano T., Tepore A., Filippo E., Micocci G., Tepore M. Characteristics of molybdenum trioxide nanobelts prepared by thermal evaporation technique. *Mater. Chem. Phys.* 2009;114(2-3):687-691. https://doi.org/10.1016/j.matchemphys.2008.10.018

21. Gupta C.K. Extractive metallurgy of molybdenum. Boca Raton: CRC Press; 1992. 404 p.

22. Nakamura I., Miras H.N., Fujiwara A., Fujibayashi M., etc. Investigating the formation of “molybdenum blues” with gel electrophoresis and mass spectrometry. *J. Am. Chem. Soc.* 2015;137(20):6524-6530. https://doi.org/10.1021/ja512758j

23. Koyun O., Gorduk S., Arvas M.B., Sahin Y. Direct, one-step synthesis of molybdenum blue using an electrochemical method, and characterization studies. *Synth. Met.* 2017;233:111-118. https://doi.org/10.1016/j.synthmet.2017.09.009

24. Kazenas E.K., Tsvetkov Yu.V. *Isparenie oksidov* (Evaporation of oxides). Moscow: Nauka; 1997. 543 p. (in Russ.).

25. Yuhnevich Yu.G. Advances in the use of IR-spectroscopy to characterize OH bonds. *Uspekhi Khimii = Russ. Chem. Rev.* 1963;32(11):1397-1423 (in Russ.).

26. Li C., Xin Q., Wang K.-L., Guo X. FT-IR Emission spectroscopy studies of molybdenum oxide and supported molybdena on alumina, silica, zirconia, and titania. *Appl. Spectrosc.* 1991;45(5):874-882. https://doi.org/10.1366/0003702914336651

27. Chen D., Liu M., Yin L., Li T. *et al.* Single-crystalline MoO$_3$ nanoplates: topochemical synthesis and enhanced ethanol-sensing performance. *J. Mater. Chem.* 2011;21(25):9332-9342. https://doi.org/10.1039/C1JM11447F

28. Pavlova S.S., Kotvanova M.K. IR-spectra and electromechanical properties of transition metal oxide bronzes. *Vestnik Yugorskogo gosudarstvennogo universiteta = Yugra State University Bulletin.* 2008;10(3):61-63 (in Russ.).

17. Pergament A.L., Malinenko V.P., Aleshina L.A., Kazakova E.L., Kuldin N.A. Electrical switching in thin film structures based on molybdenum oxides. *J. Exp. Phys.* 2014;2014:6 p. https://doi.org/10.1155/2014/951297

18. Chiang T.H., Yeh H.C. The synthesis of α-MoO$_3$ by ethylene glycol. *Materials.* 2013;6(10):4609-4625. https://doi.org/10.3390/ma6104609

19. Parviz D., Kazemeini M., Rashidi A.M., Jozani J. Synthesis and characterization of MoO$_3$ nanostructures by solution combustion method employing morphology and size control. *J. Nanopart. Res.* 2010;12(4):1509-1521. https://doi.org/10.1007/s11051-009-9727-6

20. Siciliano T., Tepore A., Filippo E., Micocci G., Tepore M. Characteristics of molybdenum trioxide nanobelts prepared by thermal evaporation technique. *Mater. Chem. Phys.* 2009;114(2-3):687-691. https://doi.org/10.1016/j.matchemphys.2008.10.018

21. Gupta C.K. Extractive metallurgy of molybdenum. Boca Raton: CRC Press; 1992. 404 p.

22. Nakamura I., Miras H.N., Fujiwara A., Fujibayashi M., etc. Investigating the formation of «molybdenum blues» with gel electrophoresis and mass spectrometry. *J. Am. Chem. Soc.* 2015;137(20):6524-6530. https://doi.org/10.1021/ja512758j

23. Koyun O., Gorduk S., Arvas M.B., Sahin Y. Direct, one-step synthesis of molybdenum blue using an electrochemical method, and characterization studies. *Synth. Met.* 2017;233:111-118. https://doi.org/10.1016/j.synthmet.2017.09.009

24. Казенас Е.К., Цветков Ю.В. Испарение оксидов. М.: Наука; 1997. 543 с.

25. Юхневич Ю.Г. Успехи в применении ИК-спектроскопии для характеристики ОН-связей. *Успехи химии.* 1963;32(11):1397-1423.

26. Li C., Xin Q., Wang K.-L., Guo X. FT-IR Emission spectroscopy studies of molybdenum oxide and supported molybdena on alumina, silica, zirconia, and titania. *Appl. Spectrosc.* 1991;45(5):874-882. https://doi.org/10.1366/0003702914336651

27. Chen D., Liu M., Yin L., Li T. *et al.* Single-crystalline MoO$_3$ nanoplates: topochemical synthesis and enhanced ethanol-sensing performance. *J. Mater. Chem.* 2011;21(25):9332-9342. https://doi.org/10.1039/C1JM11447F

28. Павлова С.С., Котванова М.К. ИК-спектры и электромеханические свойства оксидных бронз переходных металлов. *Вестник Югорского государственного университета.* 2008;10(3):61-63.

About the authors:

Elena E. Nikishina, Assistant Professor, Department of Chemistry and Technology Rare and Dispersed Elements, Nanoscale and Composite Materials, M.V. Lomonosov Institute of Fine Chemical Technologies, MIREA – Russian Technological University (86, Vernadskogo pr., Moscow, 119571, Russia). E-mail: nikishina@mirea.ru. Scopus Author ID 6602839662, ResearherID O-7115-2014, https://orcid.org/0000-0003-3579-2194

Elena N. Lebedeva, Engineer, Department of Chemistry and Technology Rare and Dispersed Elements, Nanoscale and Composite Materials, M.V. Lomonosov Institute of Fine Chemical Technologies, MIREA – Russian Technological University (86, Vernadskogo pr., Moscow, 119571, Russia). E-mail: rare214@mail.ru. Scopus Author ID 7102162057, https://orcid.org/0000-0003-1532-8845

Dmitry V. Drobot, Professor, Department of Chemistry and Technology Rare and Dispersed Elements, Nanoscale and Composite materials, M.V. Lomonosov Institute of Fine Chemical Technologies, MIREA – Russian Technological University (86, Vernadskogo pr., Moscow, 119571, Russia). E-mail: dvdrobot@mail.ru. Scopus Author ID 35580931100, https://orcid.org/0000-0002-0379-2926

Об авторах:

Никишина Елена Евгеньевна, доцент кафедры химии и технологии редких и рассеянных элементов, наноразмерных и композиционных материалов Института тонких химических технологий им. М.В. Ломоносова ФГБОУ ВО «МИРЭА – Российский технологический университет» (119571, Россия, Москва, пр-т Вернадского, д. 86). E-mail: nikishina@mirea.ru. Scopus Author ID 6602839662, ResearherID O-7115-2014, https://orcid.org/0000-0003-3579-2194

Лебедева Елена Николаевна, инженер кафедры химии и технологии редких и рассеянных элементов, наноразмерных и композиционных материалов Института тонких химических технологий им. М.В. Ломоносова ФГБОУ ВО «МИРЭА – Российский технологический университет» (119571, Россия, Москва, пр-т Вернадского, д. 86). E-mail: rare214@mail.ru. Scopus Author ID 7102162057, https://orcid.org/0000-0003-1532-8845

Дробот Дмитрий Васильевич, профессор кафедры химии и технологии редких и рассеянных элементов, наноразмерных и композиционных материалов Института тонких химических технологий им. М.В. Ломоносова ФГБОУ ВО «МИРЭА – Российский технологический университет» (119571, Россия, Москва, пр-т Вернадского, д. 86). E-mail: dvdrobot@mail.ru. Scopus Author ID 35580931100, https://orcid.org/0000-0002-0379-2926

Submitted: July 11, 2019; Reviewed: February 10, 2020; Accepted: April 11, 2020.

Translated from Russian into English by N. Isaeva
Edited for English language and spelling by Enago, an editing brand of Crimson Interactive Inc.

ANALYTICAL METHODS IN CHEMISTRY AND CHEMICAL TECHNOLOGY

АНАЛИТИЧЕСКИЕ МЕТОДЫ В ХИМИИ И ХИМИЧЕСКОЙ ТЕХНОЛОГИИ

ISSN 2686-7575 (Online)

https://doi.org/10.32362/2410-6593-2020-15-2-77-85

UDC 577.11

Development and validation of a method for the determination of the specific activity of recombinant monoclonal antibody eculizumab

Dmitry I. Zybin[1,@], Aleksandr S. Seregin[2], Aleksandr D. Askretkov[1], Natalya V. Orlova[2], Yuri A. Seregin[2], Anna I. Prostyakova[3], Dmitry V. Kapustin[3]

[1] PHARMAPARK, Moscow, 117246 Russia
[2] Scientific Center "Kurchatov Institute," Research Institute for Genetics and Selection of Industrial Microorganisms, Moscow, 117545 Russia
[3] M.M. Shemyakin and Yu.A. Ovchinnikov Institute of Bioorganic Chemistry, Russian Academy of Sciences, Moscow, 117997 Russia
[@] Corresponding author, e-mail: zybin@pharmapark.ru

Objectives. *Developing reliable and accurate analytical methods is necessary for comparative pharmaceutical analysis using physicochemical, biological (in vitro), preclinical, and clinical trials. The main objective of this study was to develop and validate an in vitro method for determining the specific activity of the recombinant monoclonal antibody eculizumab.*
Methods. *The method of indirect enzyme immunoassay was used in the study.*
Results. *A method for determining the specific activity of the humanized recombinant monoclonal antibody eculizumab was described and validated for the first time. A comparative evaluation of the specific activity of Soliris® (Alexion Pharmaceuticals Inc., USA), and its biosimilar PRK-001 (Pharmapark, Russia) was performed using the developed method.*
Conclusions. *The similarity of PRK-001 and the original Soliris® in relation to their specific activity, that is, binding to the human complement system C5 protein, was proved.*

Keywords: *validation; paroxysmal nocturnal hemoglobinuria; reproduced drug; specific in vitro activity; enzyme-linked immunosorbent assay; complement system.*

For citation: Zybin D.I., Seregin A.S., Askretkov A.D., Orlova N.V., Seregin Yu.S., Prostyakova A.I., Kapustin D.V. Development and validation of a method for the determination of the specific activity of recombinant monoclonal antibody eculizumab. *Tonk. Khim. Tekhnol. = Fine Chem. Technol.* 2020;15(2):77-85. https://doi.org/10.32362/2410-6593-2020-15-2-77-85

Разработка и валидация метода определения специфической активности рекомбинантного моноклонального антитела экулизумаб

Д.И. Зыбин[1,@], А.С. Серегин[2], А.Д. Аскретков[1], Н.В. Орлова[2], Ю.А. Серегин[2], А.И. Простякова[3], Д.В. Капустин[3]

[1]ООО «ФАРМАПАРК», Москва, 117246 Россия
[2]НИЦ «Курчатовский институт – ГосНИИгенетика», Москва, 117545 Россия
[3]Институт биоорганической химии им. Академиков М.М. Шемякина и Ю.А. Овчинникова, Российская академия наук, Москва, 117997 Россия
[@]Автор для переписки, e-mail: zybin@pharmapark.ru

Цели. *При подтверждении биоподобности препаратов необходимо создание надежных и точных аналитических методов сравнительных исследований для доказательства схожести препаратов по результатам физико-химических, биологических (in vitro), доклинических и клинических испытаний. Основной задачей настоящей работы является разработка и валидация метода определения специфической активности рекомбинантного моноклонального антитела экулизумаб.*

Методы. *В работе использован метод непрямого иммуноферментного анализа.*

Результаты. *Впервые разработан метод определения специфической активности гуманизированного рекомбинантного моноклонального антитела экулизумаб и проведена его валидация. С использованием разработанного метода проведена сравнительная оценка специфической активности оригинального препарата Солирис® (Alexion Pharmaceuticals Inc., USA) и его биоаналога PRK-001 (ООО «Фармапарк», Россия).*

Выводы. *Доказана биоаналогичность препаратов Солирис® и PRK-001 в отношении их специфической активности.*

Ключевые слова: *валидация, воспроизведенный лекарственный препарат, пароксизмальная ночная гемоглобинурия, специфическая активность in vitro, иммуноферментный анализ, система комплемента.*

Для цитирования: Зыбин Д.И., Серегин А.С., Аскретков А.Д., Орлова Н.В., Серегин Ю.А., Простякова А.И., Капустин Д.В. Разработка и валидация метода определения специфической активности рекомбинантного моноклонального антитела экулизумаб. *Тонкие химические технологии.* 2020;15(2):77-85. https://doi.org/10.32362/2410-6593-2020-15-2-77-85

INTRODUCTION

Paroxysmal nocturnal hemoglobinuria (PNH) is an extremely rare disease (an average of three cases per million [1]) accompanied by serious epiphenomena, such as hemolytic anemia, atypical thrombosis, bone marrow failure, and renal failure. The etiology of PNH is associated with a somatic mutation in the PIG-A gene, which blocks the biosynthesis of glycosylphosphatidylinositol, a glycolipid called GPI anchor, necessary to retain a number of proteins on the cell membrane, in particular CD55 and CD59, which are inhibitors of the membrane attack complex (MAC) complement systems. The deficiency of CD55 and CD59 on the surface of the cell membrane leads to dysfunction in the suppression of MAC production, which is the main cause of erythrocyte hemolysis in PNH [2, 3]. This is determined by flow cytometry [4, 5].

Currently, the only commercially available drug, Soliris® (*Alexion Pharmaceuticals Inc.*, USA) is used for PNH therapy. The active substance of Soliris® is a recombinant kappa-monoclonal antibody of mixed type IgG2/4—eculizumab consisting of a human constant chain and determining the complementarity of murine regions grafted onto human framework regions in the variable and heavy chain with a total molecular mass of 148 kDa[1]. The mechanism of eculizumab action is the binding of the complement system to protein C5 followed by its lytic destruction in lysosomes, blocking the formation of a MAC, and subsequent cell lysis [6–8].

Due to the high cost of therapy (USD 600 000 per year for one patient) [9] and the need for its lifelong

---

[1] DRUGBANK. Eculizumab. Available from: https://www.drugbank.ca/drugs/DB01257 [Accessed October 22, 2019].

implementation, the number of pharmaceutical companies actively developing a bioanalog of Soliris® increases (*Generium Pharmaceutical,* Russia; *Samsung Bioepis,* South Korea; *Amgen*, USA). Therefore, the need for the development of reliable methods for controlling the quality of the resulting product becomes obvious. One of the most important quality indicators is its binding to protein C5 [10–12].

Currently, no method has been described to evaluate the specific activity of eculizumab with accuracy and reproducibility at all stages of production. Although the Soliris®/Eculizumab enzyme-linked immunosorbent assay (ELISA) Kit (*Arsh Biotech Pvt. Ltd.,* India) is already at the market and can help to evaluate the activity of the drug in biological fluids, because the main part of eculizumab molecules in the human body is bound to an antigen, it is impossible to evaluate its content and activity with the required level of accuracy without using additional sample preparation. In addition, it is unclear whether the use of the kit is effective at various stages of drug production, in particular, after the stages of isolation, purification, and filtration, which can significantly affect the property of the final product.

In this work, we present a new method for determining the specific activity of eculizumab. Our method is suitable for both monitoring the drug quality at various stages of development and implementing the output control of the finished product. The suggested method was used for the comparative evaluation of the specific activity of three series of Soliris® (*Alexion Pharmaceuticals Inc.,* USA) and PRK-001 (*Pharmapark,* Russia).

MATERIALS AND METHODS

We used ELISA to quantify the specific activity of eculizumab. The specific activity of a standard sample of eculizumab used in this study was confirmed by the manufacturer. Soliris® (*Alexion Pharmaceuticals Inc.,* USA) was used for comparison.

Preparation of standard solutions

Preparation of phosphate-buffered saline ("Buffer solution A")

One tablet of the dry prepared buffer (*Sigma Aldrich,* USA) was dissolved in 100 ml of deionized water. The pH of the resulting solution was adjusted to 7.4 using a pH meter *(Mettler Toledo,* USA). The resulting solution was stored in a tightly closed container at 4°C.

Preparation of phosphate-buffered saline with 0.01% Tween 20 ("Buffer solution B")

One tablet of a dry finished buffer containing 0.01% Tween 20 (*Sigma Aldrich,* USA) was dissolved in 500 ml of deionized water under constant stirring at 25°C. The solution pH was adjusted to 7.4. The resulting solution was stored in a tightly closed container at 4°C.

Blank solution preparation

1 g bovine serum albumin (*Sigma Aldrich,* USA) was dissolved in 100 ml buffer solution A. Then, the solution was stored in a tightly closed container at 4°C.

Immobilization of C5 protein on an ELISA plate

A solution of C5 protein (*Complement Technology,* USA) was diluted to a concentration of 1.5 µg/ml using buffer solution A. 100 µl of the resulting solution was added to the wells of the plate and incubated for 48 h at 4°C.

Preparation of calibration solutions

Soliris® with a specific activity of 9138000 IU per 300 mg was diluted with a blank solution according to Table 1.

Preparation of the solution of secondary antibodies

A working solution of secondary antibodies conjugated to horseradish peroxidase was diluted with a blank solution according to the manufacturer's recommendations (*Genway Biotech Inc.,* USA).

Determination of the specific activity of eculizumab

The test solution of eculizumab diluted in the blank solution, and S1–S6 calibration solutions were added into the wells of a tablet with pre-immobilized C5 protein in an amount of 100 µl per well in three repetitions each. The plate was incubated for 2 h at 4°C. Next, the wells of the plate were washed with 200-µl buffer solution B in three repetitions to remove the matrix of the sample. 100-µl solution of secondary antibodies was added into the wells of the plate and incubated for 2 h at 37°C. After incubation, the wells were washed with 200-µl buffer solution B in three repetitions to remove unbound antibodies. After removing buffer solution B, 100-µl 3,3', 5,5'-tetramethylbenzidine containing hydrogen peroxide (*Sigma Aldrich,* USA) was added into the wells of the plate. The plate was incubated for 10 min at 25°C, and the reaction was stopped using 0.5 M sulfuric acid (*CHIMMED,* Russia). The optical density was measured at 450 nm and 650 nm (reference) using a Tecan Infinite 200 Pro plate reader (*Tecan,* Switzerland). A sigmoidal curve was plotted using the calibration solutions of eculizumab in the optical density–activity coordinates. The equation describing the curve was used to calculate the activity of eculizumab in the test sample.

The results were processed using Origin 9.1 software (*OriginLab Corp.,* USA).

Method validation

The validation of the developed method was carried out in compliance with the requirements of the

Russian Federation State Pharmacopeia XIV in terms of specificity, linearity, repeatability, intermediate precision, accuracy, analytical area, and stability.

RESULTS AND DISCUSSION

First, the immobilized protein C5–eculizumab complex was obtained. Second, secondary antibodies specific for the Fc fragment of type 4 IgG and conjugated to horseradish peroxidase were bound. Finally, a chromogenic reagent was added, the reaction was stopped, and the optical density was determined. A schematic representation of the method is shown in Fig. 1.

Specificity evaluation

The method specificity was determined by the ability to evaluate the content of the studied component against the background of related substances in the protein solution [13]. To confirm the method specificity, we studied the effect of buffer solutions on PRK-001 and Soliris® (hereinafter referred to as SP1 and SP2, respectively) prepared in accordance with the manufacturer's instructions. At the same time, the effect of the components of the buffer solutions used at each stage of drug purification was evaluated. When using sample SP3, the buffer solution after purification using an affinity sorbent was used. When using sample SP4, the buffer solution after purification using an ion-exchange sorbent was used. The optical density of the investigated solutions should be in the range of ±10% of the optical density of the blank solution. The results of the study are presented in Table 2.

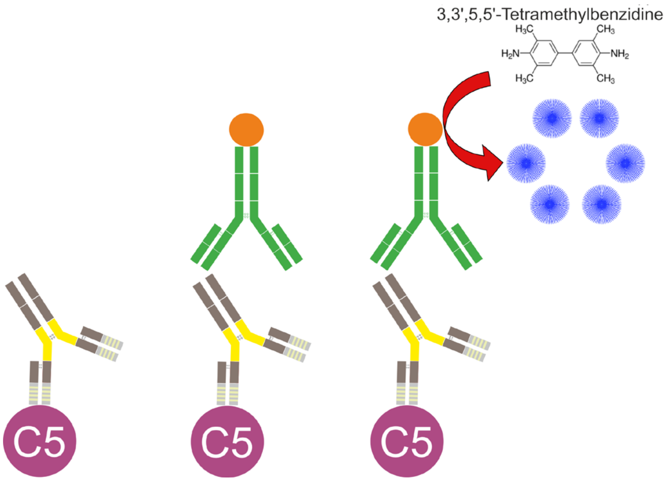

Fig 1. Schematic for determining the specific activity of eculizumab. The stages of the method are described in the text below.

Table 1. Dilution of a standard sample for the preparation of calibration solutions

Sample name	Sample volume, μl	Volume of blank solution, μl	Specific activity, IU/ml
Sample ITD 1*	10 μl of Soliris®	294.6	300 000
Sample ITD 2	100 ITD1	900	30 000
Sample ITD 3	100 ITD2	900	3000
Sample ITD 4	100 ITD3	900	300
Sample S1	500 ITD4	500	150
Sample S2	500 S1	250	100
Sample S3	400 S2	400	50
Sample S4	400 S3	400	25
Sample S5	400 S4	400	12.5
Sample S6	400 S5	140	9.3

*Samples labeled "ITD" are used as intermediate dilutions.

The obtained results indicate that the auxiliary components of the drug do not affect the analysis results. Thus, the specificity of the method was established.

Linearity evaluation

Our method does not demonstrate a linear dependence between specific activity and optical density for the selected range (from 9.3 IU/ml to 150 IU/ml). Therefore, we used a sigmoid curve described by the following equation [14–15]:

$$y = A_1 + \frac{A_2 - A_1}{1 + 10^{(LOGx_0 - x)\times p}},$$

where A_1 and A_2 are the asymptotes, x is the value of activity, IU/ml; p is the Hill coefficient; x_0 is the coordinate of the inflection point.

When plotting the calibration curve, six standard solutions with the following values of specific activity were used: 150, 100, 50, 25, 12.5, and 9.3 IU/ml. The resulting curve is presented in Fig. 2. The correlation coefficient was 0.9987, which is above the minimum allowable value of 0.99. Thus, the linearity of the method was established.

Repeatability evaluation

The repeatability of the method was evaluated by analyzing standard samples vis-à-vis specific activity values (150, 25, and 12.5 IU/ml) in six replicates each. The relative standard deviation (RSD) for each concentration should not exceed 3%. The results obtained for the method repeatability are presented in Table 3. The value of the RSD for all concentration levels does not exceed 3%, proving the repeatability of the method.

Intermediate precision and accuracy

Intermediate precision and accuracy were evaluated by conducting six analytical sessions over six days by two operators. In each analytical session, a calibration curve was plotted, and five test solutions were studied with the following values of specific activity: 150, 75, 37.5, 18.7, and 9.3 IU/ml. To establish the method accuracy, the value of the degree of extraction (R) should not go beyond 85–115%. The intermediate precision of the method is considered to be established if the RSD according to the results of six sessions for each concentration level does not exceed 15%. The results are presented in Table 4.

The obtained results meet the requirements. Thus, the intermediate precision and accuracy of the method were established.

Evaluation of the analytical field

The analytical region of the method was evaluated on the basis of the results obtained when determining the method linearity, repeatability, and accuracy

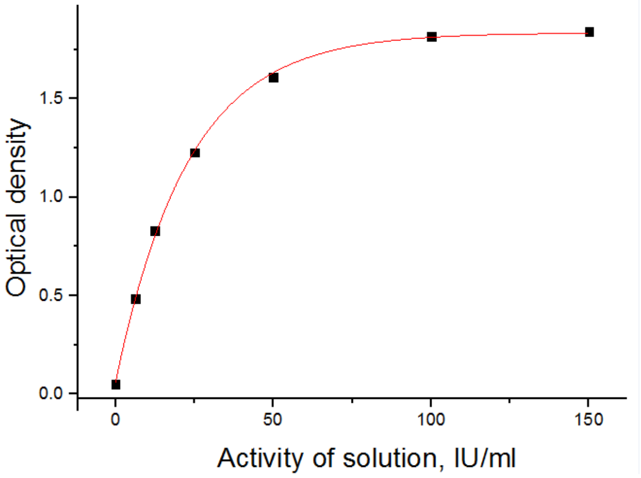

Fig. 2. The calibration curve obtained when evaluating the linearity of the method.

Table 2. Determination of method specificity

Sample name	Optical density*	Optical density* of blank solution
Sample SP1	0.0154 ± 0.0004	0.0151 ± 0.0004
Sample SP2	0.0153 ± 0.0004	
Sample SP3	0.0151 ± 0.0003	
Sample SP4	0.0155 ± 0.0004	

*The data in the table are given in the following format: average value ± standard deviation ($n = 3$).

for the activity range of 9.3–150 IU/ml. Since the technique meets all the validation requirements, we can assume that the analytical region of the method is in the range of 9.3–150 IU/ml.

Stability evaluation

The most critical parameter of the method, which may affect the result, is the storage time of the tablet with immobilized C5 protein. To evaluate the method stability, plates with immobilized C5 protein were incubated at 4°C for 7 and 14 days. Next, the test sample was analyzed with parallel analysis in the tablet (storage time 0 days). The results of determining the activity in the tablets subjected to storage were compared with the results obtained in the tablet without any long-term storage.

The deviation of the activity of the test sample from the true value obtained in the tablets subjected to storage, both for 7 and for 14 days, did not exceed the set limit (±5%). This proves the method stability with respect to the storage time of the tablet with immobilized protein C5.

Comparative study of the specific activity of PRK-001 and Soliris®

The drug manufactured by Pharmapark—PRK-001—is a reproduced biological drug. Thus, it is necessary to confirm its similarity to the original [16]. In this work, we performed a comparative evaluation of the specific activity of three series of Soliris® and PRK-001 to confirm their similar bioactivity. Soliris® 1000325 series with a known activity value was used as the standard.

Figure 3 presents the optical density dependence on the specific activity of all the drugs studied in the work.

For all the series of studied drugs, the specific activity was determined using the developed method. The study results are shown in Fig. 4.

The obtained results confirm the compliance of PRK-001 and Soliris® preparations with respect to their specific activity, that is, binding to the human complement system C5 protein. The measured specific activity of Soliris® and PRK-001 samples differed no more than 9%.

Table 3. Results of the method repeatability study

Theoretical specific activity of the sample, IU/ml	The value of the measured specific activity of the sample*, IU/ml	RSD, %
150	154.9 ± 4.4	2.8
25	25.5 ± 0.7	2.5
12.5	12.3 ± 0.1	0.8

*The data in the table are given in the format average value ± standard deviation ($n = 6$).

Table 4. Evaluation of the intermediate precision and accuracy of the method

Theoretical specific activity of the sample, IU/ml	The value of the measured specific activity of the sample*, IU/ml	RSD ($n = 6$), %	R, %
150.0	157.3 ± 15.3	9.7	104.9
75.0	75.9 ± 6.0	7.9	101.2
37.5	37.5 ± 2.2	5.9	100.0
18.7	19.9 ± 1.7	8.5	106.1
9.3	9.3 ± 0.9	8.7	108.1

*The data in the table are given in the format average value ± standard deviation ($n = 6$).

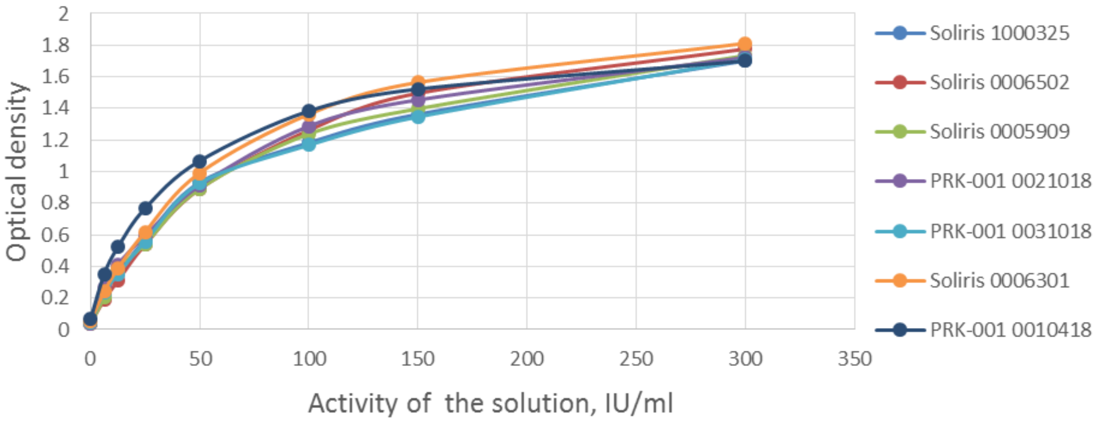

Fig. 3. "Optical density-specific activity (binding)" dependence plot obtained for Soliris® (Series 0006502, 0005909, and 0006301) and PRK-001 (Series 0010418, 0021018, and 0031018) in comparison with Soliris® Series 1000325.

Fig. 4. Specific activity of three series Soliris® and PRK-001.

CONCLUSIONS

In this work, a method for determining the specific activity of the humanized recombinant monoclonal antibody eculizumab was described and validated for the first time. A comparative evaluation of the reproduced drug PRK-001 and the original—Soliris®—was performed. The similarity of both drugs in relation to their specific activity was proved.

The authors declare no conflicts of interest.

REFERENCES

1. Hill A., Platts P.J., Smith A. The incidence and prevalence of paroxysmal nocturnal hemoglobinuria (PNH) and survival of patients in Yorkshire. *Blood.* 2006;108(11):985. https://doi.org/10.1182/blood.V108.11.985.985

2. Pu J.J., Brodsky R.A. Paroxysmal nocturnal hemoglobinuria from bench to bedside. *ClinTranslSci.* 2011;4(3):219-224. https://doi.org/10.1111/j.1752-8062.2011.00262.x

3. Devalet B., Mullier F., Chatelain B., Dogne J.M., Chatelain C. Pathophysiology, diagnosis, and treatment of paroxysmal nocturnal hemoglobinuria: a review. *Eur. J. Haematol.* 2015;95(3):190-198. https://doi.org/10.1111/ejh.12543

4. Höchsmann B., Rojewski M., Schrezenmeier H. Paroxysmal nocturnal hemoglobinuria (PNH): higher sensitivity and validity in diagnosis and serial monitoring by flow cytometric analysis of reticulocytes. *Ann. Hematol.* 2011;90(8):887-899. https://doi.org/10.1007/s00277-011-1177-4

5. Brodsky R.A., Young N.S., Antonioli E. Multicenter phase 3 study of the complement inhibitor eculizumab for the treatment of patients with paroxysmal nocturnal hemoglobinuria. *Blood.* 2008;111(4):1840-1847. https://doi.org/10.1182/blood-2007-06-094136

6. Tegla C.A., Cudrici C., Patel S. Membrane attack by complement: the assembly and biology of terminal complement complexes. *Immunol. Res.* 2011;51(1):45–60. https://doi.org/10.1007/s12026-011-8239-5

7. Ricklin D., Hajishengallis G., Yang K., Lambris J.D. Complement: a key system for immune surveillance and homeostasis. *Nat. Immunol.* 2010;11(9):785-797. https://doi.org/10.1038/ni.1923

8. Dubois E.A., Cohen A.F. Eculizumab. *Br. J. Clin. Pharmacol.* 2009;68(3):318-319. https://doi.org/10.1111/j.1365-2125.2009.03491.x

9. Khedraki R., Noor Z., Rick J. The Most Expensive Drug in the World: To Continue or Discontinue, That Is the Question. *Fed. Pract.* 2016;33(7):22-28. https://www.ncbi.nlm.nih.gov/pmc/articles/PMC6366567/

10. Harder M. J., Kuhn N., Schrezenmeier H., *et al.* Incomplete inhibition by eculizumab: mechanistic evidence for residual C5 activity during strong complement activation. *Blood.* 2016;129(8):970-980. https://doi.org/10.1182/blood-2016-08-732800

11. Kelly R. J., Höchsmann B., Szer J., *et al.* Eculizumab in Pregnant Patients with Paroxysmal Nocturnal Hemoglobinuria. *N. Engl. J. Med.* 2015;373(11):1032-1039. https://doi.org/10.1056/NEJMoa1502950

12. Wehling C., Amon O., Bommer M. Monitoring of complement activation biomarkers and eculizumab in complement-mediated renal disorders. *Clin. Exp. Immunol.* 2016;187(2):304-315. https://doi.org/10.1111/cei.12890

13. Validation of Analytical Procedures: Text and Methodology Q2(R1). In: International Conference on Harmonization (ICH) of Technical Requirements for Registration of Pharmaceuticals for Human Use. Geneva. 2005;6-13.

14. Tijssen P. Practice and Theory of Enzyme Immunoassays. Canada: Elsevier Science; 1985. 548 p.

15. Isakova O.P., Tarasevich Yu.Yu. *Obrabotka i vizualizatsiya dannykh fizicheskikh eksperimentov s pomoshch'yu paketa Origin* (Processing and visualization of physical experiment data using the Origin package). Educational and methodological guide. Astrakhan: DPO AIPKP Publ.; 2007; 67 p. (in Russ.).

16. Guideline on similar biological medicinal products. Committee for Medicinal Products for Human Use; 2014. 16 p. Available from: https://www.ema.europa.eu/en/documents/scientific-guideline/guideline-similar-biological-medicinal-products-rev1_en.pdf

About the authors:

Dmitry I. Zybin, Chief Chemist-Analyst, PHARMAPARK LLC (8, b. 1, Nauchnyi proezd, Moscow, 117246, Russia). E-mail: zybin@pharmapark.ru. Researcher ID P-8049-2016, https://orcid.org/0000-0002-5542-982X

Aleksandr S. Seregin, Postgraduate Student, Scientific Center "Kurchatov Institute", Research Institute for Genetics and Selection of Industrial Microorganisms (1, 1st Dorozhnyi pr., Moscow, 117545, Russia). E-mail: penpney@mail.ru. https://orcid.org/0000-0002-5842-7344

Aleksandr D. Askretkov, Chief Chemist-Analyst, PHARMAPARK LLC (8, b. 1, Nauchnyi proezd, Moscow, 117246, Russia). E-mail: askretkov.a.d@gmail.com. https://orcid.org/0000-0003-0110-8323

Natalya V. Orlova, Cand. of Sci., Head of Research Laboratory, Scientific Center "Kurchatov Institute," Research Institute for Genetics and Selection of Industrial Microorganisms (1, 1st Dorozhnyi pr., Moscow, 117545, Russia). E-mail: orlova.chemist@gmail.com. https://orcid.org/0000-0003-4161-5880

Yuri A. Seregin, Cand. of Sci., Deputy Director, Scientific Center "Kurchatov Institute," Research Institute for Genetics and Selection of Industrial Microorganisms (1, 1st Dorozhnyi pr., Moscow, 117545, Russia). E-mail: yuriy.seregin@pharmapark.ru. ResearcherID I-1874-2017

Anna I. Prostyakova, Cand. of Sci., Researcher, Laboratory of Polymers for Biology, M.M. Shemyakin and Yu.A. Ovchinnikov Institute of Bioorganic Chemistry, Russian Academy of Sciences (16/10, Miklukho-Maklaya ul., Moscow, 117997, Russia). E-mail: profan@list.ru. Researcher ID H-5123-2016, https://orcid.org/0000-0001-5922-6600

Dmitry V. Kapustin, Cand. of Sci., Head of Polymeric Sorbent Laboratory, M.M. Shemyakin and Yu.A. Ovchinnikov Institute of Bioorganic Chemistry, Russian Academy of Sciences (16/10, Miklukho-Maklaya ul., Moscow, 117997, Russia). E-mail: kapustin@ibch.ru. Researcher ID B-5773-2014, https://orcid.org/0000-0002-5485-9297

Об авторах:

Зыбин Дмитрий Игоревич, старший химик-аналитик ООО «Фармапарк» (117246, Россия, Москва, Научный пр-д, д. 8, стр. 1). E-mail: zybin@pharmapark.ru. Researcher ID P-8049-2016, https://orcid.org/0000-0002-5542-982X

Серегин Александр Сергеевич, аспирант НИЦ «Курчатовский институт – ГосНИИгенетика» (117545, Россия, Москва, 1-й Дорожный пр-д, д. 1). E-mail: penpney@mail.ru. https://orcid.org/0000-0002-5842-7344

Аскретков Александр Дмитриевич, старший химик-аналитик ООО «Фармапарк» (117246, Россия, Москва, Научный пр-д, д. 8, стр. 1). E-mail: askretkov.a.d@gmail.com. https://orcid.org/0000-0003-0110-8323

Орлова Наталья Владимировна, кандидат биологических наук, заведующий испытательной лаборатории НИЦ «Курчатовский институт – ГосНИИгенетика» (117545, Россия, Москва, 1-й Дорожный пр-д, д. 1). E-mail: orlova.chemist@gmail.com. https://orcid.org/0000-0003-4161-5880

Серегин Юрий Александрович, кандидат биологических наук, заместитель директора НИЦ «Курчатовский институт – ГосНИИгенетика» (117545, Россия, Москва, 1-й Дорожный пр-д, д. 1). E-mail: yuriy.seregin@pharmapark.ru. ResearcherID I-1874-2017

Простякова Анна Игоревна, кандидат химических наук, научный сотрудник лаборатории полимеров для биологии Института биоорганической химии им. академиков М.М. Шемякина и Ю.А. Овчинникова Российской академии наук (117997, Россия, Москва, ул. Миклухо-Маклая, д.16/10). E-mail: profan@list.ru. Researcher ID H-5123-2016, https://orcid.org/0000-0001-5922-6600

Капустин Дмитрий Валерьевич, кандидат химических наук, старший научный сотрудник, руководитель лаборатории полимерных сорбентов Института биоорганической химии им. академиков М.М. Шемякина и Ю.А. Овчинникова Российской академии наук (117997, Россия, Москва, ул. Миклухо-Маклая, д.16/10). E-mail: kapustin@ibch.ru. Researcher ID B-5773-2014, https://orcid.org/0000-0002-5485-9297

Submitted: November 01, 2019; Reviewed: March 12, 2020; Accepted: April 13, 2020.

Translated from Russian into English by M. Povorin

Edited for English language and spelling by Enago, an editing brand of Crimson Interactive Inc.

MIREA – Russian Technological University.
78, Vernadskogo pr., Moscow, 119454, Russian Federation.
Publication date *April 30*, 2020.
Not for sale

МИРЭА – Российский технологический университет.
119454, РФ, Москва, пр-кт Вернадского, д. 78.
Дата опубликования *30 апреля* 2020 г.
Не для продажи